

UNCLASSIFIED

AD NUMBER

AD861763

LIMITATION CHANGES

TO:

Approved for public release; distribution is unlimited.

FROM:

Distribution authorized to U.S. Gov't. agencies and their contractors; Critical Technology; NOV 1969. Other requests shall be referred to Air Force Aero Propulsion Laboratory, Attn: APTA, Wright-Patterson AFB, OH 45433. This document contains export-controlled technical data.

AUTHORITY

AFAPL ltr, 12 Apr 1972

THIS PAGE IS UNCLASSIFIED

AD 861763

AFAPL-TR-68-119
SUPPLEMENT I

EXPERIMENTAL EVALUATION OF INLET DRAG CHARACTERISTICS IN THE TRANSONIC MACH NUMBER REGIME

F.D. McVey, J.V. Rejeske, and E.J. Phillips

MCDONNELL DOUGLAS CORPORATION

TECHNICAL REPORT AFAPL-TR-68-119, SUPPLEMENT I

NOVEMBER 1969

This document is subject to special export controls and each transmittal to foreign governments or foreign nationals may be made only with prior approval of the Air Force Aero Propulsion Laboratory, Wright-Patterson Air Force Base, Ohio 45433.

Attn: APTA

Air Force Aero Propulsion Laboratory
Air Force Systems Command
Wright-Patterson Air Force Base, Ohio

CLEARING HOUSE

NOV 20 1969

119

119

INSTRUCTION FOR	
OPT.	WHITE SECTION <input type="checkbox"/>
DOC	BUFF SECTION <input checked="" type="checkbox"/>
UNANNOUNCED	
JUSTIFICATION	
BY	
DISTRIBUTION / AVAILABILITY CODES	
DIST.	AVAIL and/or SPECIAL

NOTICE

When Government drawings, specifications, or other data are used for any purpose other than in connection with a definitely related Government procurement operation, the United States Government thereby incurs no responsibility nor any obligation whatsoever; and the fact that the government may have formulated, furnished, or in any way supplied the said drawings, specifications, or other data, is not to be regarded by implication or otherwise as in any manner licensing the holder or any other person or corporation, or conveying any rights or permission to manufacture, use, or sell any patented invention that may in any way be related thereto.

Copies of this report should not be returned unless return is required by security considerations, contractual obligations, or notice on a specific document.

AFAPL-TR-68-119

SUPPLEMENT I

EXPERIMENTAL EVALUATION OF INLET DRAG CHARACTERISTICS IN THE TRANSonic MACH NUMBER REGIME

F.D. McVey, J.V. Rejeske, and E.J. Phillips

MCDONNELL DOUGLAS CORPORATION

This document is subject to special export controls and each transmittal to foreign governments or foreign nationals may be made only with prior approval of the Air Force Aero Propulsion Laboratory, Wright-Patterson Air Force Base, Ohio 45433.

FOREWORD

This report was prepared by the McDonnell Aircraft Company, St. Louis, Missouri, under an amendment to United States Air Force contract F33615-68-C-1520, "Experimental Evaluation of Propulsion System Component Drag and Stability Characteristics in the Transonic Mach Number Regime." The test program was sponsored by the Air Force Aero Propulsion Laboratory, Harlan J. Gratz/APTA, Project Engineer, as in the first phase of the contract effort. The drag balance is U. S. Government property under loan to the McDonnell Aircraft Company, St. Louis. The test models and other test apparatus were furnished by the McDonnell Aircraft Company, St. Louis.

The contract period extended from 4 December 1968 to 15 September 1969. The Phase II experimental effort was carried out at NASA-Ames in the 6 x 6 ft. supersonic wind tunnel in two parts. The Phase II - Part A series was conducted in October 1968 and the Phase II - Part B series in June 1969, with the assistance of ARO, Inc., Ames Division Personnel C. Prunty and A. R. Boone. This report was prepared by F. D. McVey, J. V. Rejeske, and E. J. Phillips of the McDonnell Aircraft Company, St. Louis. The authors are indebted to T. C. Rochow, Dr. B. M. Sharp, and E. D. Spong for development of the analytic techniques, and to D. R. Chamberlain, D. N. Kendall, and D. A. Kopp for assistance in model design and test direction.

Publication of this report does not constitute Air Force approval of the report's findings or conclusions. It is published only for the exchange and stimulation of ideas.

ABSTRACT

This report presents the results of a test program to determine the drag of supersonic inlets operating at transonic Mach number conditions. It is a supplement to Air Force Report AFAPL-TR-68-119 describing the results of additional tests conducted under Air Force Contract F33615-68-C-1520.

Data are presented showing the additive drag and total inlet drag of the F-4 aircraft inlet measured in the presence of the aircraft forebody and in an undisturbed stream. Inlet drag test data are also presented for a series of thirteen configurations where the sideplate geometry is the primary variable. All thirteen configurations are variations on a single two-dimensional inlet.

Tests to reproduce some of the data reported in AFAPL-TR-68-119 were conducted to evaluate the accuracy of the experimental procedure.

TABLE OF CONTENTS

<u>SECTION</u>		<u>PAGE</u>
I	INTRODUCTION	1
II	DESCRIPTION OF TEST EQUIPMENT	4
	1. Drag Balance and Model Support	4
	2. Inlet Models	4
	a. Axisymmetric Inlet Models	4
	b. F-4 Inlet Models	5
	c. Two-Dimensional Inlet Models	6
	3. Drag Balance Modifications	8
III	TEST PROGRAM AND TEST TECHNIQUES	16
	1. Test Summary	16
	2. Test Procedures	16
	3. Accuracy and Repeatability of the Test Data	20
IV	TEST RESULTS	22
	1. F-4 Inlet Drag Data	22
	2. Axisymmetric Inlet Drag Data	23
	3. Two-Dimensional Inlet Drag Data	24
V	CONCLUSIONS	56
VI	REFERENCES	57
	APPENDIX A - RUN SUMMARY	59
	APPENDIX B - TEST RESULTS FOR THE F-4 INLET MODELS	65
	APPENDIX C - AXISYMMETRIC INLET PRESSURE DISTRIBUTIONS	84
	APPENDIX D - TEST RESULTS FOR THE TWO-DIMENSIONAL INLET MODELS	93

LIST OF ILLUSTRATIONS

<u>FIGURE</u>		<u>PAGE</u>
1	F-4 and Two-Dimensional Inlet Model Components	3
2	Axisymmetric, F-4, and Two-Dimensional Inlet Geometry	9
3	F-4 Inlet Model - Typical Assembly with Splitter Plate	10
4	F-4 Inlet Model - Typical Assembly with Forebody	11
5	F-4 Inlet Model and Splitter Plate Test Assembly	12
6	F-4 Inlet Model and Forebody Test Assembly	13
7	Two-Dimensional Inlet Model Test Assemblies and Geometry	14
8	Two-Dimensional Inlet Model Sideplate Configurations	15
9	Forebody Effects on the F-4 Inlet Drag, $F_1, M_\infty = 0.70, \alpha = 0^\circ$	27
10	Forebody Effects on the F-4 Inlet Drag, $F_1, M_\infty = 0.90, \alpha = 0^\circ$	28
11	Forebody Effects on the F-4 Inlet Drag, $F_3, M_\infty = 0.70, \alpha = 0^\circ$	29
12	Forebody Effects on the F-4 Inlet Drag, $F_3, M_\infty = 0.90, \alpha = 0^\circ$	30
13	Forebody Effects on the F-4 Inlet Drag, $F_3, M_\infty = 2.0, \alpha = 0^\circ$	31
14	Forebody Effects on the F-4 Inlet Drag, $F_3, M_\infty = 0.70, \alpha = 6^\circ$	32
15	Forebody Effects on the F-4 Inlet Drag, $F_3, M_\infty = 0.90, \alpha = 6^\circ$	33
16	Forebody Effects on the F-4 Inlet Drag, $F_3, M_\infty = 2.0, \alpha = 6^\circ$	34
17	Forebody Effects on the F-4 Inlet Drag, $F_1, M_\infty = 0.70, \alpha = 12^\circ$	35
18	Forebody Effects on the F-4 Inlet Drag, $F_1, M_\infty = 0.90, \alpha = 12^\circ$	36
19	Forebody Effects on the F-4 Inlet Drag, $F_1, M_\infty = 1.05, \alpha = 12^\circ$	37

LIST OF ILLUSTRATIONS (Continued)

<u>FIGURE</u>		<u>PAGE</u>
20	Forebody Effects on the F-4 Additive Drag, $F_1, M_\infty = 0.70, \alpha = 0^\circ$	38
21	Forebody Effects on the F-4 Additive Drag, $F_1, M_\infty = 0.90, \alpha = 0^\circ$	39
22	Forebody Effects on the F-4 Additive Drag, $F_1, M_\infty = 0.70, \alpha = 12^\circ$	40
23	Forebody Effects on the F-4 Additive Drag, $F_1, M_\infty = 0.90, \alpha = 12^\circ$	41
24	Forebody Effects on the F-4 Additive Drag, $F_1, M_\infty = 1.05, \alpha = 12^\circ$	42
25	Inlet Drag Coefficient, Configuration A10, $\alpha = 0^\circ$	43
26	Additive Drag Coefficient, Configuration A10, $\alpha = 0^\circ$	44
27	Cowl Drag Coefficient, Configuration A10, $\alpha = 0^\circ$	45
28	Comparison of Theoretical and Experimental Cowl Pressure Coefficient, Configuration A10	46
29	Comparison of Theoretical and Experimental Innerbody Pressure Coefficient, Configuration A10	47
30	Effect of Sideplate Geometry on Inlet Drag, $M_\infty = 0.70, \alpha = 0^\circ$	48
31	Effect of Sideplate Geometry on Inlet Drag, $M_\infty = 0.90, \alpha = 0^\circ$	49
32	Effect of Sideplate Geometry on Inlet Drag, $M_\infty = 0.70, \alpha = 0^\circ$	50
33	Effect of Sideplate Geometry on Inlet Drag, $M_\infty = 0.90, \alpha = 0^\circ$	51
34	Effect of Cowl on Inlet Drag, $M_\infty = 0.70, \alpha = 0^\circ$	52
35	Effect of Cowl on Inlet Drag, $M_\infty = 0.90, \alpha = 0^\circ$	53

LIST OF ILLUSTRATIONS (Continued)

<u>FIGURE</u>		<u>PAGE</u>
36	Effect of Splitter Plate on Inlet Drag, $M_{\infty} = 0.70, \alpha = 0^\circ$	54
37	Effect of Splitter Plate on Inlet Drag, $M_{\infty} = 0.90, \alpha = 0^\circ$	55

APPENDIX B

B.1	Inlet Drag Coefficient, $F_{lf}, \alpha = 0^\circ$	66
B.2	Inlet Drag Coefficient, $F_{lf}, \alpha = 6^\circ$	67
B.3	Inlet Drag Coefficient, $F_{lf}, \alpha = 12^\circ$	68
B.4	Inlet Drag Coefficient, $F_{3f}, \alpha = 0^\circ$	69
B.5	Inlet Drag Coefficient, $F_{3f}, \alpha = 6^\circ$	70
B.6	Inlet Drag Coefficient, $F_{lo}, \alpha = 0^\circ$	71
B.7	Inlet Drag Coefficient, $F_{ls}, \alpha = 12^\circ$	72
B.8	Inlet Drag Coefficient, $F_{3s}, \alpha = 6^\circ$	73
B.9	Additive Drag Coefficient, $F_{lf}, \alpha = 0^\circ$	74
B.10	Additive Drag Coefficient, $F_{lf}, \alpha = 6^\circ$	75
B.11	Additive Drag Coefficient, $F_{lf}, \alpha = 12^\circ$	76
B.12	Additive Drag Coefficient, $F_{lo}, \alpha = 0^\circ$	77
B.13	Additive Drag Coefficient, $F_{ls}, \alpha = 12^\circ$	78
B.14	Ramp Drag Coefficient, $F_{lf}, \alpha = 0^\circ$	79
B.15	Ramp Drag Coefficient, $F_{lf}, \alpha = 6^\circ$	80
B.16	Ramp Drag Coefficient, $F_{lf}, \alpha = 12^\circ$	81
B.17	Ramp Drag Coefficient, $F_{lo}, \alpha = 0^\circ$	82
B.18	Ramp Drag Coefficient, $F_{ls}, \alpha = 12^\circ$	83

LIST OF ILLUSTRATIONS (Continued)

<u>FIGURE</u>		<u>PAGE</u>
APPENDIX C		
C.1	Cowl Pressure Coefficient, Configuration A10, $M_{\infty} = 0.70$	85
C.2	Cowl Pressure Coefficient, Configuration A10, $M_{\infty} = 0.90$	86
C.3	Cowl Pressure Coefficient, Configuration A10, $M_{\infty} = 1.05$	87
C.4	Cowl Pressure Coefficient, Configuration A10, $M_{\infty} = 2.00$	88
C.5	Innerbody Pressure Coefficient, Configuration A10, $M_{\infty} = 0.70$	89
C.6	Innerbody Pressure Coefficient, Configuration A10, $M_{\infty} = 0.90$	90
C.7	Innerbody Pressure Coefficient, Configuration A10, $M_{\infty} = 1.05$	91
C.8	Innerbody Pressure Coefficient, Configuration A10, $M_{\infty} = 2.00$	92
APPENDIX D		
D.1	Inlet Drag Coefficient, Configuration 1, $\alpha = 0^\circ$	94
D.2	Inlet Drag Coefficient, Configuration 2, $\alpha = 0^\circ$	95
D.3	Inlet Drag Coefficient, Configuration 3, $\alpha = 0^\circ$	96
D.4	Inlet Drag Coefficient, Configuration 4, $\alpha = 0^\circ$	97
D.5	Inlet Drag Coefficient, Configuration 5, $\alpha = 0^\circ$	98
D.6	Inlet Drag Coefficient, Configuration 6, $\alpha = 0^\circ$	99
D.7	Inlet Drag Coefficient, Configuration 8, $\alpha = 0^\circ$	100
D.8	Inlet Drag Coefficient, Configuration 11, $\alpha = 0^\circ$	101
D.9	Inlet Drag Coefficient, Configuration 12, $\alpha = 0^\circ$	102
D.10	Inlet Drag Coefficient, Configuration 1s, $\alpha = 0^\circ$	103

LIST OF ILLUSTRATIONS (Continued)

<u>FIGURE</u>		<u>PAGE</u>
D.11	Inlet Drag Coefficient, Configuration 1, $\alpha = 6^\circ$	104
D.12	Inlet Drag Coefficient, Configuration 2, $\alpha = 6^\circ$	105

LIST OF TABLES

<u>TABLE</u>		<u>PAGE</u>
I	Test Summary - Phase II - Part A	17
II	Test Summary - Phase II - Part B	18

SYMBOLS AND NOMENCLATURE

A_B	Axisymmetric inlet body area.
A_c	Inlet capture area.
A_{LIP}	Flow area at the inlet lip station.
A_o	Captured freestream tube area.
A_{THROAT}	The minimum flow area of the internally contracted inlets.
A_c/A_B	Ratio of inlet capture area to model body area.
A_{LIP}/A_c	Inlet lip to inlet capture area ratio.
A_o/A_c	Mass flow ratio (capture area ratio).
$(A_o/A_c)_{max}$	Maximum theoretical inlet mass flow ratio (capture area ratio).
A_{THROAT}/A_c	Inlet throat to inlet capture area ratio.
B.L.	Indicates a Butt Line
C_{ADD}	Additive drag coefficient based on inlet capture area - $F_{ADD}/q_o A_c$.
C_c	Cowl drag coefficient based on inlet capture area - $F_c/q_o A_c$.
C_I	Inlet drag coefficient ($C_{ADD} + C_c$) based on inlet capture area - $F_I/q_o A_c$.
C_p	Pressure Coefficient ($P - P_o/q_o$).
C_R	Ramp drag coefficient based on inlet capture area - $F_R/q_o A_c$.
F_{ADD}	Inlet additive drag force.
F_c	Cowl drag force.
F_I	Inlet drag force [$F_{ADD} + F_c$].
F_R	Ramp drag force.
F.S.	Indicates a Fuselage Station.
M_D	Inlet design Mach number.

M_∞	Freestream Mach number.
P_∞	Freestream static pressure.
P_{T_∞}	Freestream total pressure.
q_∞	Freestream dynamic pressure $\left \frac{P_\infty \gamma M_\infty^2}{2} \right $
R_{LIP}	Axisymmetric cowl lip leading edge radius.
W.L.	Indicates a Water Line
α	Angle of attack.
γ	Ratio of specific heats.
δ_1	F-4 fixed leading ramp angle.
δ_2	F-4 variable second ramp angle.
θ_c	Axisymmetric or Two-Dimensional cowl angle.
θ_{IB}	Axisymmetric innerbody half-angle.
θ_l	Two-Dimensional inlet ramp angle.
ψ	Yaw angle

SECTION I

INTRODUCTION

The inlet drag investigations described in the first report (Phase I) of this program (Reference 1), yielded data defining the transonic drag characteristics of Axisymmetric Single Cone and Normal Shock inlets, the basic F-4 inlet, and an unique design Opposed-Ramp inlet. The purpose of the extension of this program was to:

- o Determine forebody effects on inlet drag,
- o Define the details of the cowl lip pressure of an axisymmetric inlet, and
- o Determine drag characteristics as influenced by radical variations in sideplate geometry on a series of Two-Dimensional inlets which were readily formed by simple modifications of the available model hardware.

The forebody effects were determined with an F-4 inlet and F-4B aircraft forebody configuration. F-4 inlet drag was determined with the forebody attached, with the splitter plate configuration used in Phase I and with neither forebody nor splitter plate.

In the Phase I tests the drag determined from surface pressure integrations showed consistent disagreement with force determined inlet drag. Insufficient definition of the cowl pressure in the region of the cowl lip was believed to be a possible source of this difference. In this program one axisymmetric configuration (A10) was instrumented with additional cowl lip pressures in an effort to resolve this question. Force data was also obtained with this model to provide a correlation with the Phase I test results.

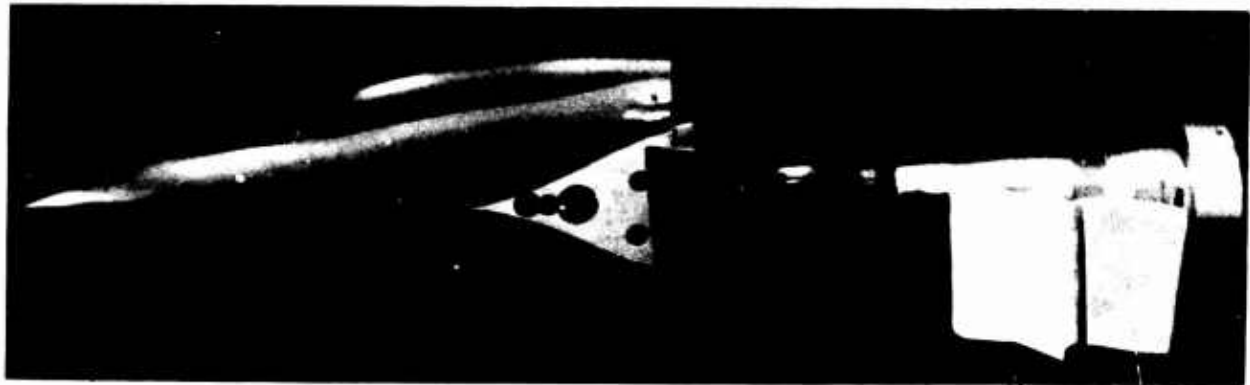
The Opposed-Ramp model of Phase I was modified to permit investigation of sideplate geometry and cowl shape. The modifications to the ramps and cowls provided a nominal two-dimensional inlet shape. Inlet configurations with and without internal contraction were tested. Figure 1 presents

photographs of the F-4 and Two-Dimensional inlet components.

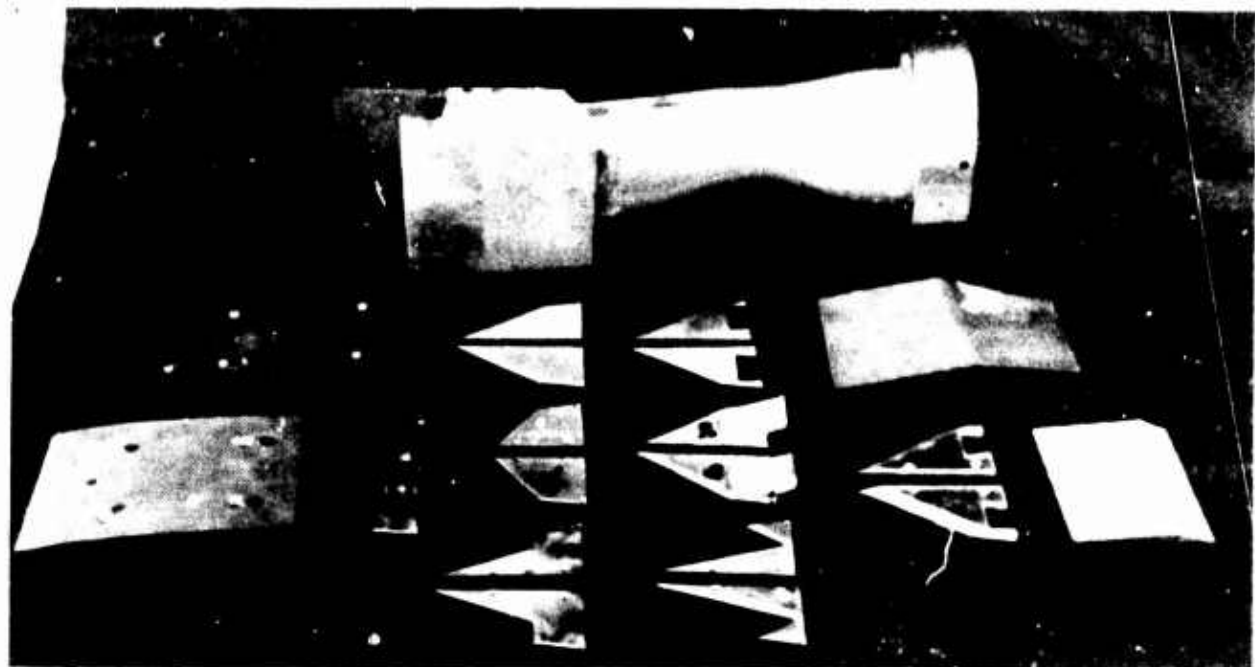
Due to a drag balance malfunction during initial Phase II testing, these tests were divided into two parts. In Phase II - Part A the forebody effects were evaluated on the F-4 inlet model and the Axisymmetric inlet was tested. In the Phase II - Part B series the Two-Dimensional inlet configurations were tested. The inlet drag balance was repaired and recalibrated between the tests of Phase II A and B. The order of the testing and a complete record of the test activity is present in the "run summary" of Appendix A.

The complete test program was accomplished at the NASA-Ames Research Center in the 6 x 6 ft. supersonic wind tunnel. The program involved tests at transonic Mach numbers ranging from .7 to 1.05, and tests of selected configurations at supersonic Mach numbers of 1.8 and 2.0. Only those models and test equipment that were not employed in the Phase I tests are described in this report.

The inlet drag data presented herein includes the results of both the force and pressure tests. Force data was obtained on all models, whereas pressure data was taken with the F-4 and Axisymmetric inlets only. The inlet drag data is presented for each configuration and comparisons between these are shown where appropriate. Selected surface pressure distribution data is also presented.



F-4 INLET COMPONENTS



TWO-DIMENSIONAL INLET COMPONENTS

FIGURE 1 - F-4 AND TWO-DIMENSIONAL INLET MODEL COMPONENTS

SECTION II

DESCRIPTION OF TEST EQUIPMENT

1. Drag Balance and Model Support

The drag balance and model support used in this test program was the same as that employed in the previous drag program (Phase I), which is described in detail in Reference 1.

A new balance calibration rig was designed and fabricated for this test series allowing axial calibrations through the zero load point with normal forces applied in any plane.

2. Inlet Models

One axisymmetric inlet model, five configurations of the F-4 inlet, forebody and splitter plates, and thirteen configurations of a basic two-dimensional inlet model are described in the following paragraphs. The F-4 models are exactly 7.5% scale. Since the other configurations fit the same balance and handle approximately the same mass flow they may also be considered as approximately 7.5% scale models.

a. Axisymmetric Inlet Model

The axisymmetric inlet model employed in these tests was configuration A10 used in the Phase I drag program. The geometry of configuration A10 is given below and illustrated in Figure 2.

Capture Area Ratio, $A_c/A_B = .620$

Cowl Angle, $\theta_c = 20^\circ$

Innerbody Half-Angle, $\theta_{IB} = 20^\circ$

Cowl Lip Radius, $R_{LIP} = 0.008"$

Inlet Design Mach Number, $M_D = 2.70$

Inlet Lip Area Ratio, $A_{LIP}/A_c = .620$

Additional surface pressure taps were added on the A10 model at the inlet lip station. Five (5) pressure taps were added to the cowl lip, and two (2) to the innerbody. These new pressure tap locations are shown in the following table:

Axisymmetric Inlet Additional Pressure Instrumentation

<u>Components</u>	<u>Axial Location</u>	<u>Measured From</u>
Cowl	0.00"	Cowl Lip Leading Edge
	0.024"	
	0.048"	
	0.072"	
	0.050" (Internal)	
	2.896"	
Innerbody	3.096"	Innerbody Tip

The original six (6) cowl and eight (8) innerbody pressure taps were also employed in these tests. Their locations are given in Reference 1.

b. F-4 Inlet Models

The F-4 inlet configuration was tested with and without the splitter plate used in Phase I and in the presence of the F-4B aircraft forebody. Figure 3 and 4 present typical inlet model assemblies. The second ramp angle was tested at two positions to represent appropriate values for the range of test Mach numbers. The first ramp angle was not variable. The configuration geometry is listed below and described in Figure 2.

Configura-tion	Leading Ramp Angle (δ_1)	Second Ramp Angle (δ_2)	A_{LIP}/A_c	A_{THROAT}/A_c	Forebody
F1s	10°	0°	0.649	0.609	Splitter Plate
F1f	10°	0°			F-4B Aircraft
Flo	10°	0°			None
F3s	10°	8°	0.541	0.487	Splitter Plate
F3f	10°	8°			F-4B Aircraft

To identify the models in the above table the notation incorporates the suffix (s), (f), and (o) to refer to the splitter plate, F-4B aircraft forebody, and no forebody, respectively.

Schematic drawings of the F-4 inlet with the splitter plate and with the F-4B forebody are presented in Figures 5 and 6. The mounting of the aircraft forebody did not involve any changes to the windshield or support hardware used in Phase I. The model geometry of the F-4 boundary layer diverter was incorporated.

Pressure instrumentation was employed on configuration F1 only and included cowl, ramp, forebody, and boundary layer diverter pressures. The instrumentation locations on the ramp and cowl are presented in Reference 1.

c. Two-Dimensional Inlet Models

The Two-Dimensional inlet models were fabricated using the existing Opposed-Ramp hardware from the Phase I tests. Simple modifications to the inlet were made to allow replacement of the ramp, cowl and sideplates. Thirteen Two-Dimensional inlet models were employed in the program to represent two basic inlet types. Eight (8) models were representative of single-ramp external compression inlets, and five were Opposed-Ramp inlets similar in design to that tested in Phase I. The inlet geometry for these thirteen configurations is given in the table below. A schematic of the Two-Dimensional inlet, with its nomenclature, is presented in Figure 2.

Two-Dimensional Inlet Geometry

<u>Configura-</u> <u>tion</u>	<u>Ramp Angle</u> <u>(θ_1)</u>	<u>Sideplate</u>	<u>Cowl</u> <u>(θ_c)</u>	<u>A_{LIP}/A_c</u>	<u>A_{THROAT}/A_c</u>
1	8°	#1 Full	None	.787	.710
2	8°	#2 Ported			
3	8°	#3 Partial			
4	8°	#4 Partial			
5	8°	#5 Partial			
6	8°	None			
8	8°	#1 Full	15°		
11	8°	#7 Partial	None		
12	8°	#8 Louvered			
16	17.75°	#1 Full	15°	.540	.502
17	17.75°	#1 Full	11°		
18	12°	#2A Ported (Plexiglas)	None	.696	.574

The inner cowl angle is fixed at 0° relative to the model centerline on all configurations. The capture area for all models is 5.312 in².

Figure 7 presents a drawing of the Two-Dimensional inlet model with pertinent dimensions, illustrating the ramp, cowl, and sideplate assembly, and Figure 8 presents a schematic of the sideplate shapes also with pertinent dimensions.

The Two-Dimensional models were included in the program to evaluate the transonic drag of inlets of the Opposed-Ramp type and to compare these data with the drag of inlets of more conventional designs. With the Opposed-Ramp inlet a large quantity of flow spills through the sideplate downstream of the cowl lip as opposed to spilling the flow over the cowl as in fully two-dimensional configurations. The drag associated with an alteration of the side spill mechanisms was evaluated using sideplates 2, 7, and 8 shown in Figure 8. These sideplates were variations on the Opposed-Ramp model illustrated as configuration 6 of Figure 8. With each of these designs, the inlet was configured to operate properly at Mach 2.0. In adapting these configurations to the available Opposed-Ramp model of Reference 1, a

slight internal contraction (7%) downstream of the throat station resulted. As mentioned, this contraction was low enough to allow starting at Mach numbers of 2.0 and above.

In order to produce some comparative data for configurations representative of simple two-dimensional inlets, additional sideplate configurations were fabricated (Sideplates 1, 3, 4, and 5). Of course, the configurations developed in this fashion cannot be operated over the same range of mass flow ratios, but do provide the required comparative data. This data also illustrates the effect of sideplate geometry on two-dimensional inlets which operate with similar Mach number conditions at the cowl lip station.

3. Drag Balance Modifications

Two problems were encountered with the drag balance during the Phase II - Part A tests.

- a. A zero shift (difference) developed in the zero readings taken before and after a run.
- b. Normal loads on the balance were found to affect the balance zero shift.

Inspection of the balance revealed that the metric portion had become loose and misaligned due to the failure of 4 of the 8 bearing supports. This resulted in an interference between the metric and non-metric elements and caused the zero load output of the load cell to be erratic.

The balance was refurbished by replacing the failed bearing supports, and by properly supporting and realigning the metric section.

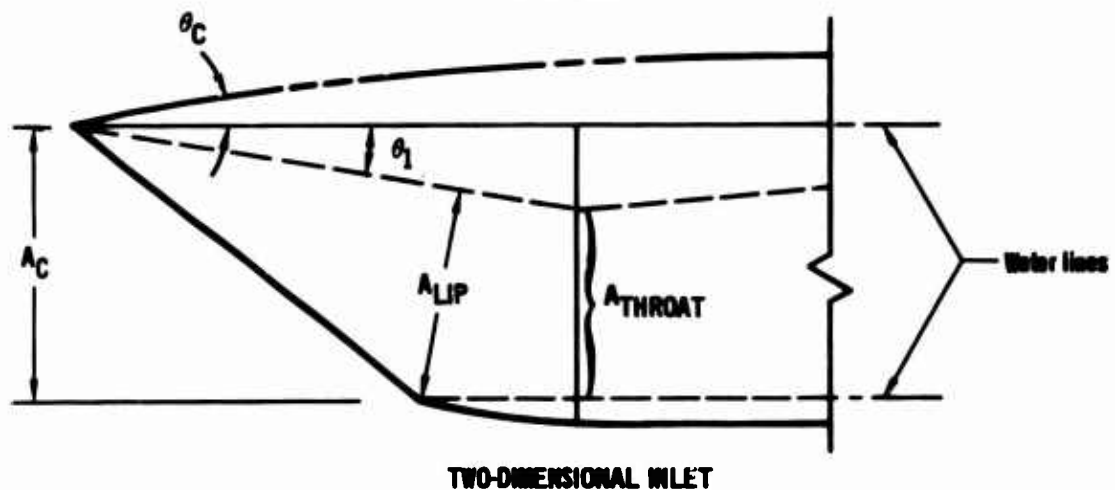
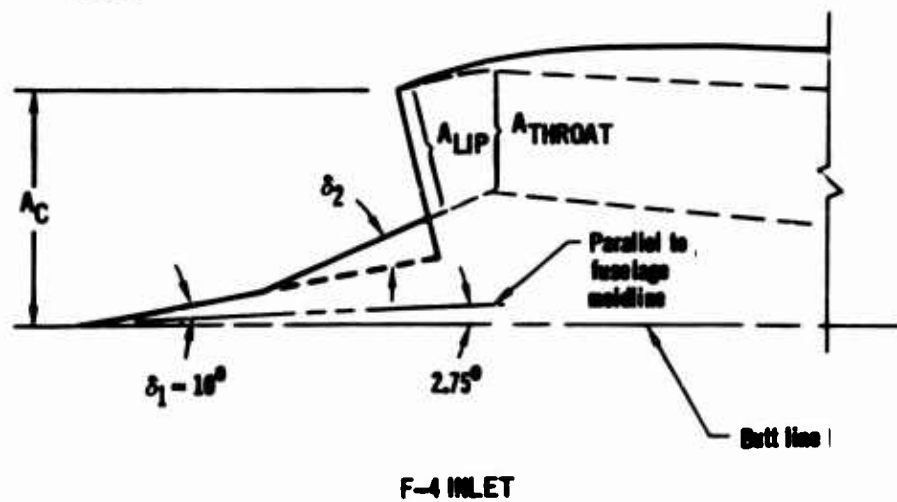
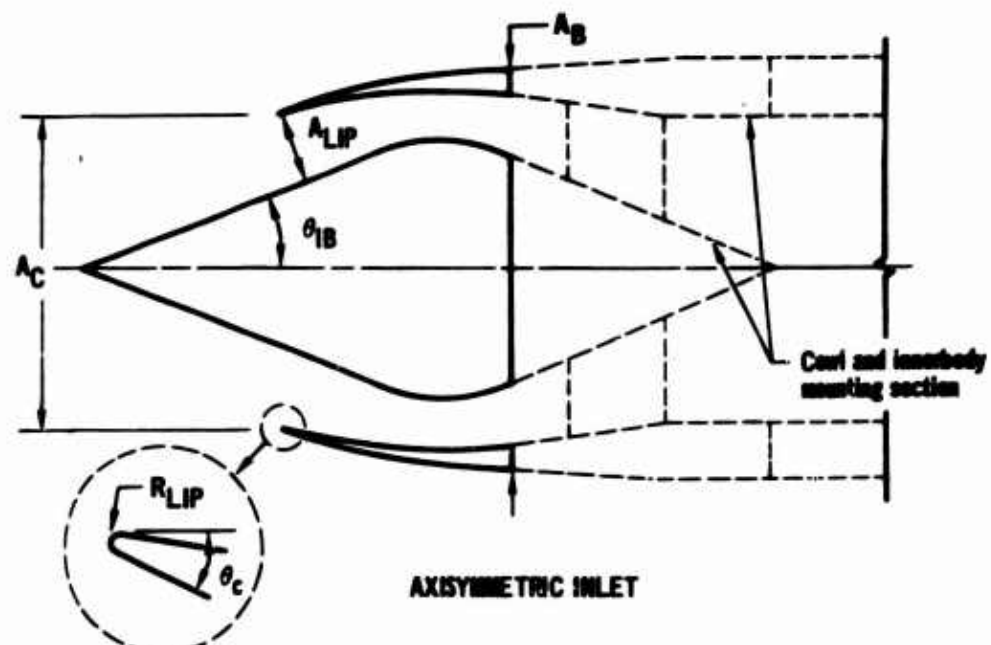
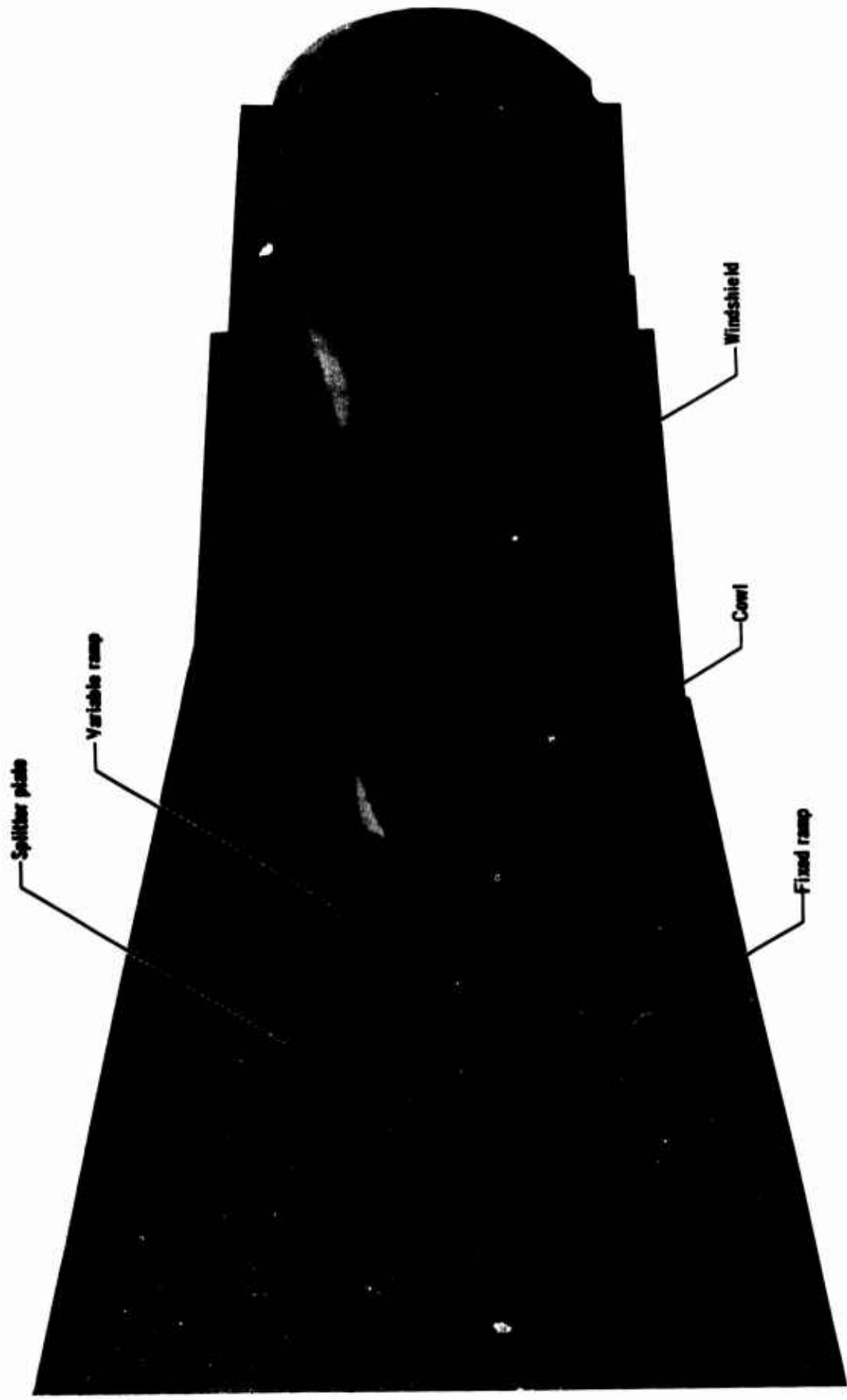


FIGURE 2 – AXISYMMETRIC, F-4, AND TWO-DIMENSIONAL INLET GEOMETRY



**FIGURE 3 - F-4 INLET MODEL
TYPICAL ASSEMBLY WITH SPLITTER PLATE**

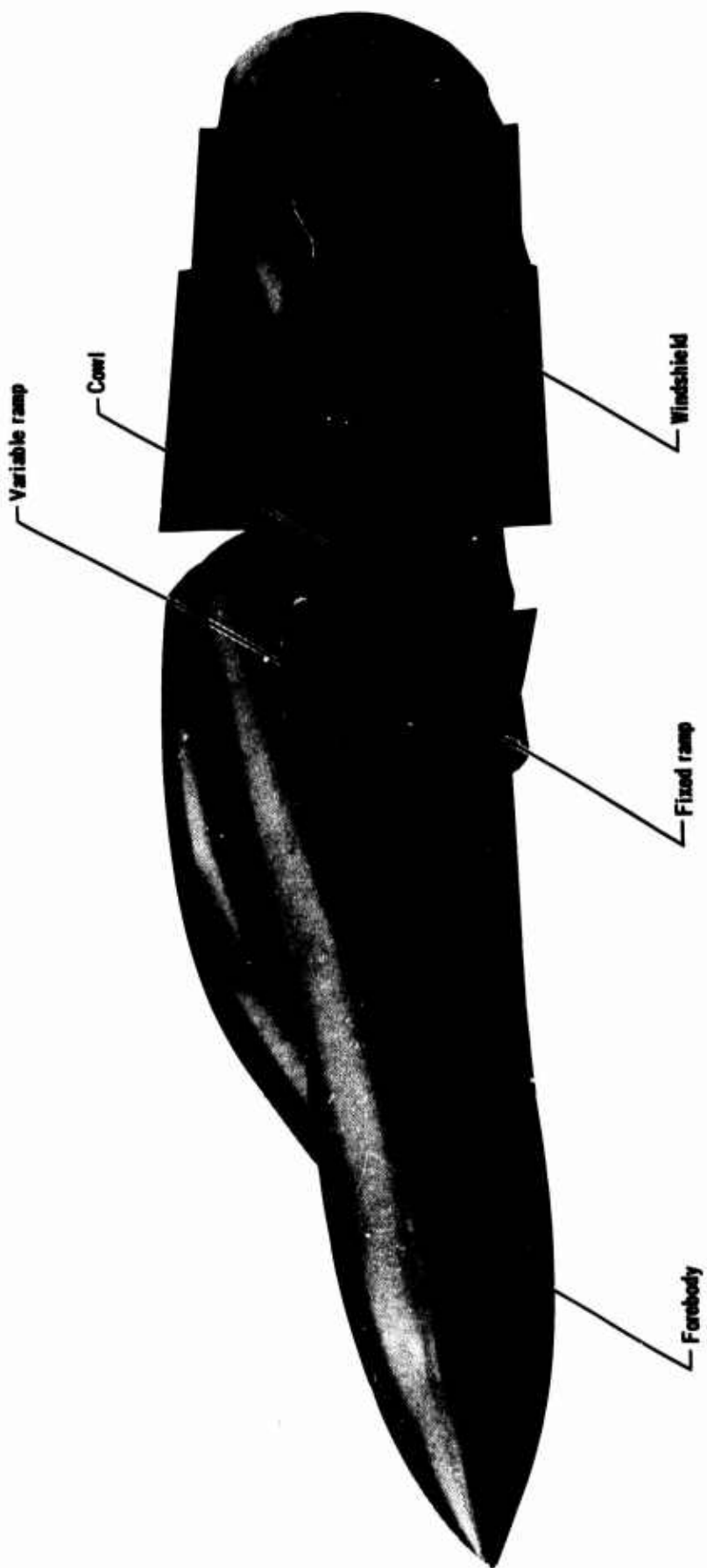


FIGURE 4 - F-4 INLET MODEL
TYPICAL ASSEMBLY WITH FOREBODY

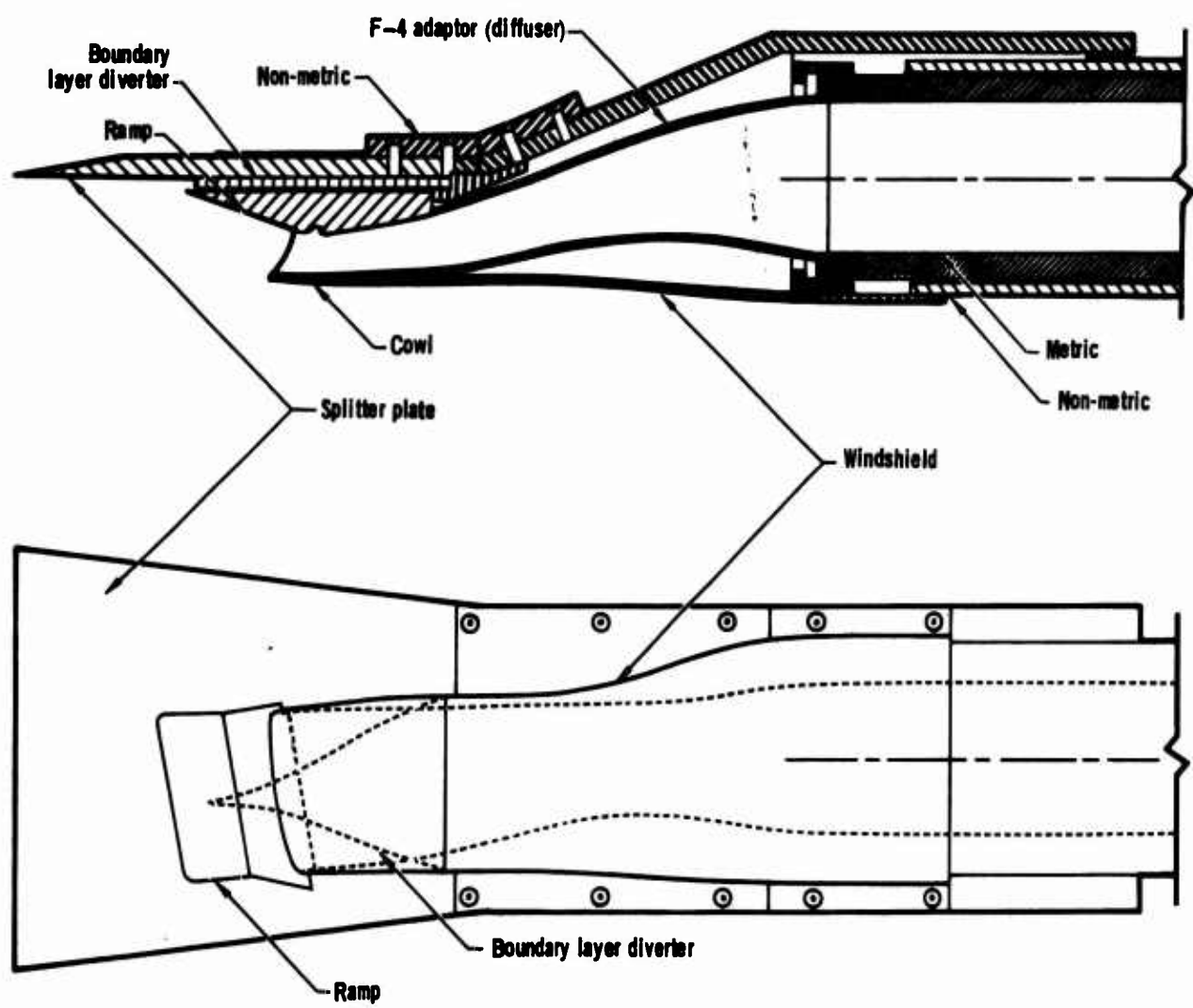


FIGURE 5 – F-4 INLET MODEL AND SPLITTER PLATE TEST ASSEMBLY

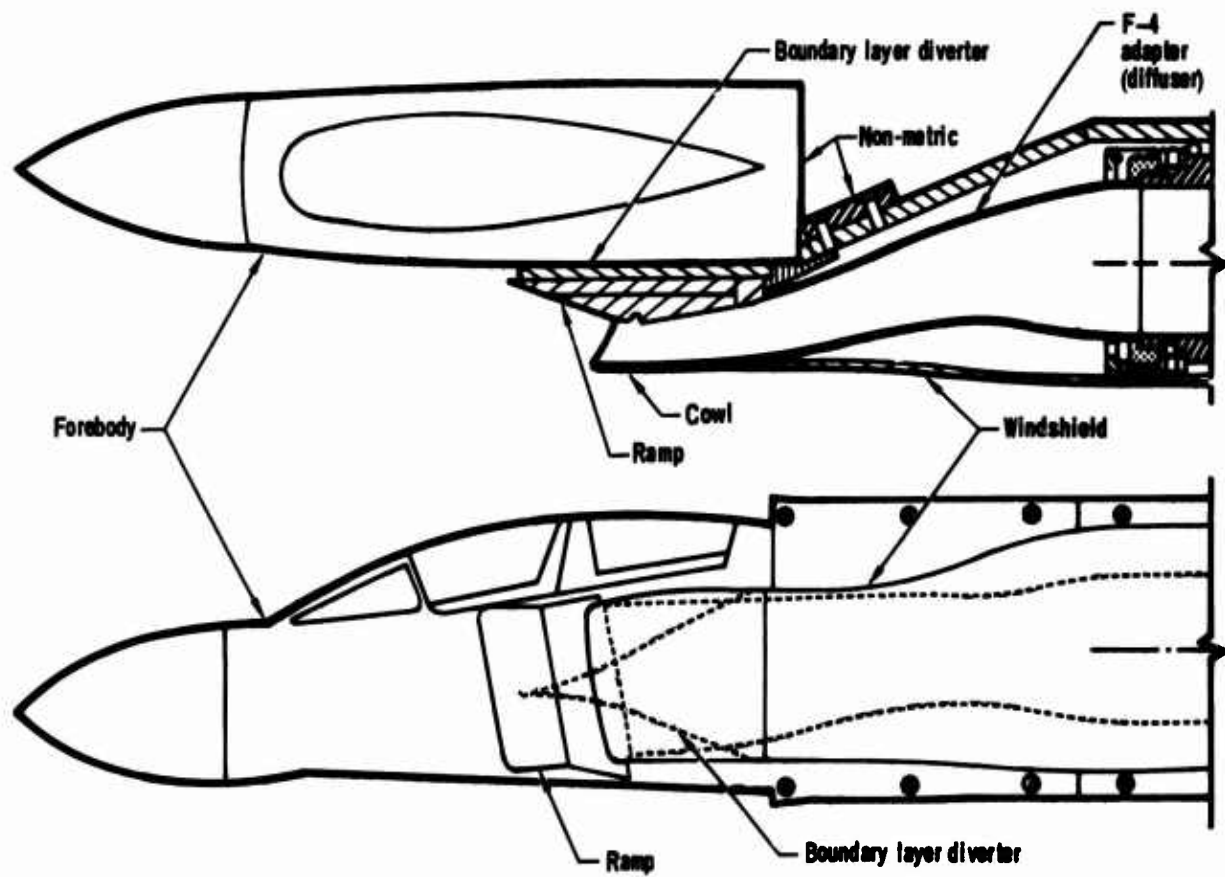


FIGURE 6 – F-4 INLET MODEL AND FOREBODY TEST ASSEMBLY

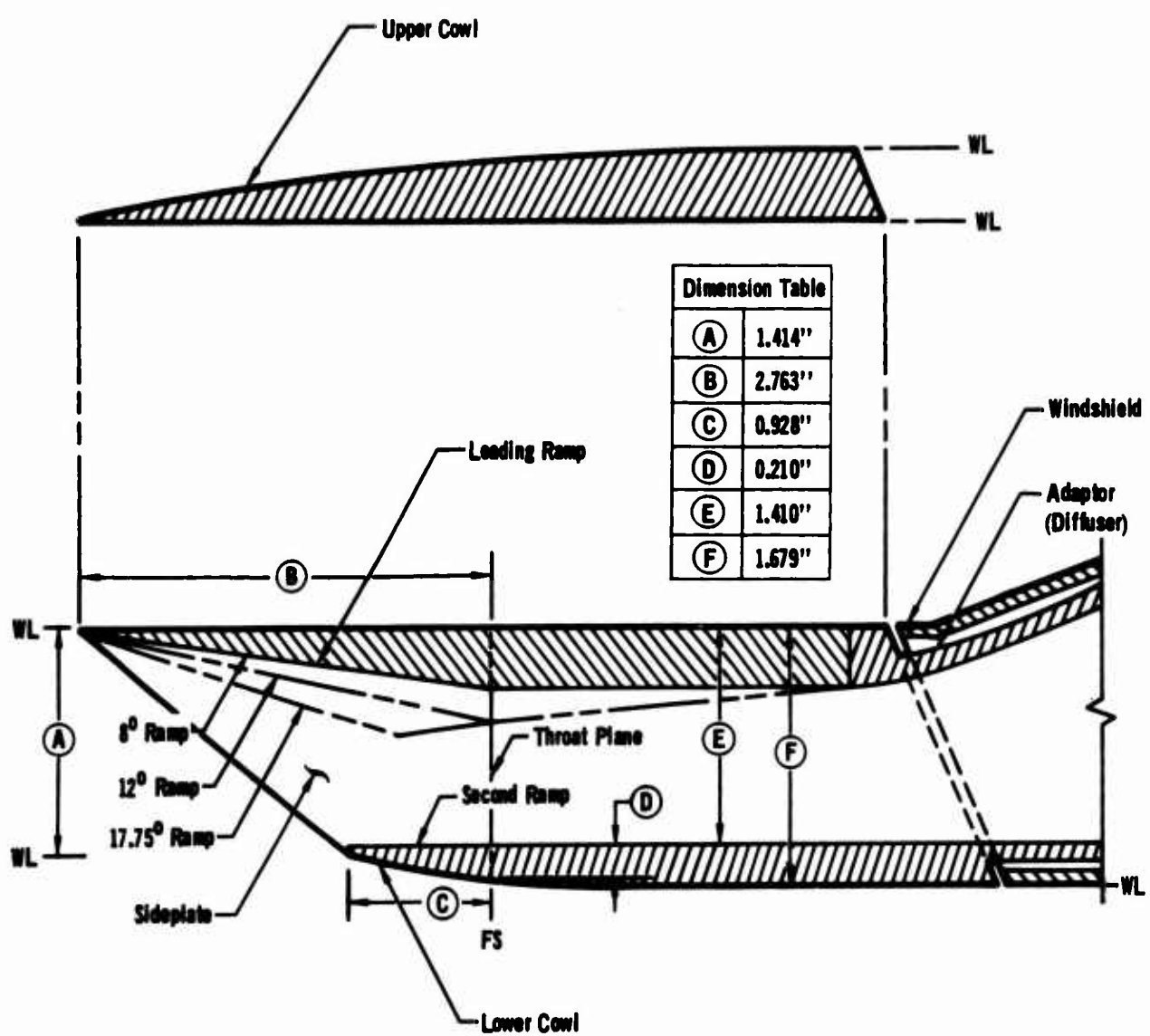


FIGURE 7 - TWO-DIMENSIONAL INLET MODEL TEST ASSEMBLIES AND GEOMETRY

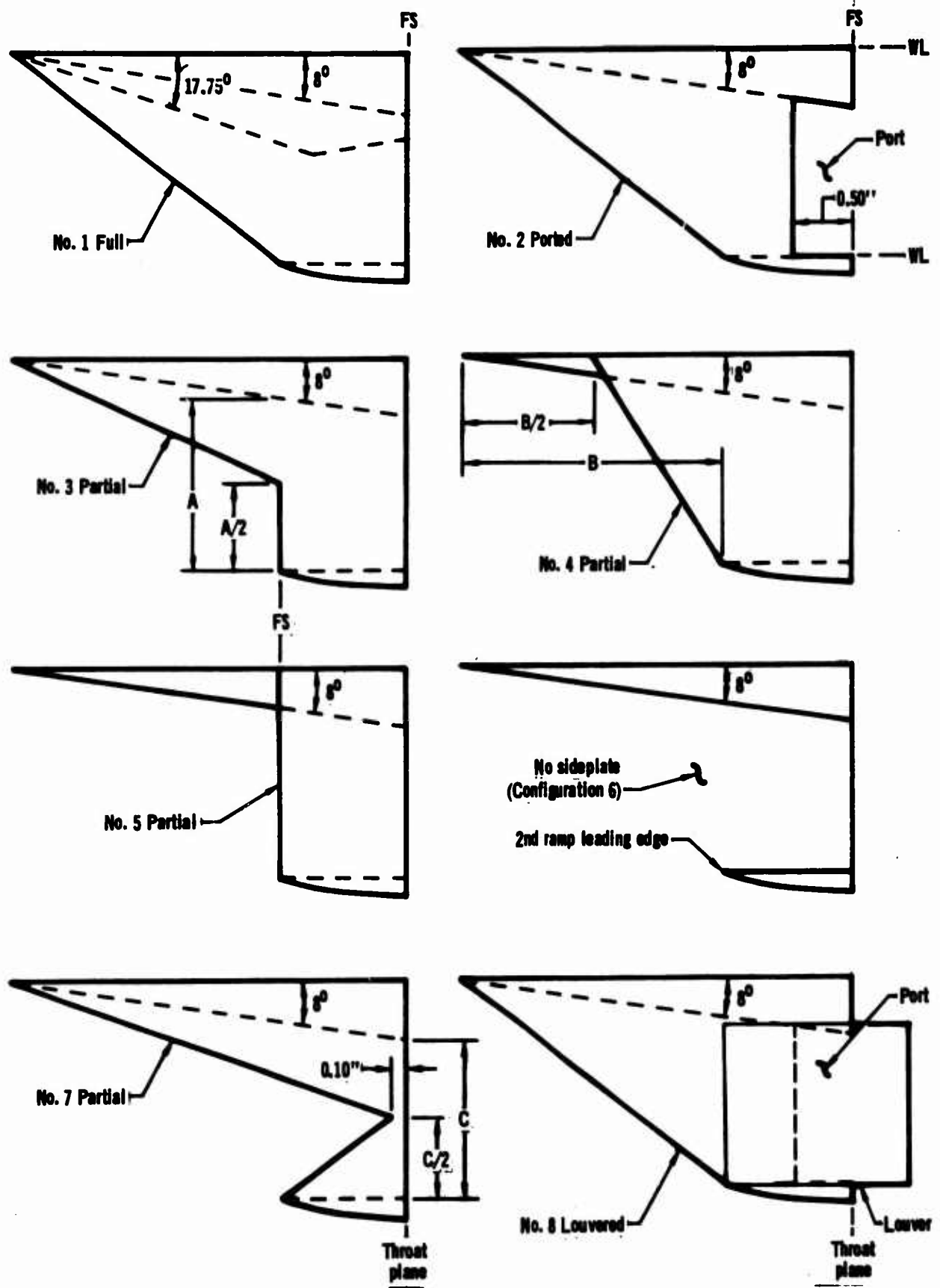


FIGURE 8 - TWO-DIMENSIONAL INLET MODEL SIDEPLATE CONFIGURATIONS

SECTION III

TEST PROGRAM AND TEST TECHNIQUES

1. Test Summary

The test program was conducted at the NASA-Ames Research Center in the 6 x 6 ft. continuous flow supersonic wind tunnel. The Phase II - Part A series was accomplished in October 1968 and the Part B series in June 1969.

In Part A, a total of 79 force and pressure runs were performed on 6 inlet configurations; 5 F-4 models and 1 Axisymmetric model. Four of the F-4 models were tested at several angles of attack. Table I presents a test summary of the Phase II - Part A test program, and Appendix A describes the complete run summary.

In the Part B test series, a total of 59 runs were performed on 15 inlet configurations; 2 F-4 models and 13 Two-Dimensional models. All runs in this series were force runs. Three of the two-dimensional models were run at angle of attack conditions. Table II presents a test summary of the Phase II - Part B test program, and Appendix A describes the complete run summary.

2. Test Procedures

The drag balance was calibrated extensively before each of the two test series. With the balance installed in the wind tunnel, axial loadings ranging from 0 to 50 lbs were applied in both the thrust and drag directions. The effects of side and vertical loads of up to 50 lbs on the axial force measurements were also examined. Post-test balance calibrations were also performed.

During the tests of Phase II - Part A, the balance was oriented to position the splitter plate on the F-4 inlet model in the vertical plane. In the later tests, Phase II - Part B, the balance was rolled 90° to

TABLE I
TEST SUMMARY

PHASE II - PART A

Configuration	Mach Number - M_∞					α			Type Test	
	0.70	0.80	0.90	1.05	2.0	0°	6°	12°	Pres.	Force
F1s	x		x	x ¹		x		x	x	x
F1f	x	x ²	x	x		x	x	x	x	x
Flo	x		x			x			x	x
F3s	x		x		x	x	x			x
F3f	x		x		x	x	x			x
A10	x		x	x	x	x			x	x

(1) $\theta \alpha = 12^\circ$ only

(2) Pressure Run $\theta \alpha = 0^\circ$ only.

TABLE II
TEST SUMMARY

PHASE II - PART B

Configuration	Mach Number - M_∞				α		Type Test	
	0.70	0.90	1.8	2.0	0°	6°	Pres.	Force
F3s	x	x ¹		x ¹	x		x	
F3f	x	x		x	x		x	
1	x	x			x	x	x	
1s	x	x			x		x	
2	x	x	x ²	x ³	x	x	x	
3	x	x			x		x	
4	x	x			x		x	
5	x	x			x		x	
6	x	x	x	x	x		x	
8	x	x			x		x	
11	x	x	x	x	x		x	
12	x	x	x	x	x		x	
16				x	x		x	
17				x	x		x	
18				x ⁴	x	x	x	

(1) Also ran $\theta \psi = +2^\circ$ (yaw)(2) $\theta \alpha = 0^\circ$ only(3) Also ran $\theta \alpha = 10^\circ, 14^\circ, 16^\circ$ (4) Also ran $\theta \alpha = 3^\circ, 10^\circ, 12^\circ$

position the splitter plate horizontally. This was to allow evaluation of the effects of angle of attack in that plane and to insure that all side loads (weight and aerodynamic forces) were in the same plane.

Pre-test and post-test balance zero readings were recorded for each series of runs on a given configuration. The pre-test zero reading was used in the data reduction, and the post-test zero return was used to evaluate the accuracy and validity of the drag measurements for each inlet configuration tested. When the balance failed to return to its initial zero reading within certain established limits (.5 lbs), the runs were repeated.

Repeatability checks were performed throughout the test programs. Certain mass flow ratios were repeated during a given run, and selected runs were also repeated.

Tests of each inlet configuration were accomplished at a given Mach number and angle of attack while varying the mass flow rate with the remotely operated flow control plug. Data were obtained at six (6) different mass flow ratios during each run, including at least two (2) at the maximum flow rate.

The flow field was monitored with the Schlieren system throughout the test program, and photos were taken at conditions where significant flow field changes were observed.

The adaptor cavity on all two-dimensional models was sealed to prevent airflow circulation within the metric cavity. This cavity was vented to the local ambient pressure downstream of the model in order to minimize the force on the adapter. Slack diaphragm gages were used for the more sensitive pressure measurements. Reference pressures for the scanivalve transducers, used to record all remaining pressures, were carefully selected to permit use of low range transducers.

It should be understood that the pressure recovery information available

from this test data is not representative of the particular inlet configurations tested since no attempt was made to incorporate bleeds or efficient subsonic diffusers.

3. Accuracy and Repeatability of the Test Data

When comparing the results of the F-4 tests of this program with the test results of Reference (1), a difference in the data shows up as a consistent increment in the total inlet drag which is essentially independent of Mach number and mass flow conditions. This increment, in terms of the inlet drag coefficient (C_I), was approximately .06 at both subsonic and supersonic conditions. It must be noted that the drag increments between various F-4 configurations, and the drag slopes of each, were consistent with those measured in the Phase I program.

The axisymmetric (A10) data comparison between the first and the second test series was in near perfect agreement at all test Mach numbers.

It was concluded that the weight, large adapter area and asymmetrical balance loadings of the two-dimensional inlets result in a larger tolerance on absolute drag than indicated by Reference (1). The above increments in drag coefficient for the repeated tests of the F-4 models can be viewed as a tolerance on the accuracy of the absolute drag measurement of all two-dimensional models tested in Phase I and Phase II - Part A. However, it should be recognized that the drag variation with mass flow ratio, and drag comparisons within a particular test program are quite accurate as indicated by the data of repeated runs.

The pressure determined additive drags, and also the cowl pressure distributions, obtained in Phases I and II for the F-4 inlets agreed very closely at all test Mach numbers. This was also true for the axisymmetric A10 inlet.

The data obtained by repeating a mass flow setting during a single run

provides a measure of the accuracy of the slope of the drag versus mass flow curves. The standard deviations of the drag coefficient for these repeated data points are .005 for the A10 inlet, .006 for the F-4 inlet models, and .030 for the Two-Dimensional inlet models.

The balance zero readings taken before and after each series of runs on a particular inlet configuration indicate the tolerance on drag coefficient for each class of configurations. The standard deviation indicated by these readings was .04 lbs for the A10 model, .34 lbs for the F-4 models, and .31 lbs for the Two-Dimensional models. The following table presents the standard deviation applicable to the drag coefficient of the three types of inlet configurations.

Standard Deviation in Inlet Drag Coefficient

<u>M₀</u>	<u>Axisymmetric (A10) Inlet</u>	<u>F-4 Inlet</u>	<u>Two-Dimensional Inlet</u>
.7	.001	.016	.018
.9	.001	.012	.011
2.0	.001	.018	.016

The two-dimensional models were mounted so that their weight applied a larger moment on the balance bearings than the axisymmetric models. This loading and the additional load due to the normal force on the two-dimensional model were the apparent reasons for the mechanical difficulties experienced with the balance and are the apparent cause of the lower accuracy obtained with these models.

The test results of repeated runs support the data in the above table. The maximum difference in drag coefficient obtained in these runs is .02 for the F-4 models.

SECTION IV

TEST RESULTS

1. F-4 Inlet Drag Data

All of the F-4 inlet drag data obtained in the Phase II - Part A test program is presented in Appendix B. This includes the inlet drag determined from force measurements, and the additive and ramp drags determined from surface pressure measurements. The drag data is presented as a function of mass flow ratio for the various test Mach numbers and angles of attack. Figures B.1 through B.8 present the inlet drag data for the F-4 inlet model with the F-4B aircraft forebody, with no forebody, and with the splitter plate attached. The splitter plate configuration data presented in the Appendix is additional data which had not been obtained in the Phase I tests. Figures B.9 through B.18 present the additive and ramp drag data for the F-4 pressure models for these same configurations. The additive drags were calculated from the pressure integrated ramp drag, and by assuming one-dimensional flow and 100% total pressure recovery at the inlet lip station.

The comparisons of the drag data presented in the Appendix illustrating the forebody effects on F-4 inlet drag and additive drags are presented in Figures 9 through 24 in the text. In all cases the inlet alone (no forebody) tests showed the highest drag.

The reduction in drag which occurred when the splitter plate or the aircraft forebody was installed was expected. The splitter plate reduces spill across the leading edge of the first ramp insuring that all spill takes place in a region where the deflected stream can produce a reduced cowl force. With the F-4B forebody, the drag reduction is most likely due to the reduced flow angularity at the inlet plane. The drag levels are

different between isolated and integrated configurations, but the drag variation with mass flow (drag slope) is the same.

The $(A_o/A_c)_{\max}$ indicated on all F-4 drag data presentations is based upon the inlet throat geometry presented in Section II assuming 100% pressure recovery at the inlet throat plane.

2. Axisymmetric Inlet Drag Data

The axisymmetric single cone inlet, additive, and cowl drag data, at Mach numbers of .7, .9, 1.05, and 2.0 are presented in Figures 25, 26, and 27. Excellent agreement with the Phase I (Reference 1) data was obtained in both the force and pressure tests. The inlet drag data was obtained by force measurement, the cowl drag was obtained from surface pressure integrations, and the additive drag was determined by subtracting the pressure determined cowl drag from the force determined inlet drag. It was felt that the pressure determined cowl drags were more accurate than the pressure determined additive drags, especially at supersonic Mach numbers.

As was the case with the F-4 inlets, the $(A_o/A_c)_{\max}$ shown on the curves for the subsonic Mach numbers is based upon the inlet throat geometry presented in Section II, assuming 100% pressure recovery at the inlet lip plane. The supersonic $(A_o/A_c)_{\max}$ (at $M_o = 2.0$) is also the theoretical value, as determined from the information presented in Reference 2.

The A10 inlet was included in the Phase II test program to determine the cowl drag by integration of surface pressure data using improved instrumentation, and to establish repeatability with the Phase I data. The additional pressure instrumentation is described in Section II. The use of this additional instrumentation did not improve the determination of the total inlet drag relative to that measured in Phase I. The effects of this added cowl lip and innerbody pressure instrumentation on the calculation of the total inlet drag was minor. The table below presents a summary of the pressure integrated cowl drag computed using the instrumentation of

Reference 1 (6 pressure taps), and the improved instrumentation (10 pressure taps).

Comparison of Cowl Drag Coefficients
Determined from Pressure Data

<u>M_o</u>	<u>A_o/A_c</u>	<u>10 Tap Data</u>	<u>6 Tap Data</u>
0.90	0.266	-0.4133	-0.4192
	0.488	-0.1628	-0.1609
	0.607	-0.0640	-0.0790
2.0	0.808	0.1774	0.1620

Based upon this comparison it appears that the increment between the pressure and force data of Reference 1 was due to the assumed flow angularity at the inlet lip used to evaluate the additive drag. The difference in pressure and force determined total inlet drag coefficients was approximately 0.05 in the Phase I tests.

The cowl and innerbody pressure distributions measured with the improved instrumentation are presented in Appendix C in Figures C.1 through C.8 for the full range of test conditions.

Figures 28 and 29 present comparisons between experimental cowl and innerbody pressures with theoretical estimates obtained using References 3 and 4.

3. Two-Dimensional Inlet Drag Data

The Two-Dimensional inlet drag data obtained in the Phase II - Part B test program is presented in Figures D.1 through D.12 in Appendix D. Since pressure runs were not performed with these models, only total inlet drag (cowl plus additive) is illustrated. The data is presented as a function of mass flow ratio for each configuration at the respective test Mach numbers.

Comparisons of the inlet drag data illustrating the effects of side-plate geometry, cowl geometry, and splitter plate are presented in Figures 30 through 37. Figures 30 and 31 present the effects of sideplate geometry on the single-ramp external compression inlets which spill flow forward of the cowl lip (Configurations 1, 3, 4, and 5). Figures 32 and 33 present the drag data showing the effect of spilling flow through sideplates downstream of the cowl. For clarity, only the curves faired through the test data are shown. The minor variations in subsonic drag level and slope illustrated by this data lie within the tolerance on data accuracy. Only the louvered configuration (config. 12) exhibited a drag characteristic distinctly different from the other configurations. The drag for the louvered model was higher at the maximum mass flow ratio, but did not increase with decreased mass flow ratio as rapidly as the other configurations. It would be anticipated that the external louver drag would increase inlet drag at low values of spill, and that the louver would increase the axial component of momentum of the spilled flow.

Figures 34 and 35 illustrate the drag effect of a cowl attached to the outer surface of the first ramp, shown schematically in Figure 7. Although the presence of this cowl did not affect the drag slope, it did cause a reduction in drag. Apparently, there is sufficient spill around the ramp leading edge to induce a reduced pressure on the upper cowl.

Figures 36 and 37 demonstrate the effect of the splitter plate on inlet drag at subsonic conditions. As would be expected the effect is the same as was noted for the F-4 configurations discussed previously.

The $(A_o/A_c)_{max}$ shown on all Two-Dimensional inlet drag data presentations is based upon the inlet throat area assuming 100% pressure recovery at the inlet throat plane. The " A_o/A_c Test Limit" shown on all figures is the

theoretical maximum airflow actually obtainable with these Two-Dimensional inlet models due to the constriction in the subsonic diffuser portion of the models, described previously in Section II.

A limited number of supersonic tests were planned to measure the drag of the configurations which could capture the full airflow. However, the lack of boundary layer bleed on these models apparently restricted their operation and no data was obtained where the inlets operated at their maximum theoretical capture. As a result, the data is not summarized in the Appendix.

Comparisons of the slope of the curves of drag versus mass flow ratio presented in the following table shows the effect of the sideplate geometry on the "subcritical" drag.

Drag Slope Comparison

$$M_\infty = 2.0 \quad \alpha = 0^\circ$$

<u>Configuration</u>	<u>$\Delta C_D / \Delta (A_\infty / A_c)$</u>	<u>Sideplate</u>	<u>Geometry</u>
2	-1.40	#2 Ported	
6	-1.20	None	
11	-1.45	#7 Partial	
12	-0.62	#8 Louvered	
16	-1.70	#1 Full	
17	-1.70	#1 Full	
F-4	-1.50	None	

The F-4 drag slope is presented for comparison. All configurations except the louvered sideplate exhibit nearly the same characteristics.

F-4 7.5% Model
 Ramp Configuration (10° - 0°)
 $M_\infty = 0.7$
 $\alpha = 0^\circ$

Inlet Drag Coefficient - C_I

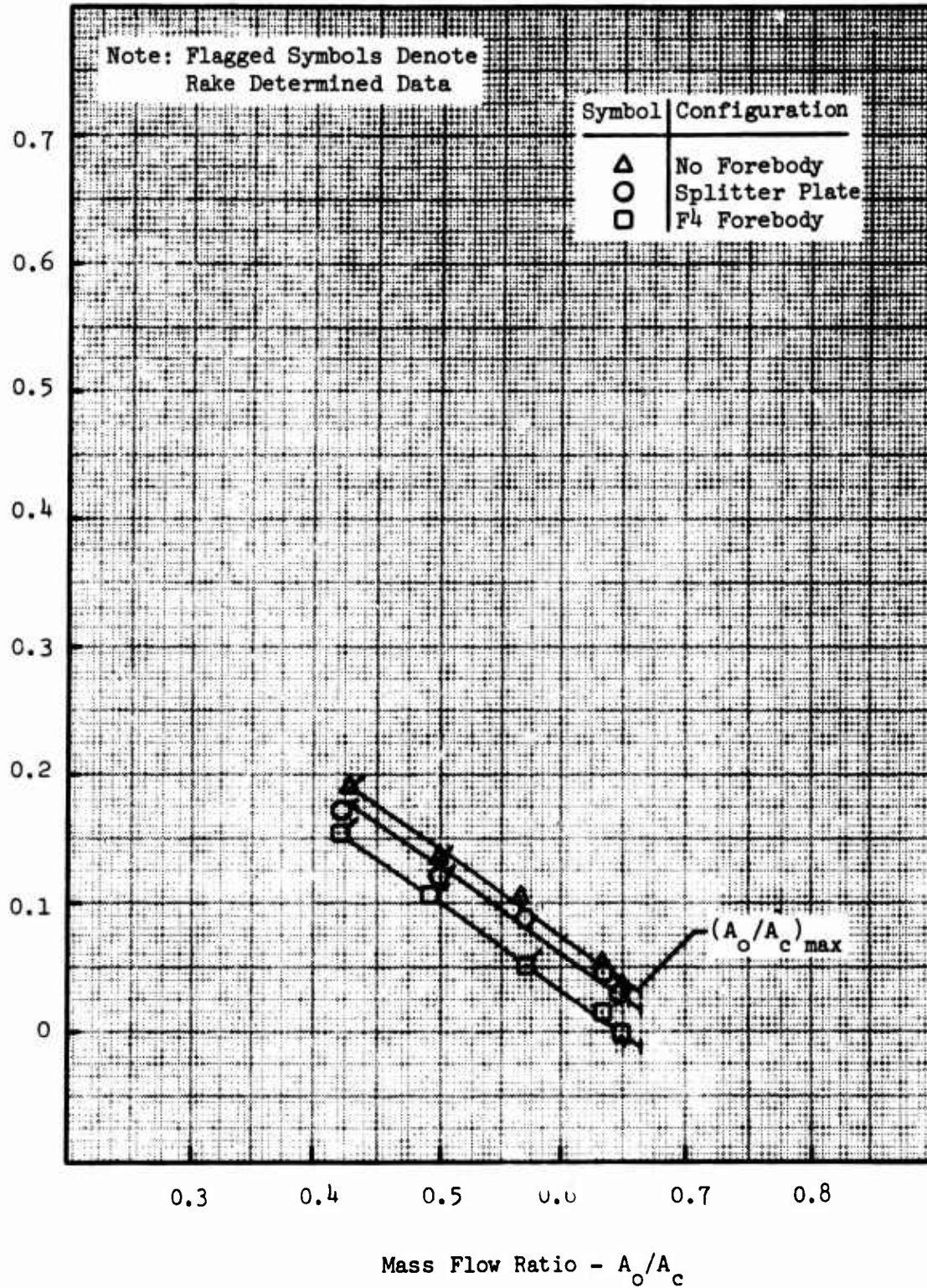


FIGURE 9 - FOREBODY EFFECTS ON THE F-4 INLET DRAG

F-4 7.5% Model
 Ramp Configuration (10° - 0°)
 $M_\infty = 0.9$
 $\alpha = 0^\circ$

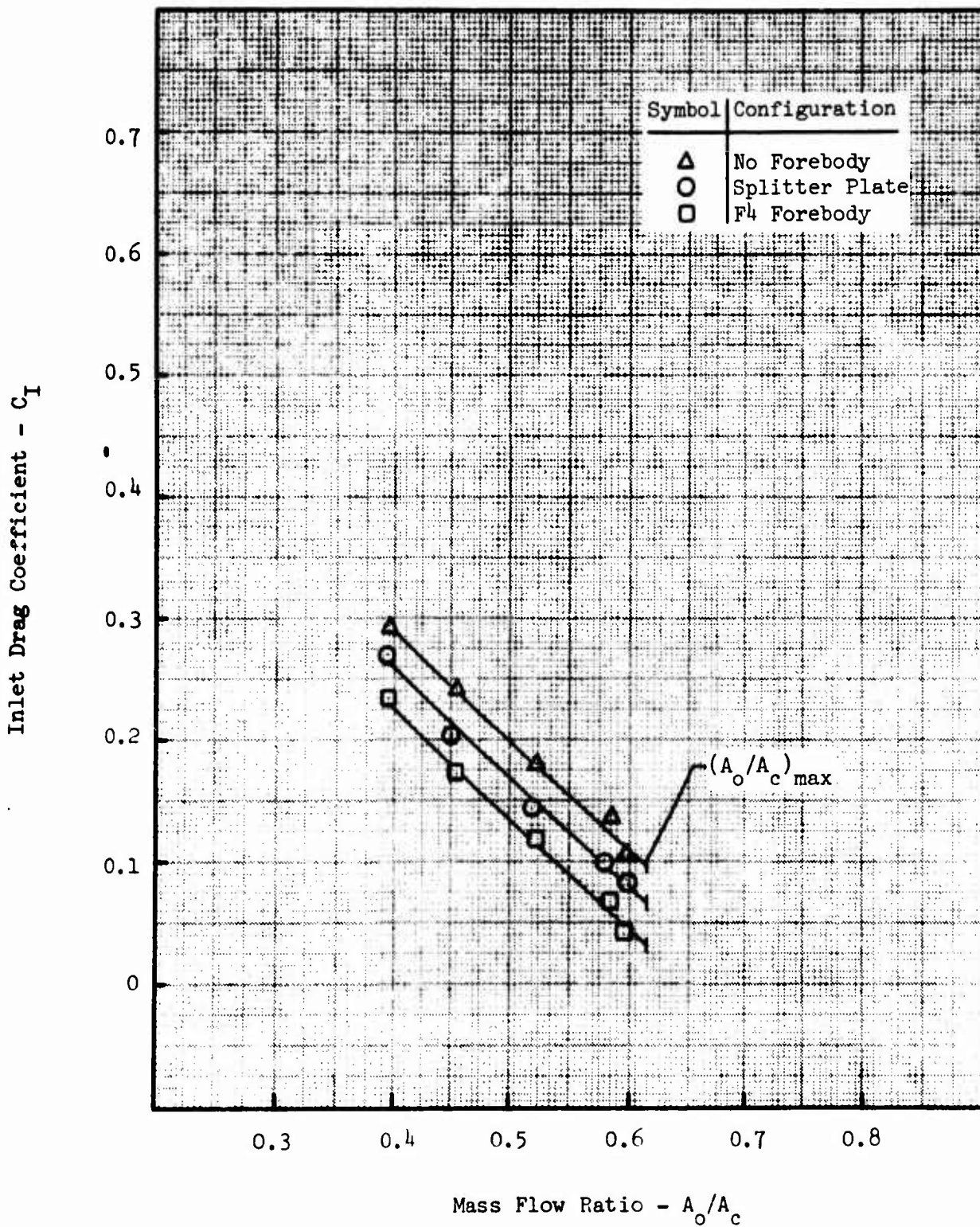


FIGURE 10 - FOREBODY EFFECTS ON THE F-4 INLET DRAG

F-4 7.5% Model
 Ramp Configuration (10° - 8°)
 $M_\infty = 0.70$
 $\alpha = 0^\circ$

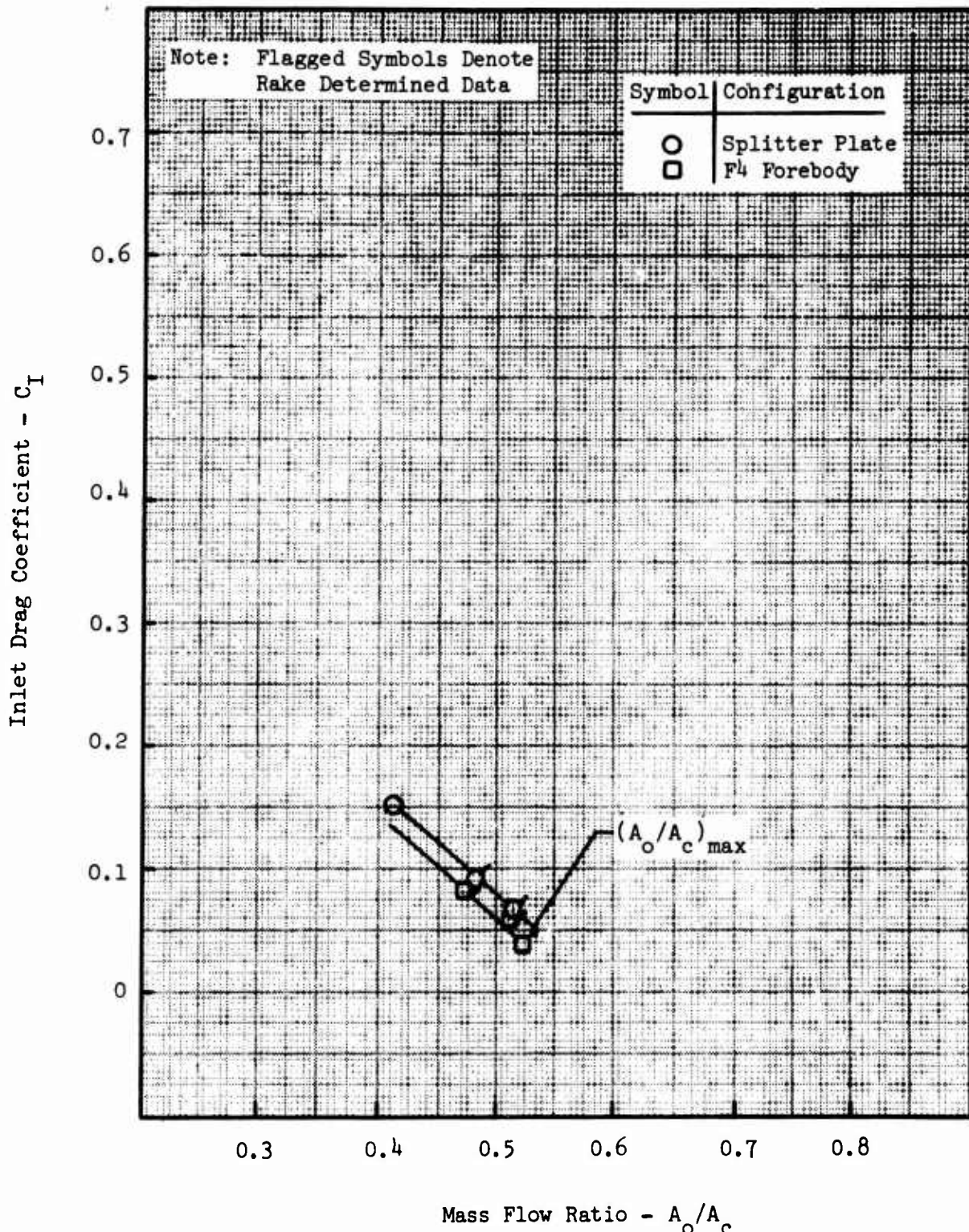


FIGURE 11 - FOREBODY EFFECTS ON THE F-4 INLET DRAG

F-4 7.5% Model
 Ramp Configuration (10° - 8°)
 $M_\infty = 0.90$
 $\alpha = 0^\circ$

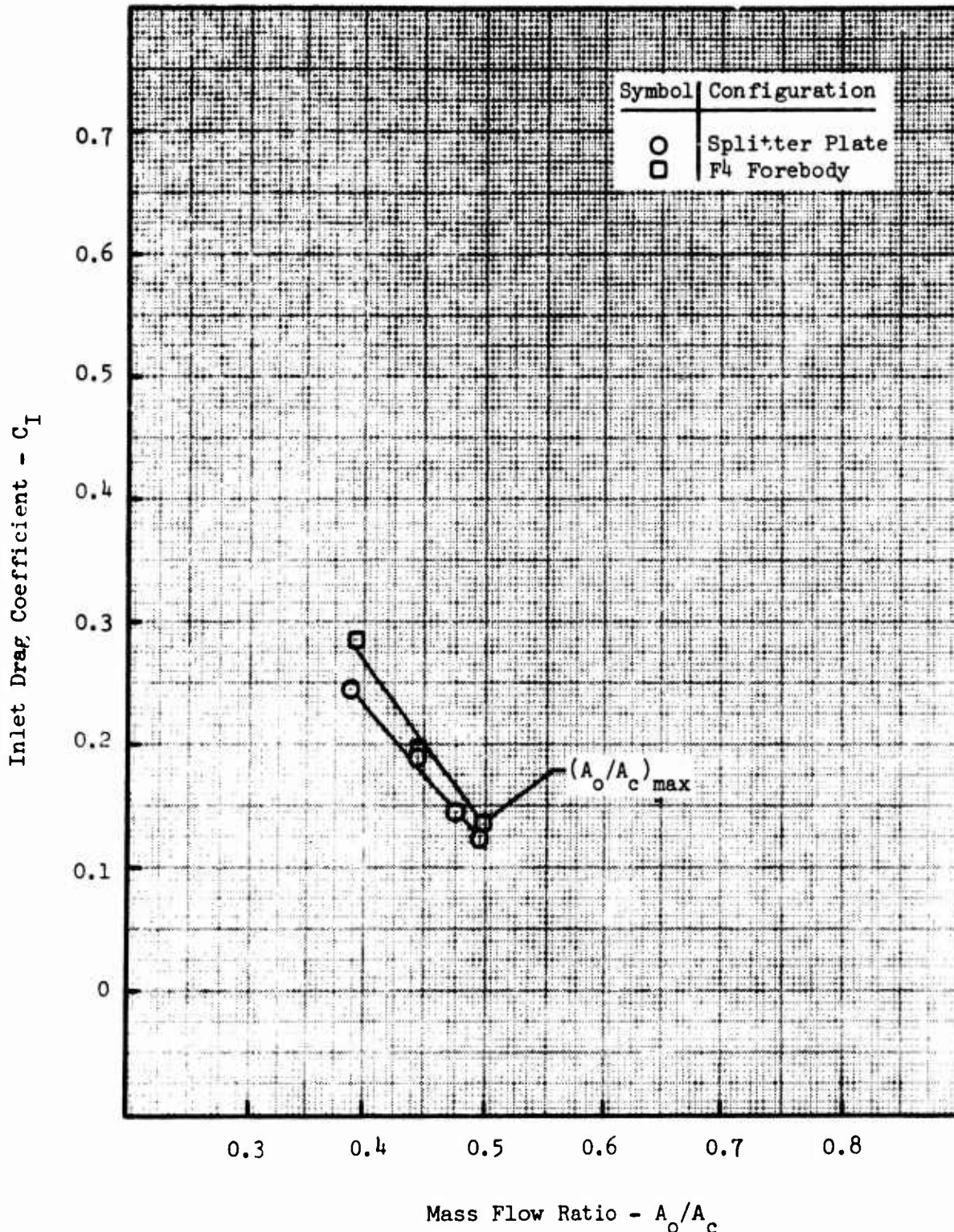


FIGURE 12 - FOREBODY EFFECTS ON THE F-4 INLET DRAG

F-4 7.5% Model
 Ramp Configuration (10°-8°)
 $M_\infty = 2.0$
 $\alpha = 0^\circ$

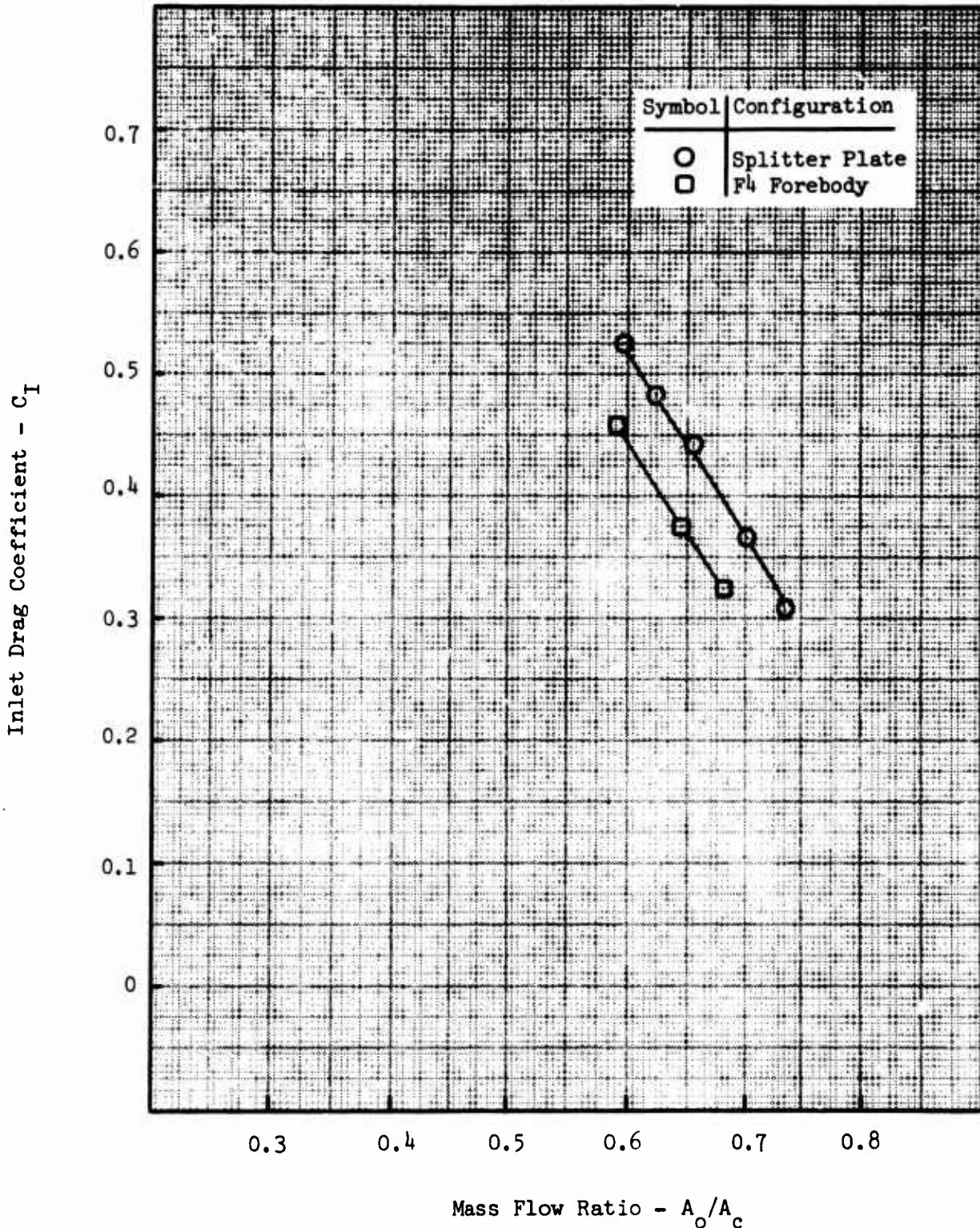


FIGURE 13 - FOREBODY EFFECTS ON THE F-4 INLET DRAG

F-4 7.5% Model
 Ramp Configuration (10° - 8°)
 $M_\infty = 0.70$
 $\alpha = 6^\circ$

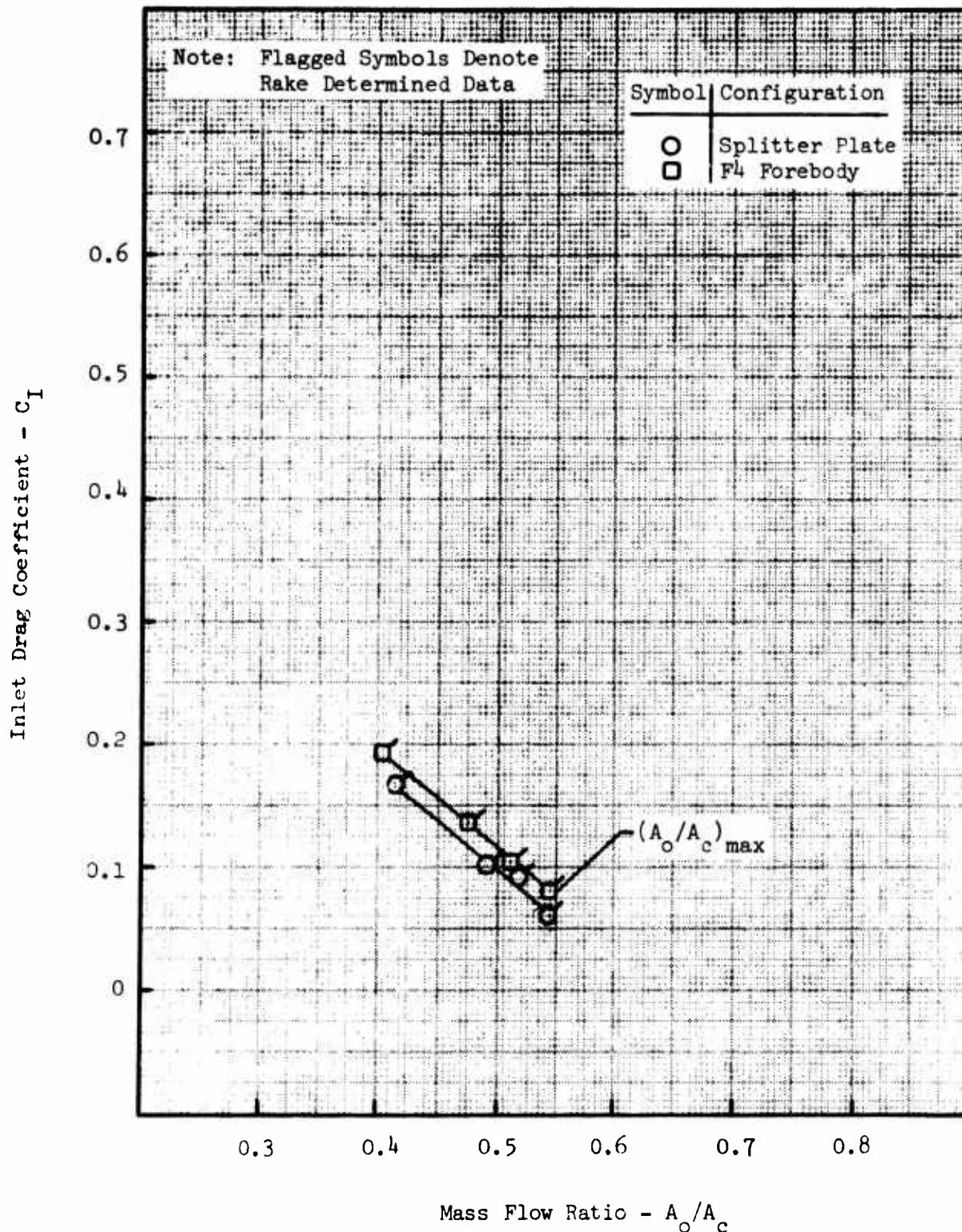


FIGURE 14 - FOREBODY EFFECTS ON THE F-4 INLET DRAG

F-4 7.5% Model
 Ramp Configuration (10° - 8°)
 $M_\infty = 0.90$
 $\alpha = 6^\circ$

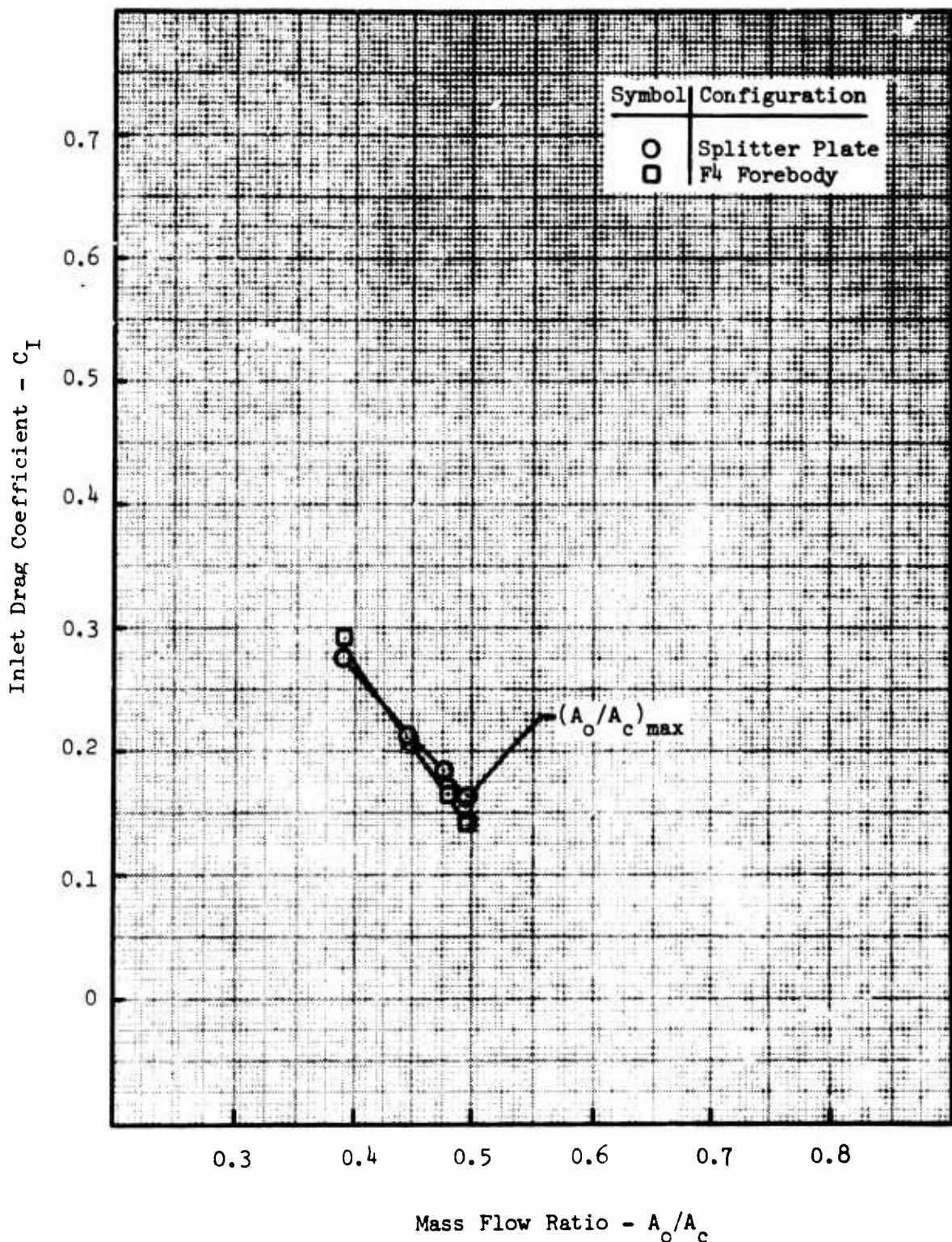


FIGURE 15 - FOREBODY EFFECTS ON THE F-4 INLET DRAG

F-4 7.5% Model
Ramp Configuration (10° - 8°)
 $M_\infty = 2.0$
 $\alpha = 6^\circ$

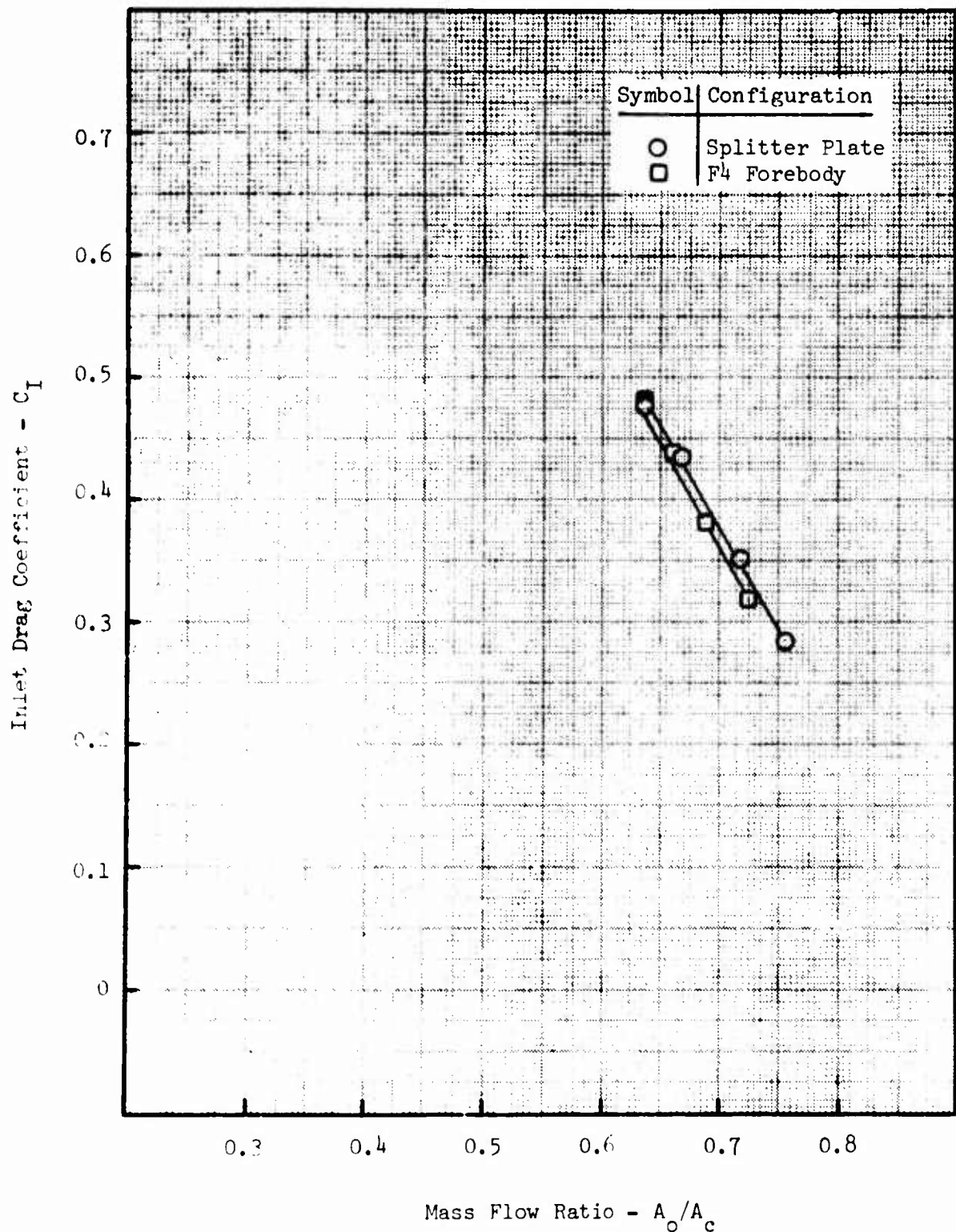


FIGURE 16 - FOREBODY EFFECTS ON THE F-4 INLET DRAG

F-4 7.5% Model
 Ramp Configuration (10°-0°)
 $M_\infty = 0.70$
 $\alpha = 12^\circ$

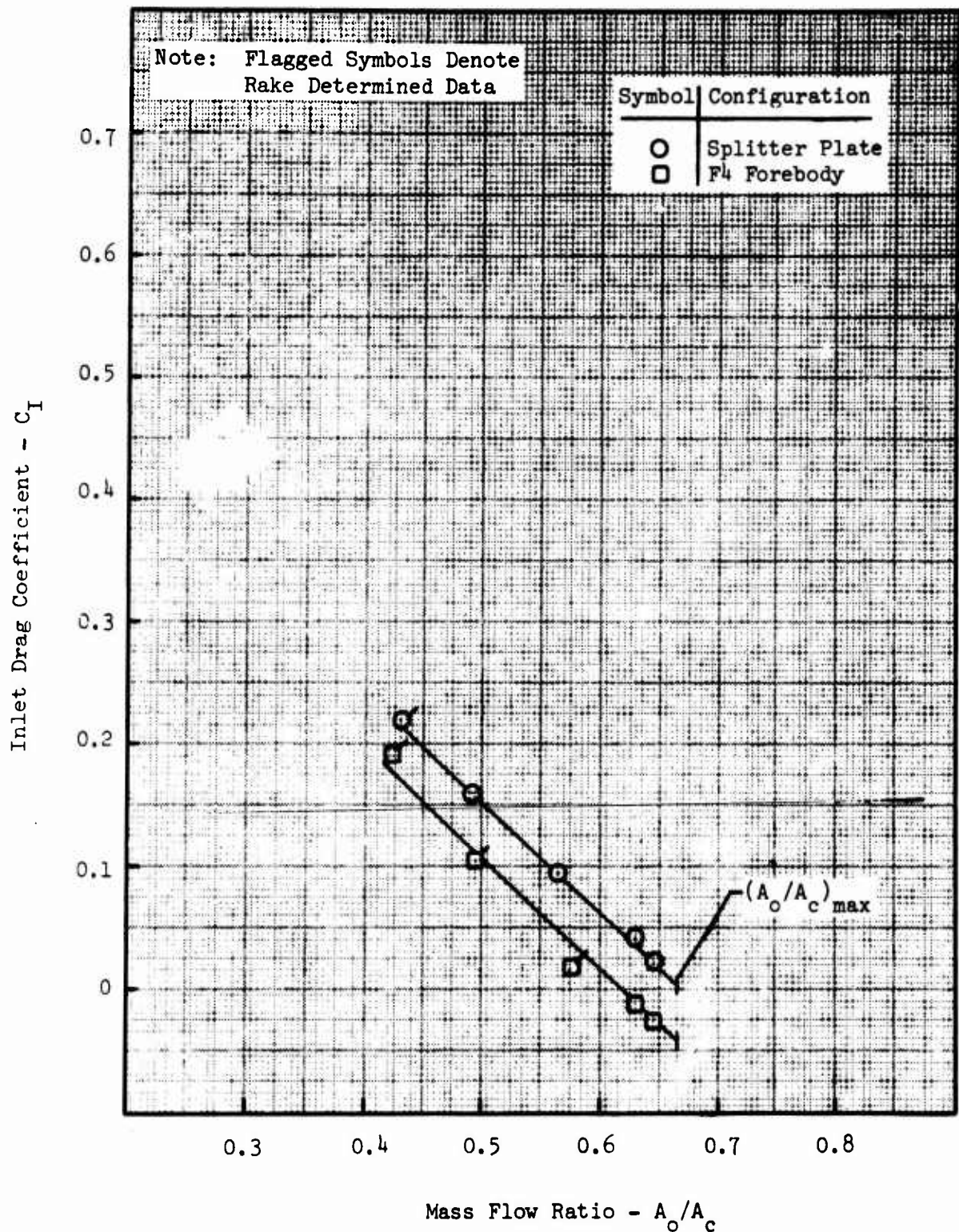


FIGURE 17 - FOREBODY EFFECTS ON THE F-4 INLET DRAG

F-4 7.5% Model
 Ramp Configuration (10° - 0°)
 $M_\infty = 0.90$
 $\alpha = 12^\circ$

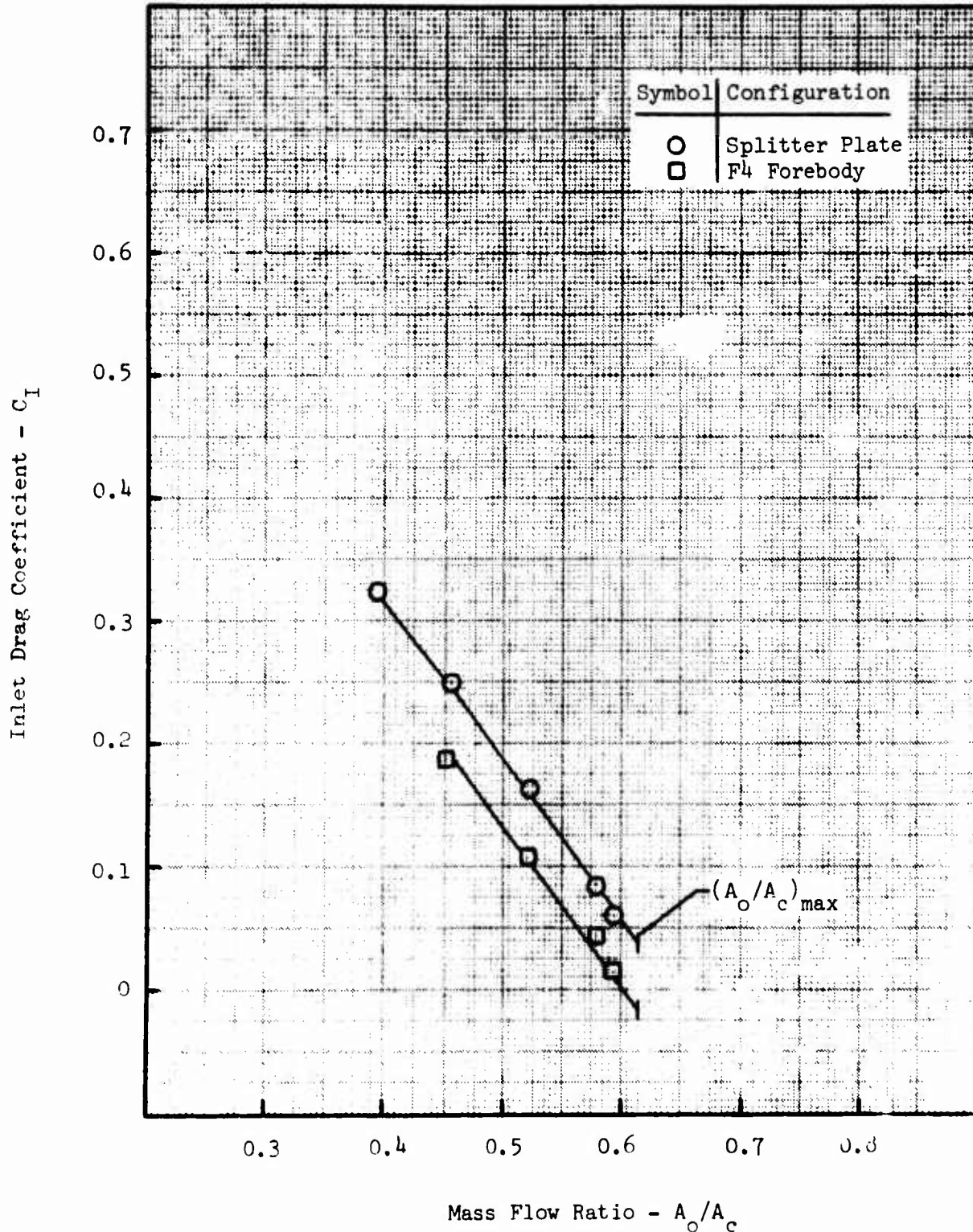


FIGURE 18 - FOREBODY EFFECTS ON THE F-4 INLET DRAG

F-4 7.5% Model
 Ramp Configuration (10° - 0°)
 $M_\infty = 1.05$
 $\alpha = 12^\circ$

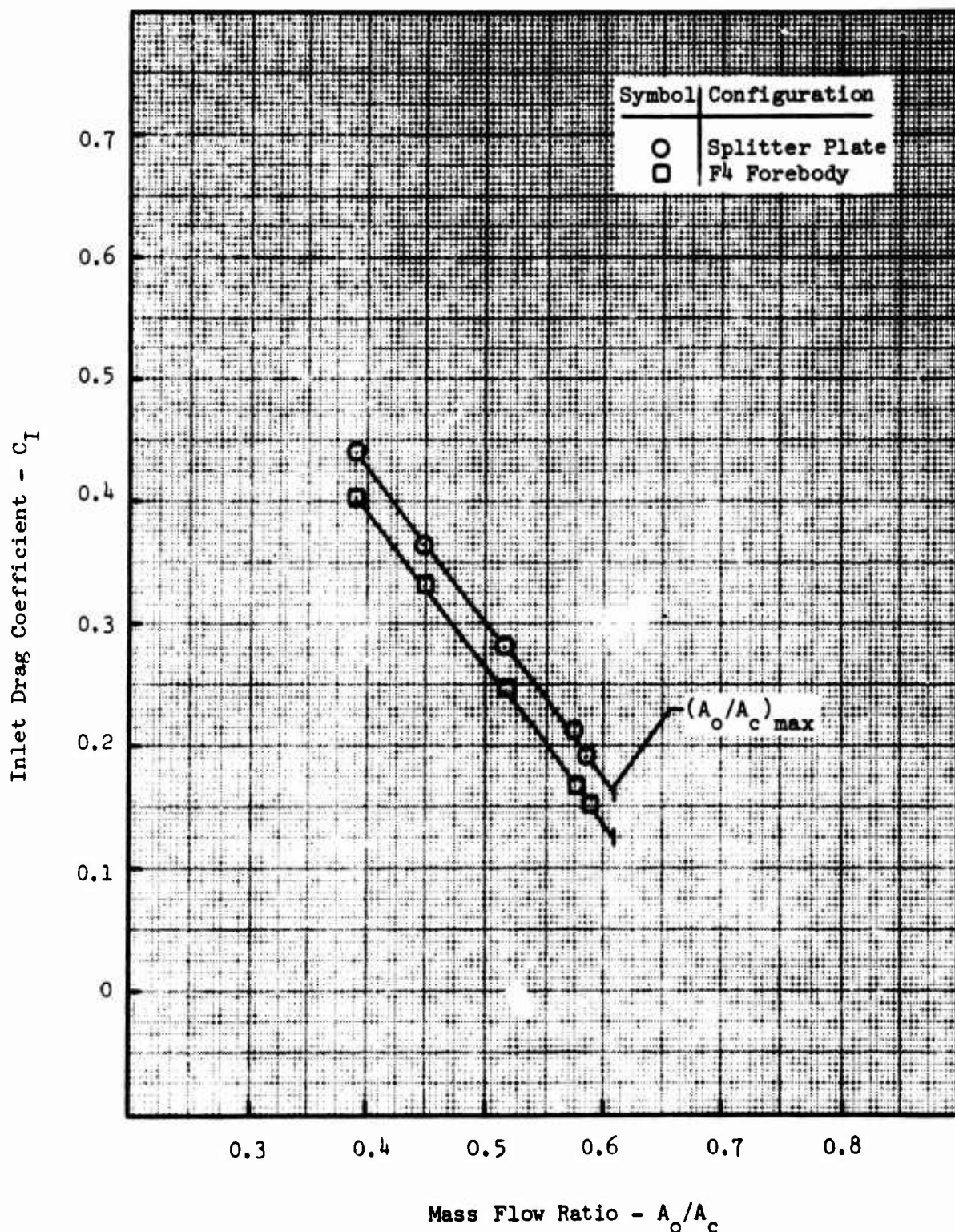


FIGURE 19 - FOREBODY EFFECTS ON THE F-4 INLET DRAG

F-4 7.5% Model
 Ramp Configuration (10° - 0°)
 $M_\infty = 0.70$
 $\alpha = 0^\circ$

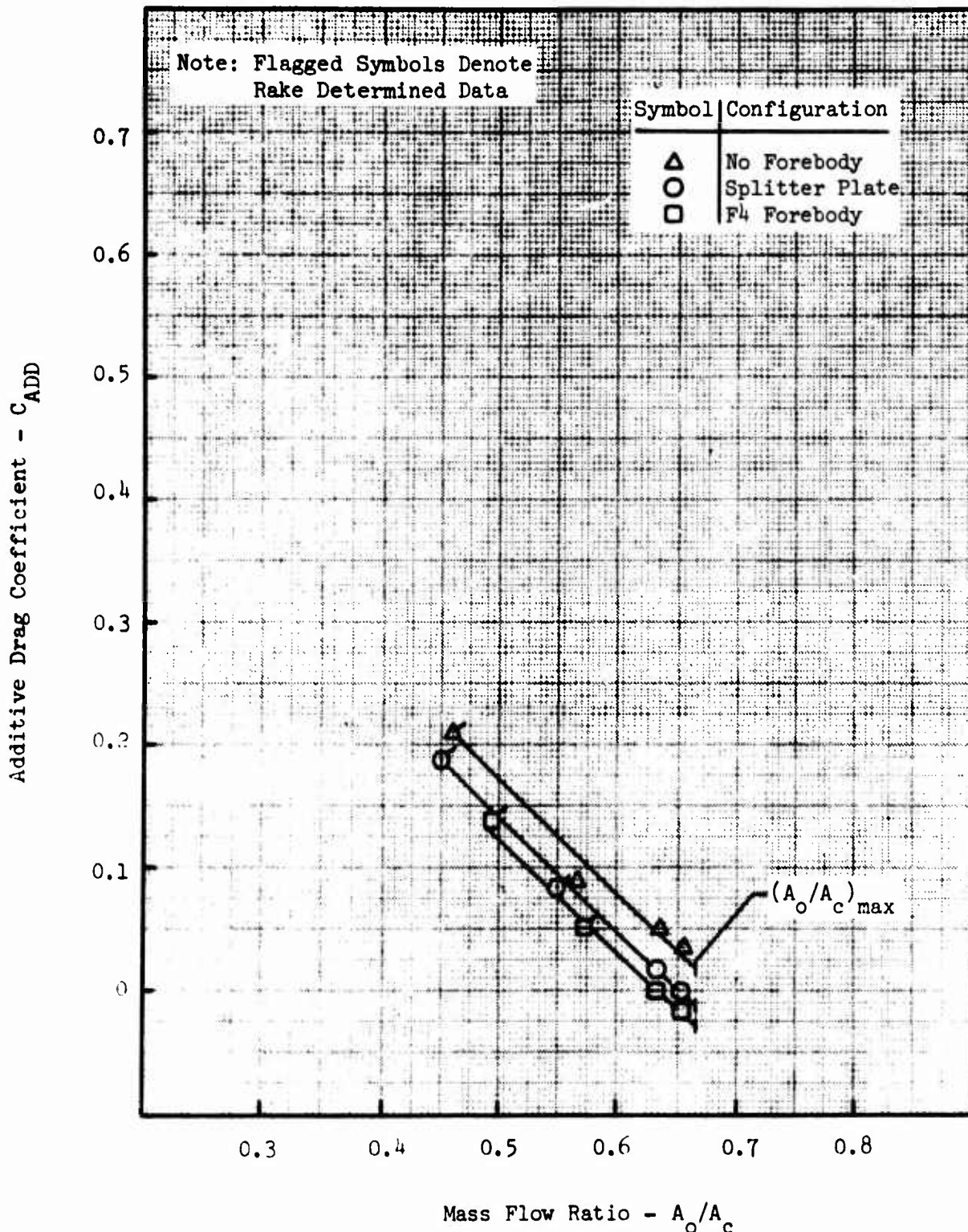


FIGURE 20 - FOREBODY EFFECTS ON THE F-4 ADDITIVE DRAG

Additive Drag Coefficient - C_{ADD}

F-4 7.5% Model
Ramp Configuration (10°-0°)
 $M_\infty = 0.90$
 $\alpha = 0^\circ$

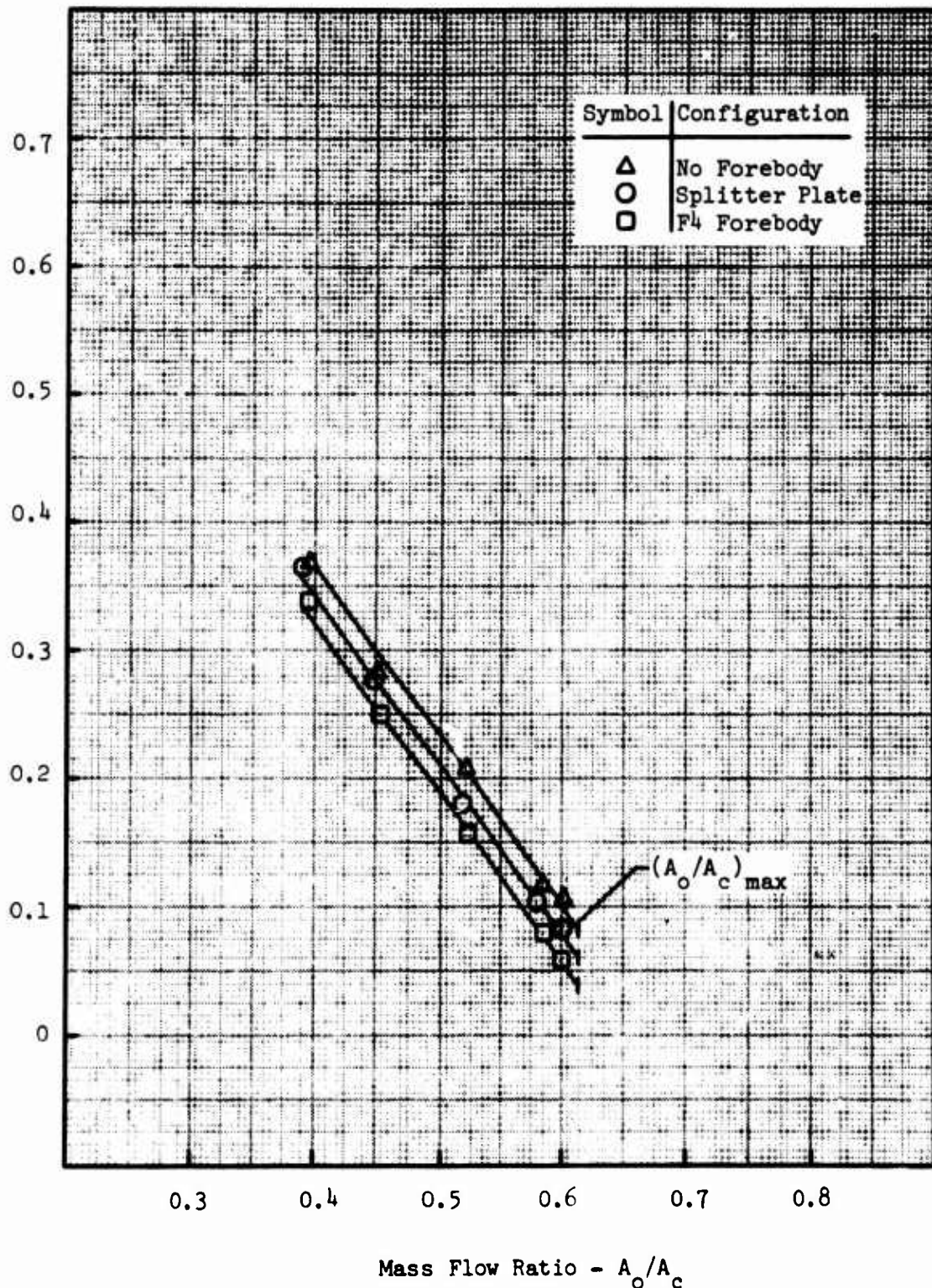


FIGURE 21 - FOREBODY EFFECTS ON THE F-4 ADDITIVE DRAG

F-4 7.5% Model
 Ramp Configuration ($10^\circ - 0^\circ$)
 $M_\infty = 0.70$
 $\alpha = 12^\circ$

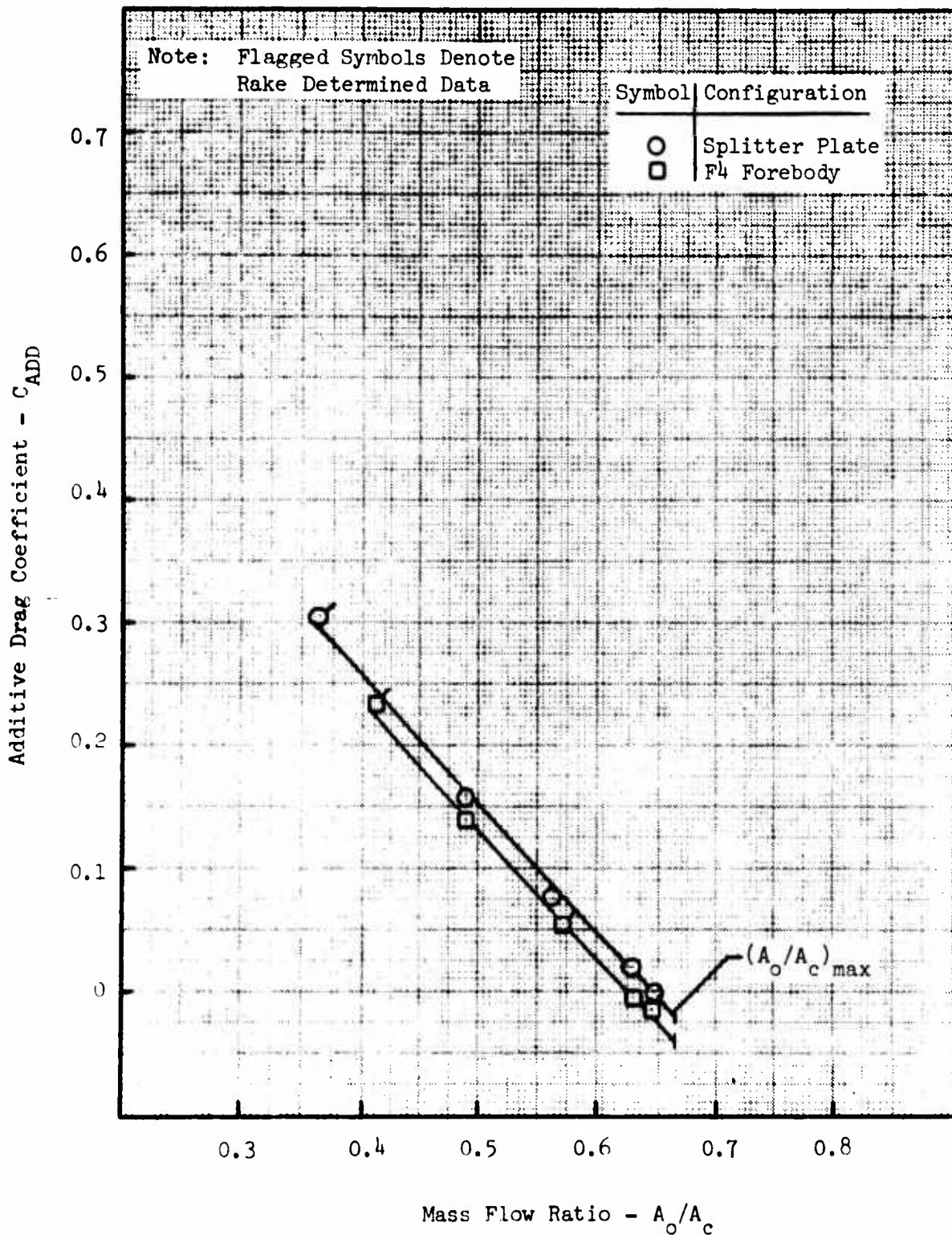


FIGURE 22 - FOREBODY EFFECTS ON THE F-4 ADDITIVE DRAG

F-4 7.5% Model
 Ramp Configuration (10° - 0°)
 $M_\infty = 0.90$
 $\alpha = 12^\circ$

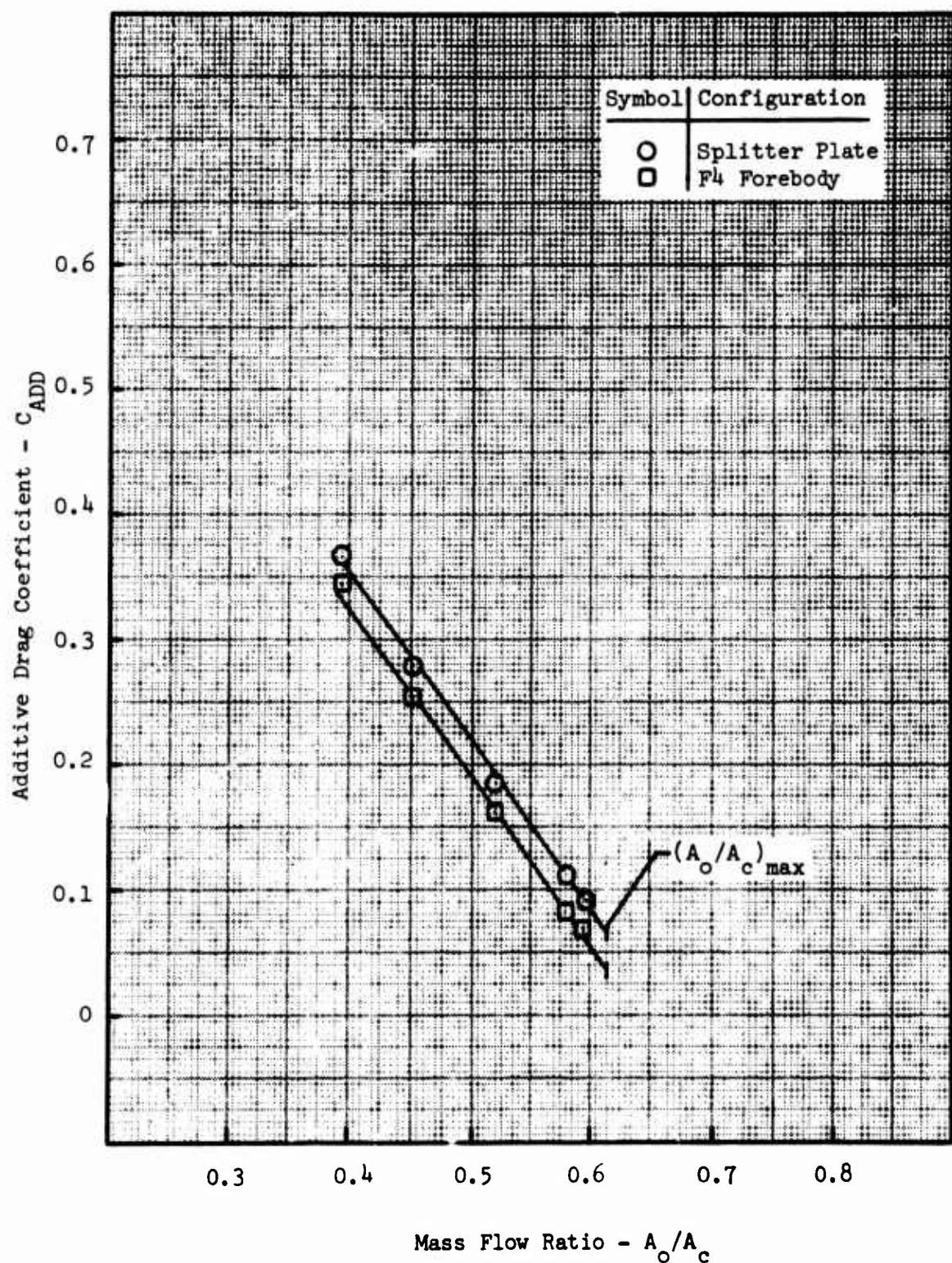


FIGURE 23 - FOREBODY EFFECTS ON THE F-4 ADDITIVE DRAG

F-4 7.5% Model
 Ramp Configuration (10° - 0°)
 $M_\infty = 1.05$
 $\alpha = 12^\circ$

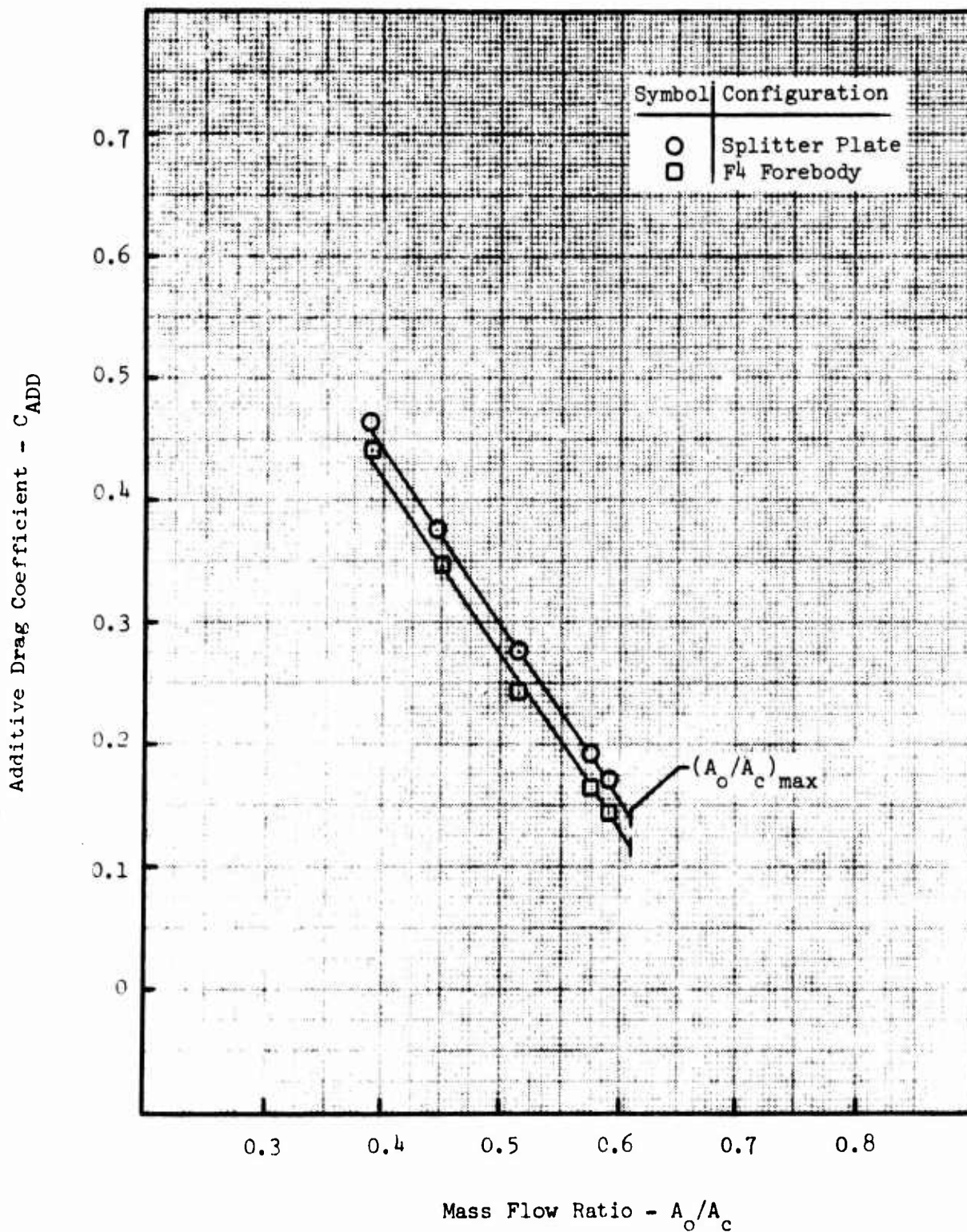


FIGURE 24 - FOREBODY EFFECTS ON THE F-4 ADDITIVE DRAG

Axisymmetric Single Cone Inlet Model
Configuration A10
 $\alpha = 0^\circ$

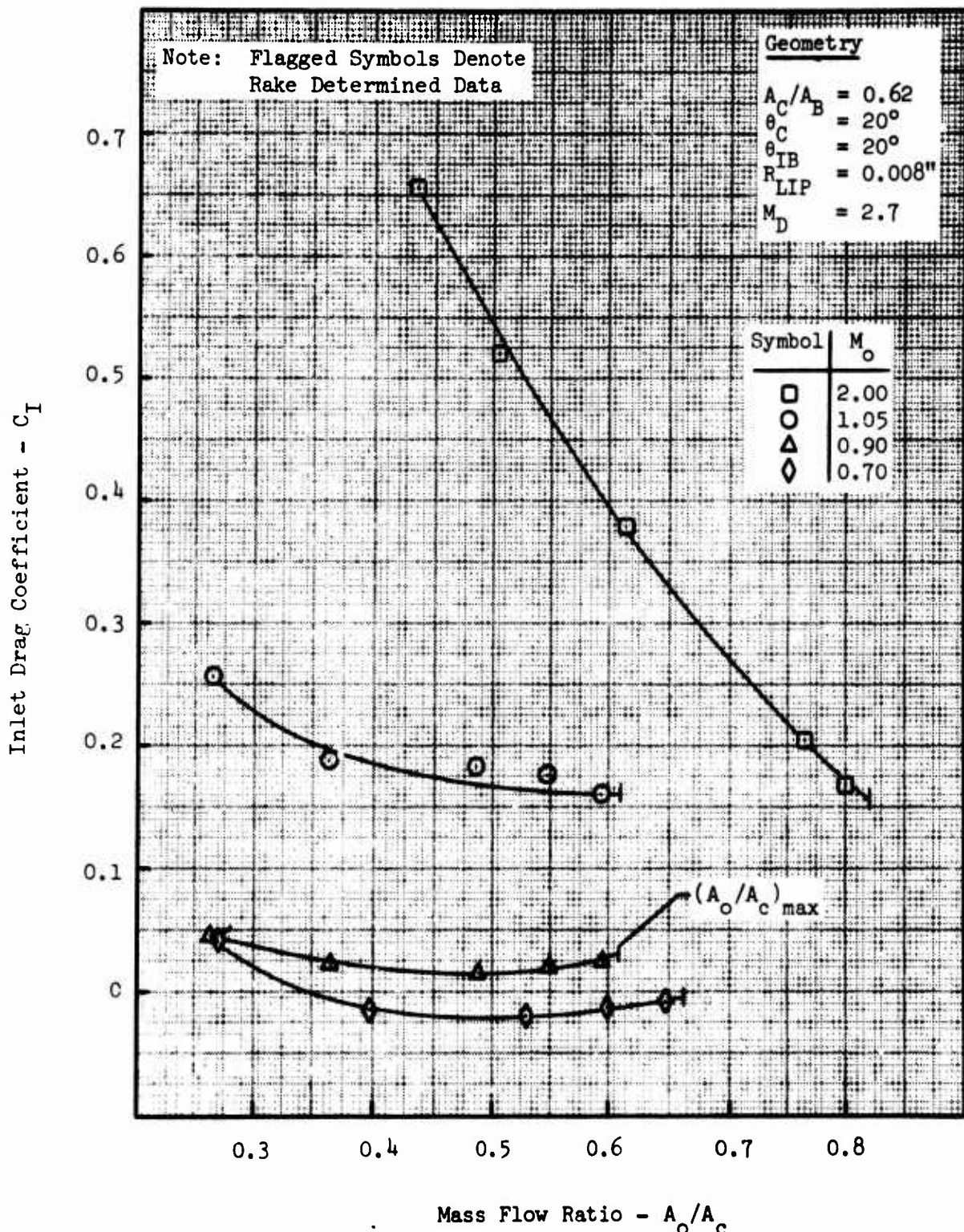


FIGURE 25 - INLET DRAG COEFFICIENT

Axisymmetric Single Cone Inlet Model
Configuration A10
 $\alpha = 0^\circ$

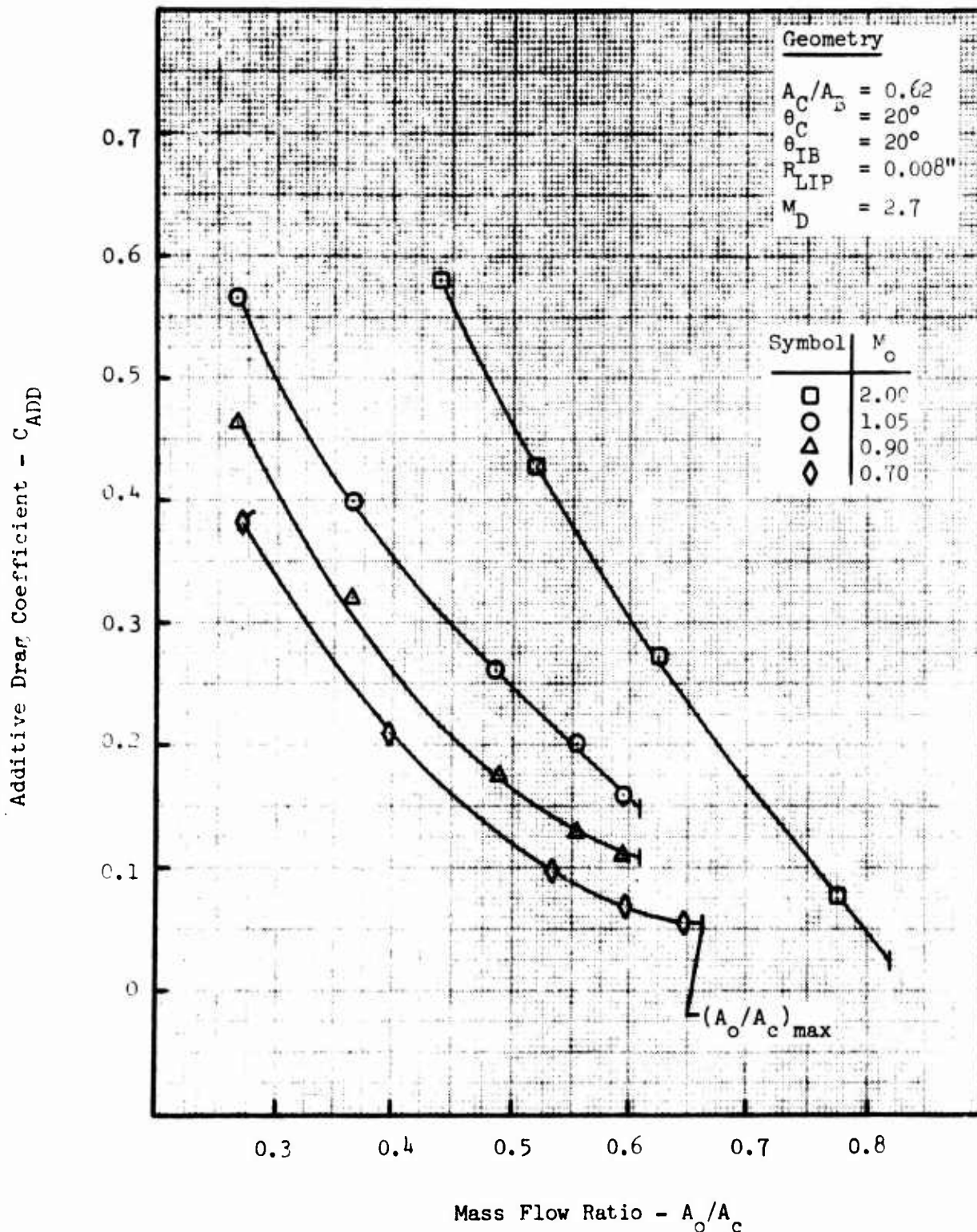


FIGURE 26 - ADDITIVE DRAG COEFFICIENT

Axisymmetric Single Cone Inlet Model
Configuration A10
 $\alpha = 0^\circ$

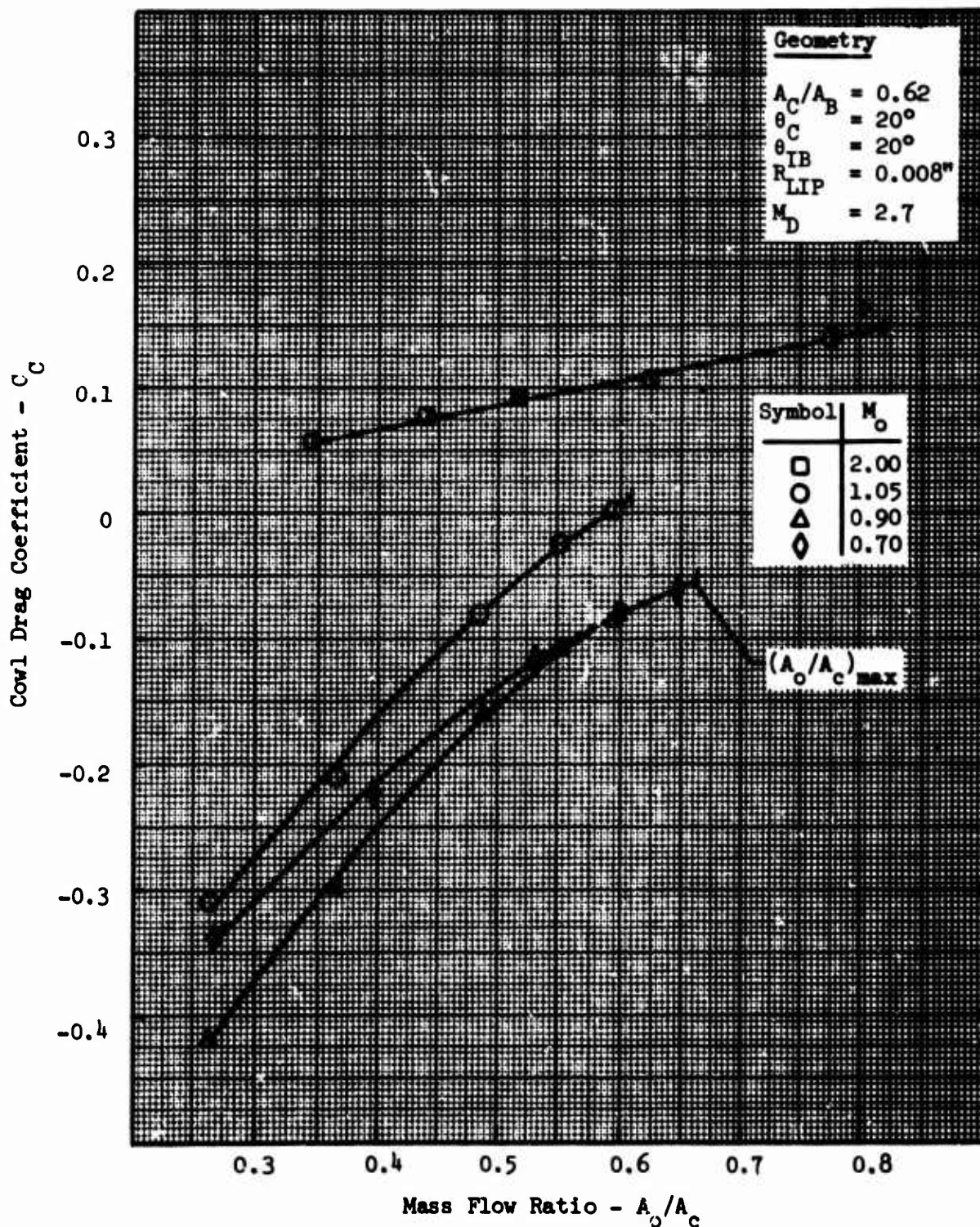


FIGURE 27 - COWL DRAG COEFFICIENT

Axisymmetric Single Cone Inlet Model
Configuration A10

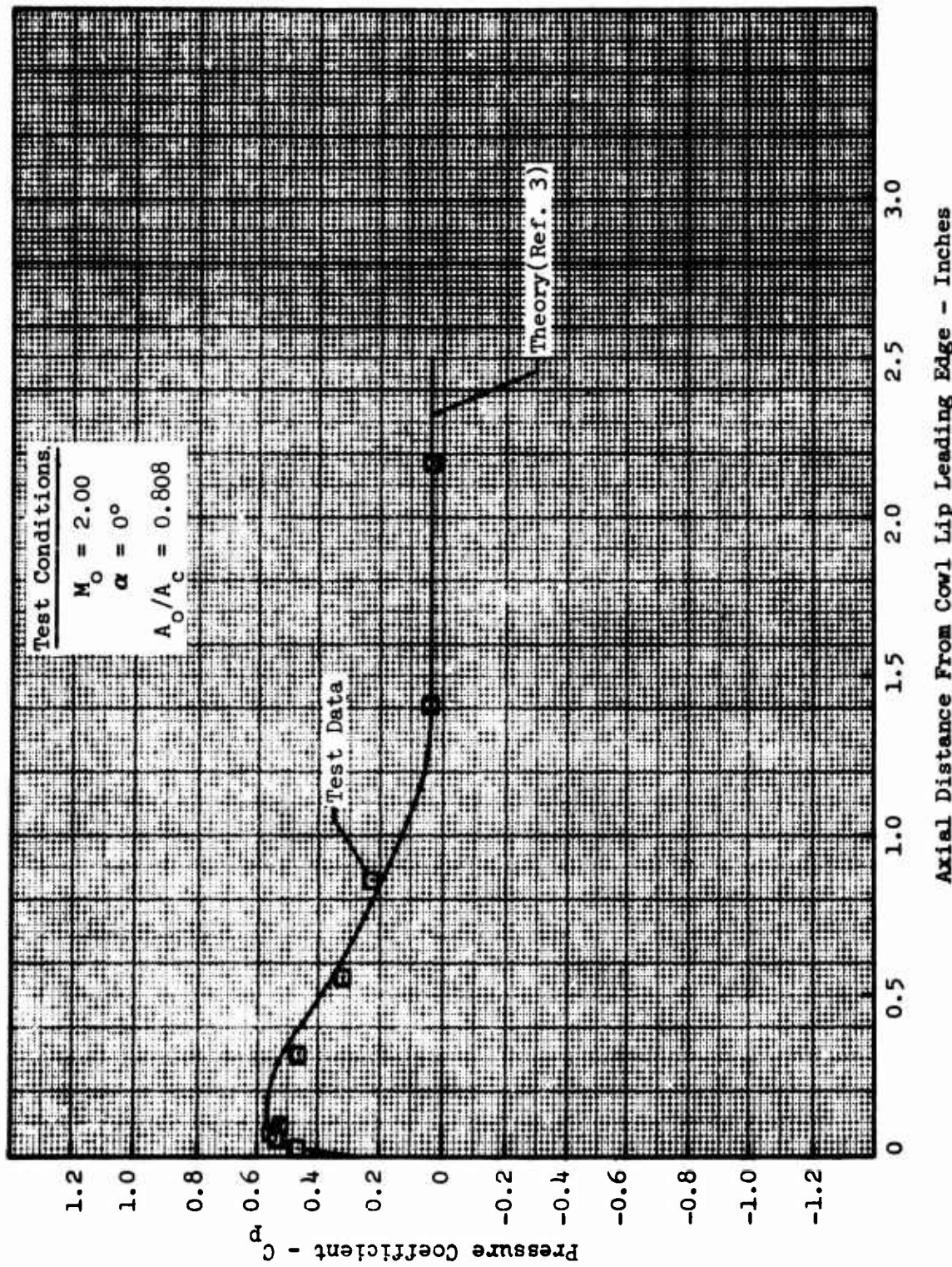


FIGURE 28 - COMPARISON OF THEORETICAL AND EXPERIMENTAL
COWL PRESSURE COEFFICIENT

Axisymmetric Single Cone Inlet Model
Configuration A10

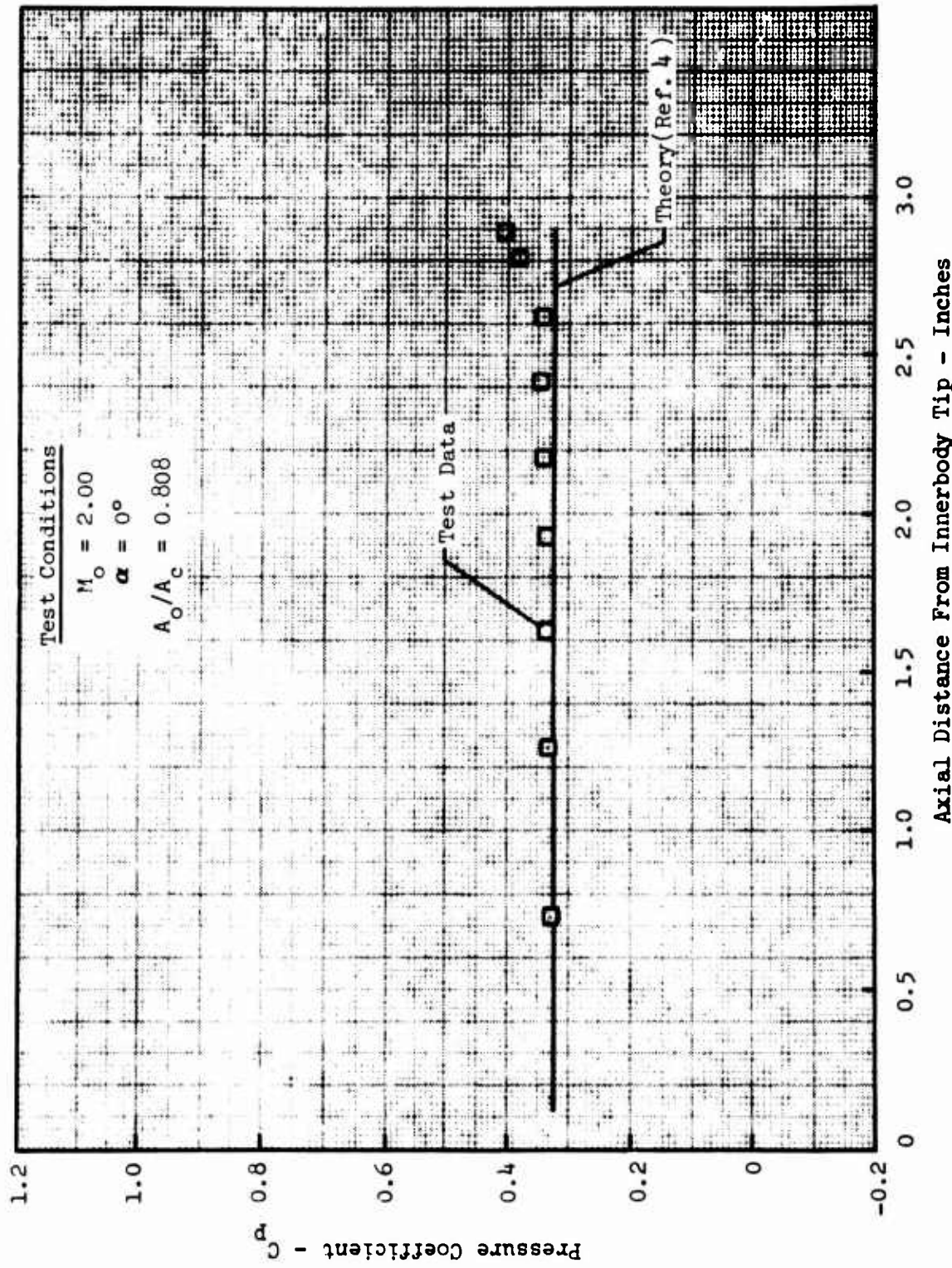


FIGURE 29 - COMPARISON OF THEORETICAL AND EXPERIMENTAL
INNERBODY PRESSURE COEFFICIENT

Two-Dimensional Inlet Model

Ramp Angle = δ'

$M_\infty = 0.70$

$\alpha = 0^\circ$

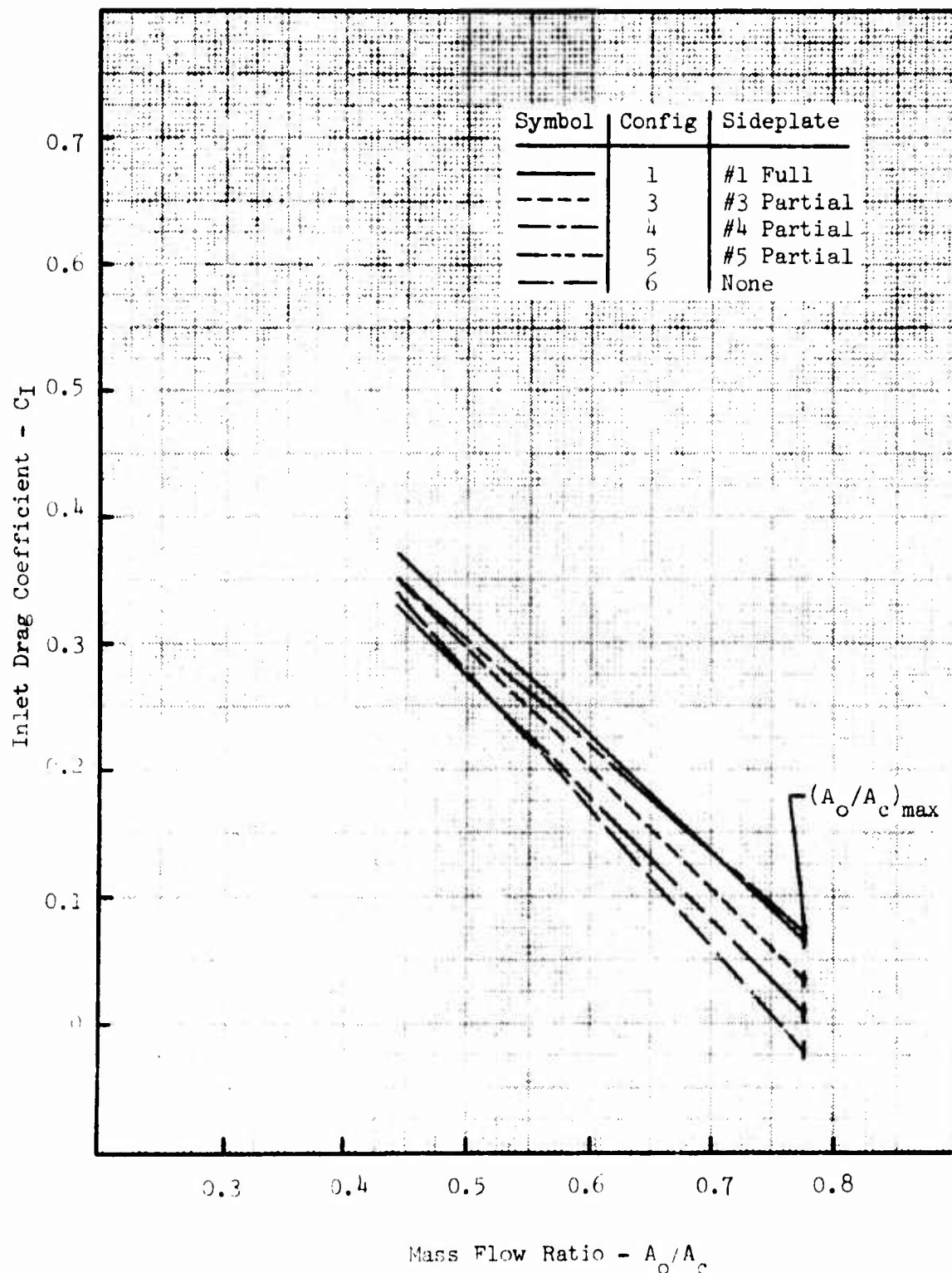


FIGURE 30 - EFFECT OF SIDEPLATE GEOMETRY ON INLET DRAG

Two-Dimensional Inlet Model
 Ramp Angle = 8°
 $M_0 = 0.90$
 $\alpha = 0^\circ$

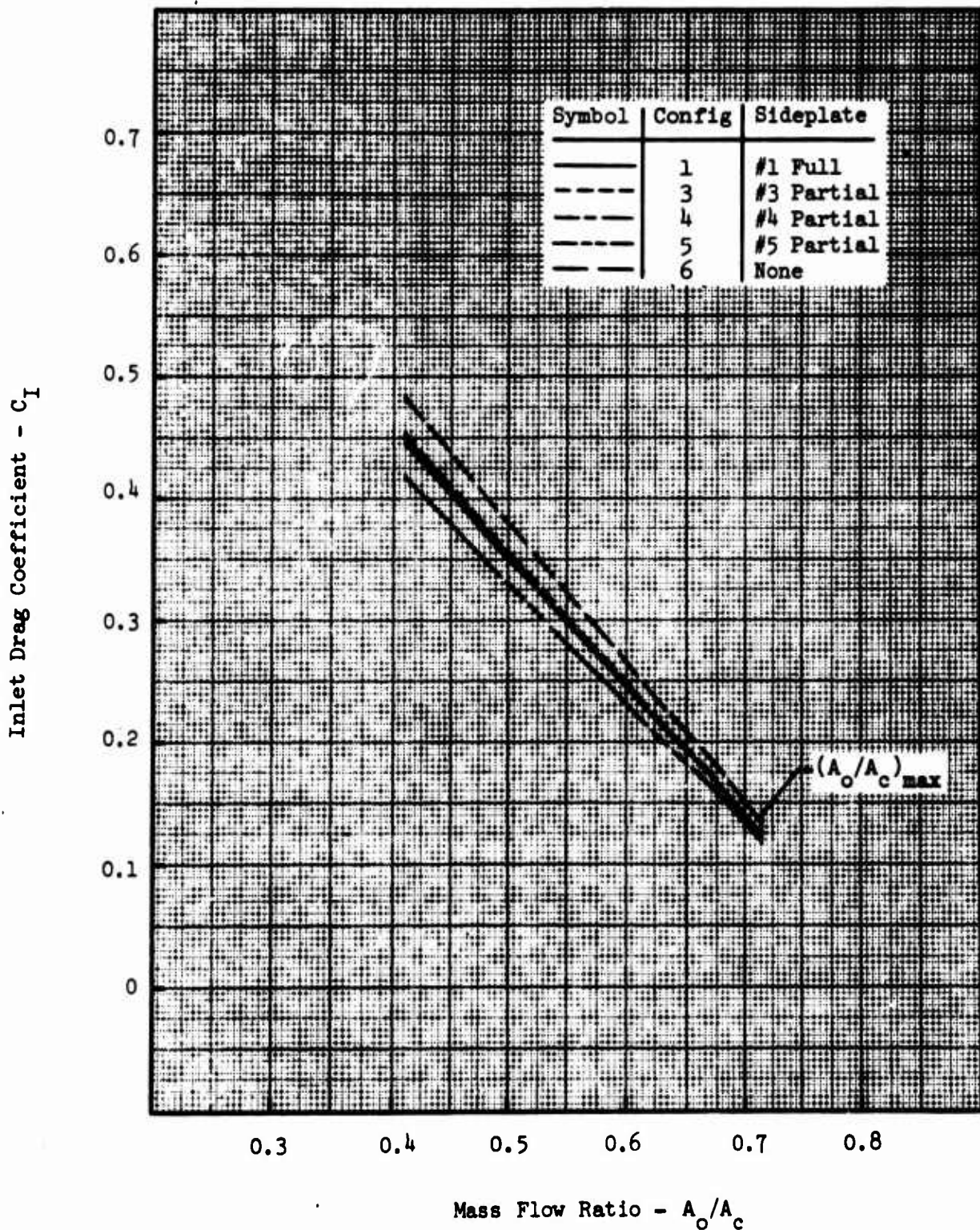


FIGURE 31 - EFFECT OF SIDEPLATE GEOMETRY ON INLET DRAG

Two-Dimensional Inlet Model

Ramp Angle = 8°

$M_\infty = 0.70$

$\alpha = 0^\circ$

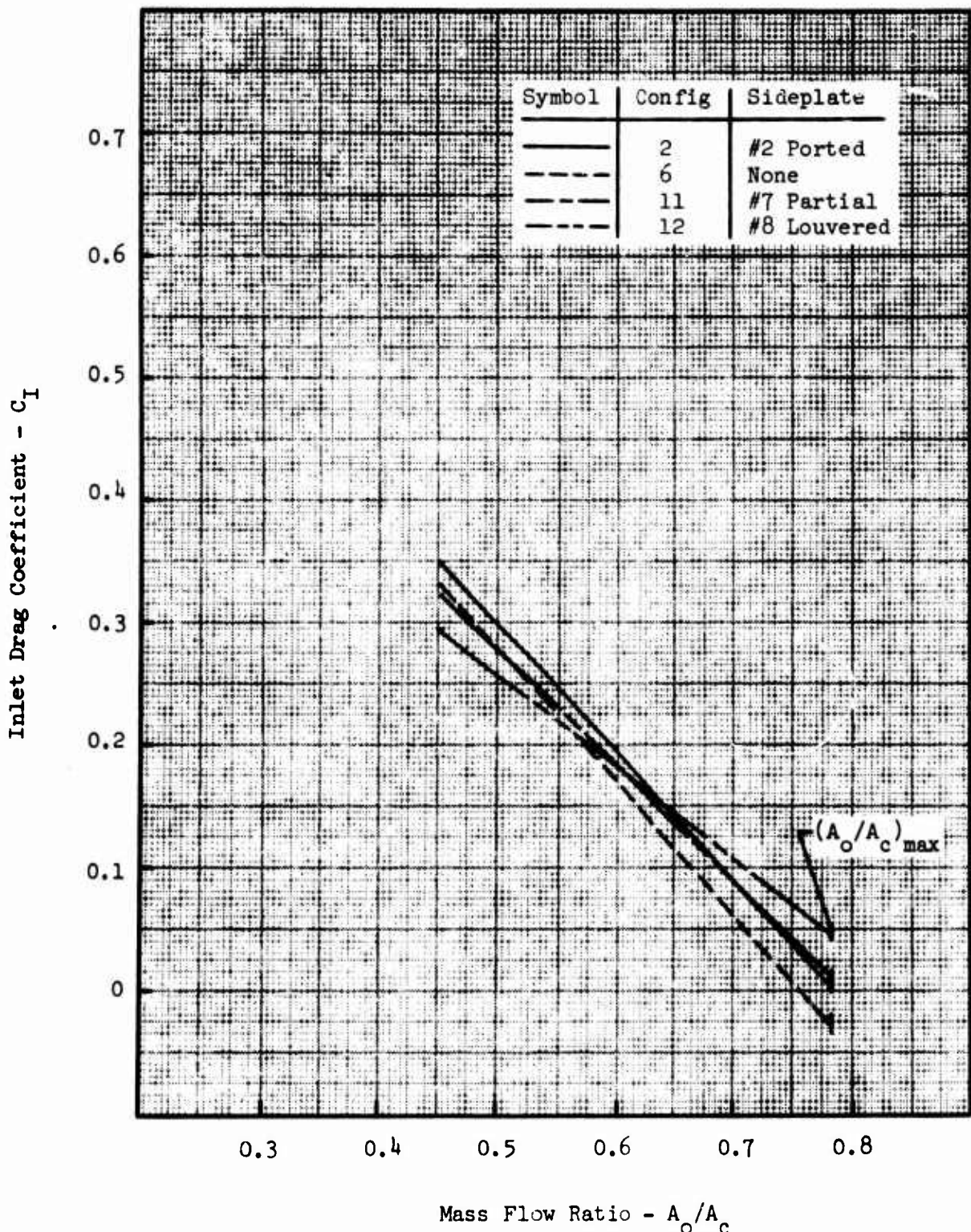


FIGURE 32 - EFFECT OF SIDEPLATE GEOMETRY ON INLET DRAG

Two-Dimensional Inlet Model

Ramp Angle = 8°

$M_0 = 0.90$

$\alpha = 0^\circ$

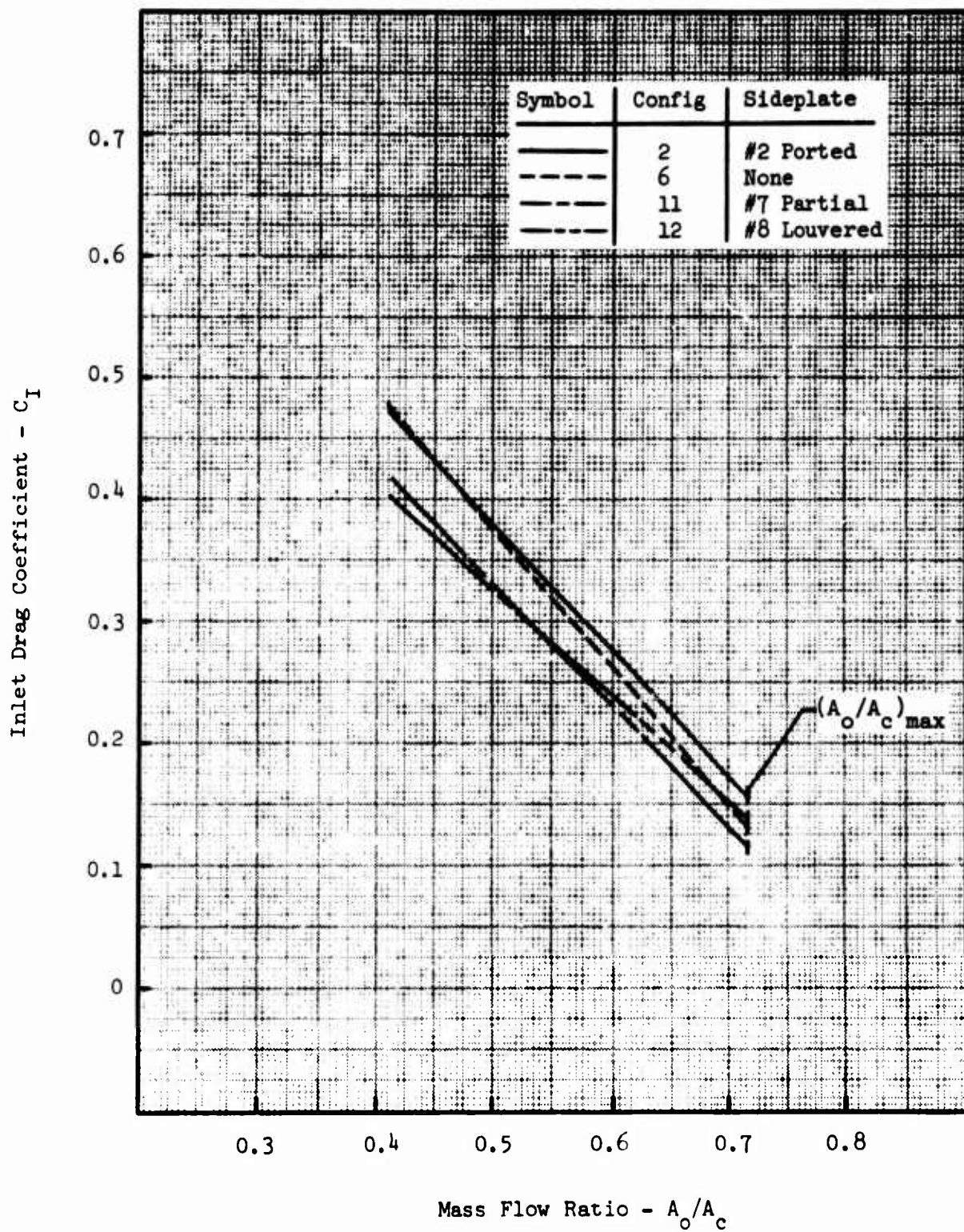


FIGURE 33 - EFFECT OF SIDEPLATE GEOMETRY ON INLET DRAG

Two-Dimensional Inlet Model

$M_\infty = 0.70$

$\alpha = 0^\circ$

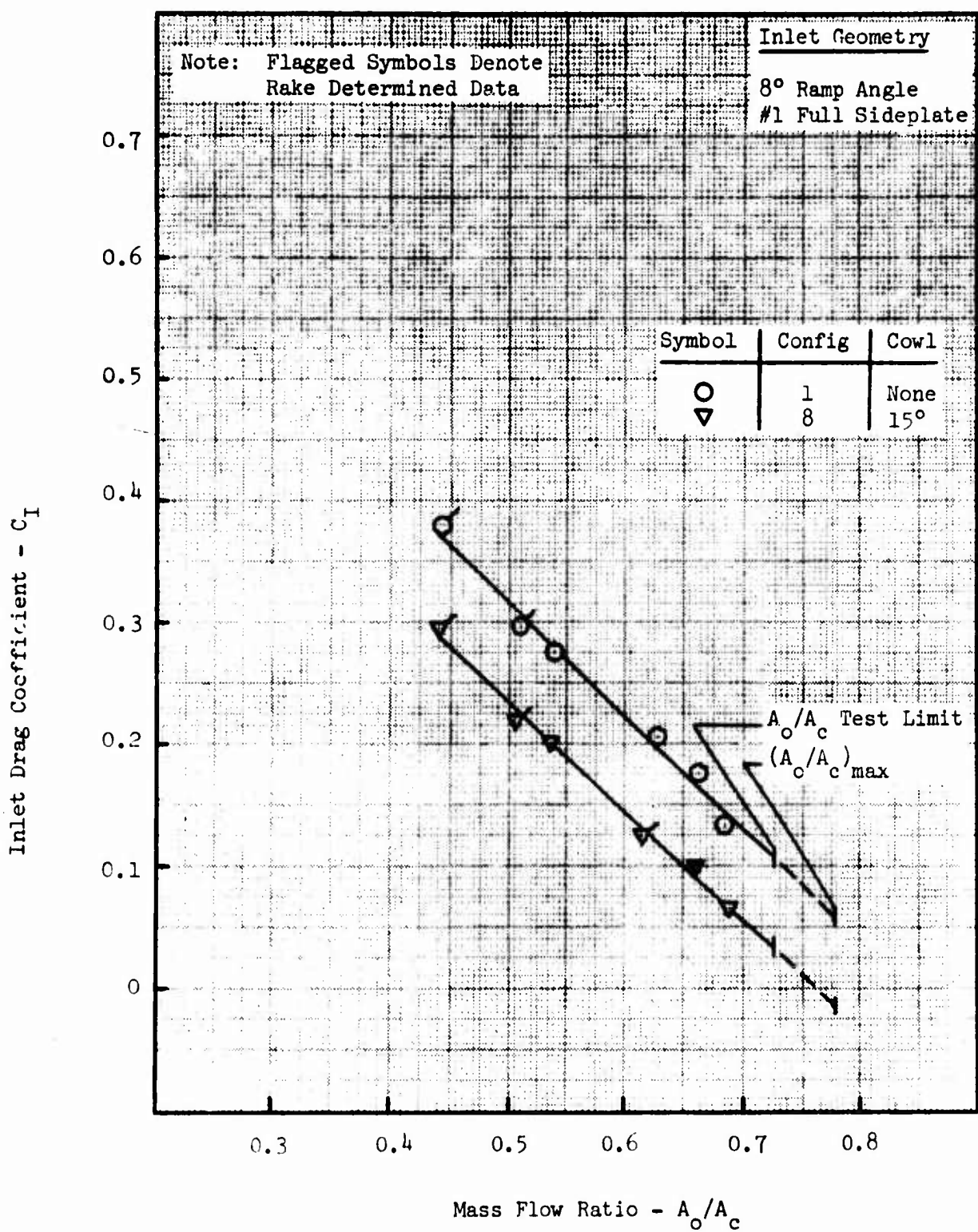


FIGURE 34 - EFFECT OF COWL ON INLET DRAG

Two-Dimensional Inlet Model

$M_\infty = 0.90$

$\alpha = 0^\circ$

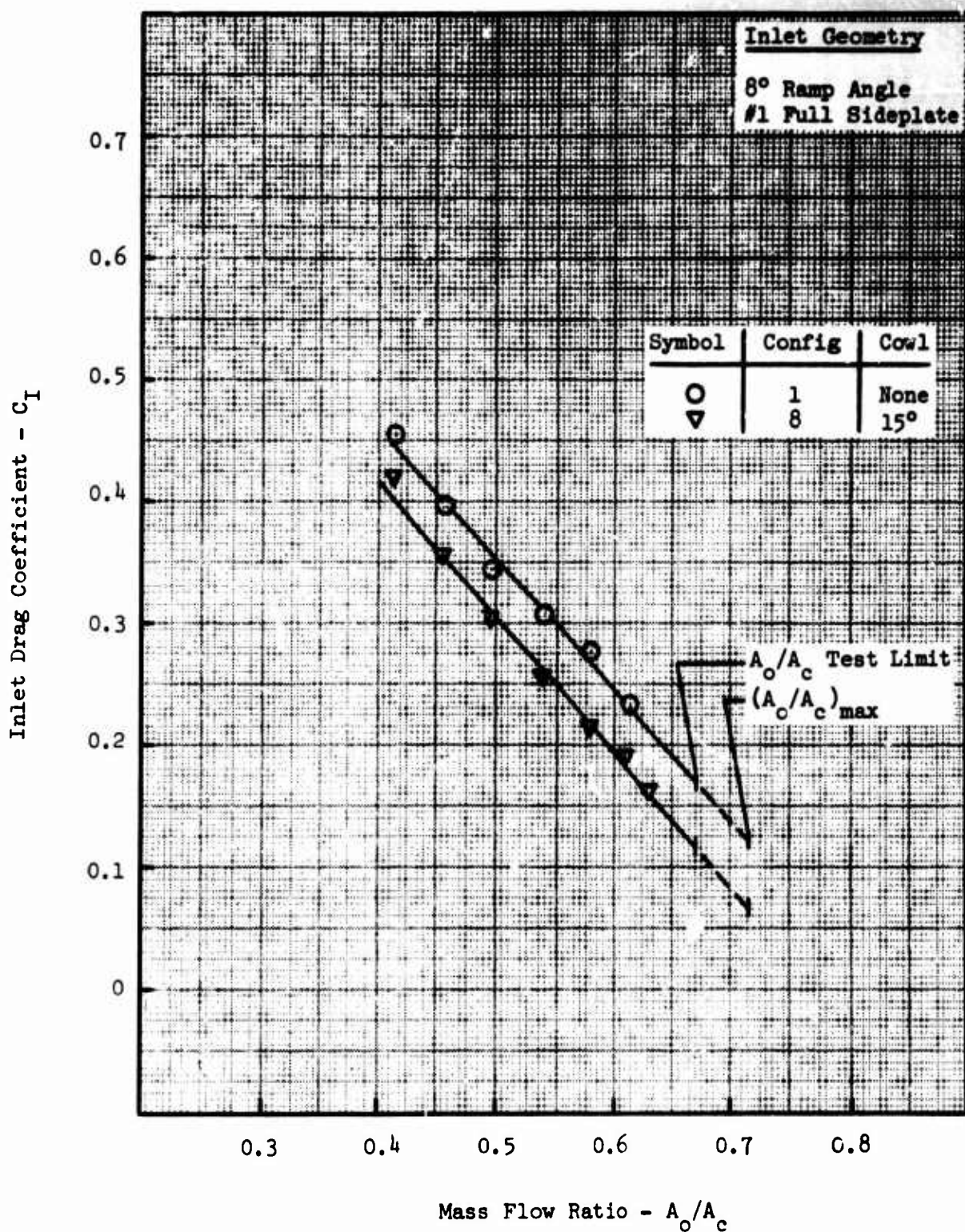


FIGURE 35 - EFFECT OF COWL ON INLET DRAG

Two-Dimensional Inlet Model

$M_\infty = 0.70$
 $\alpha = 0^\circ$

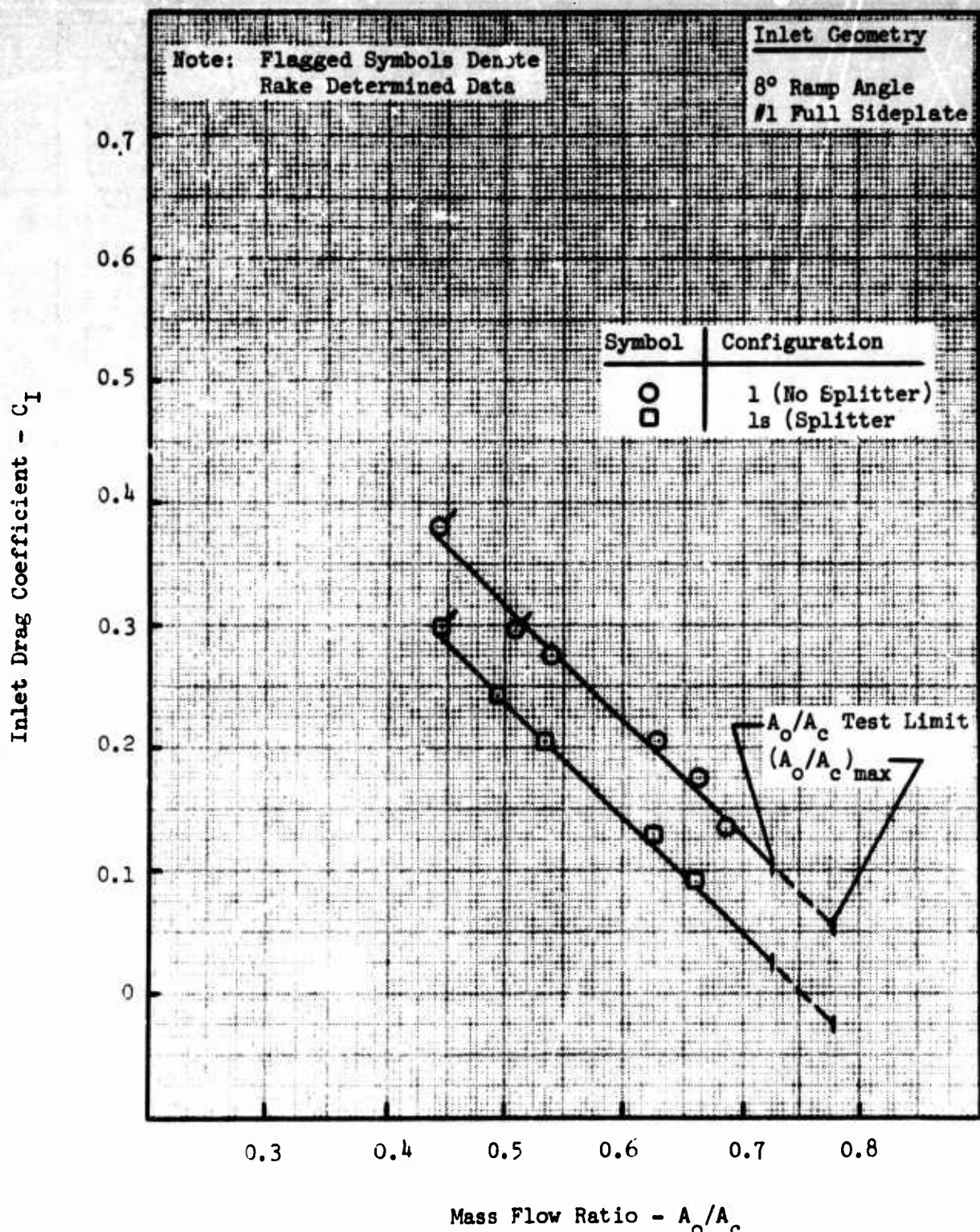


FIGURE 36 - EFFECT OF SPLITTER PLATE ON INLET DRAG

Two-Dimensional Inlet Model

$M_\infty = 0.90$

$\alpha = 0^\circ$

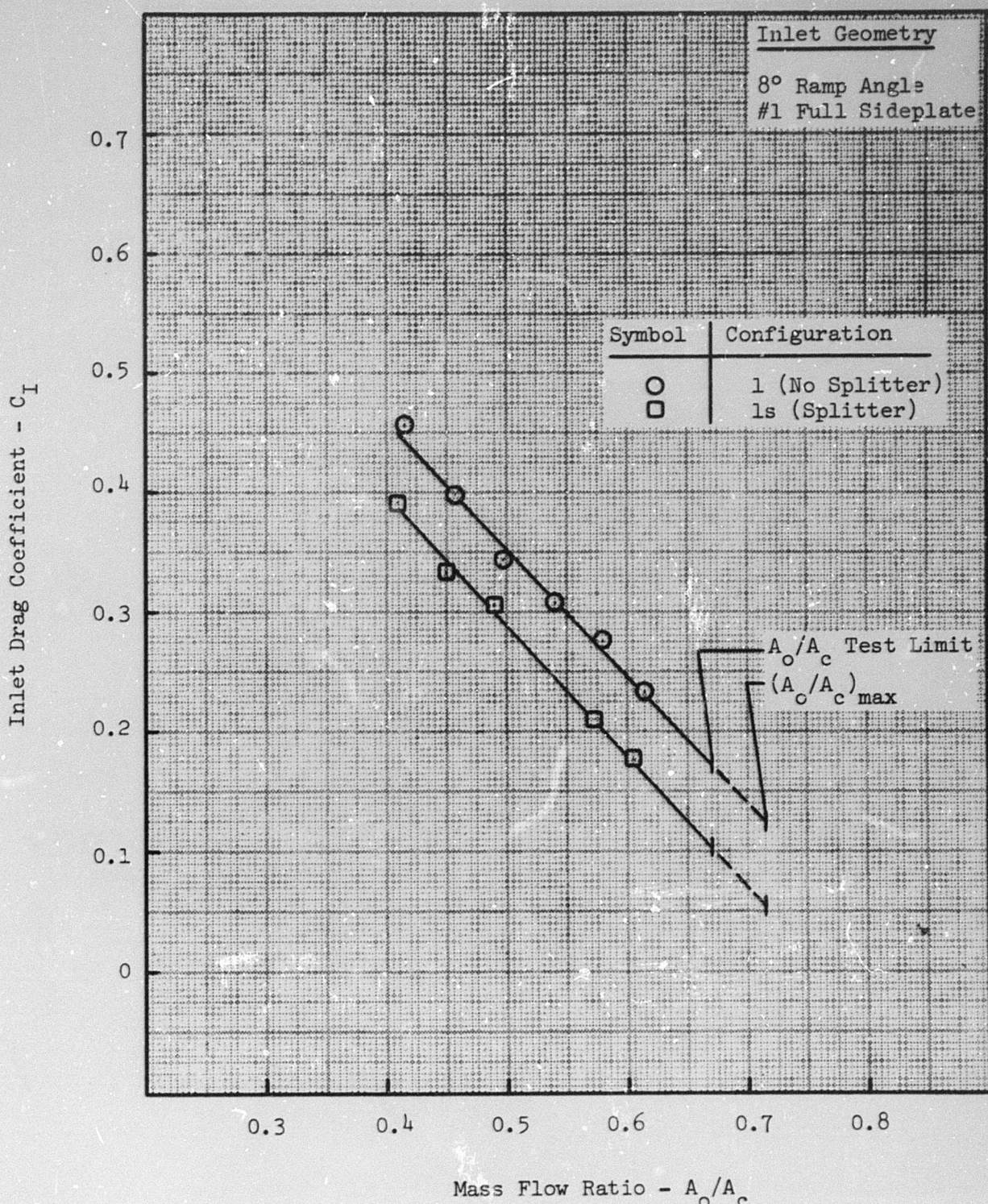


FIGURE 37 - EFFECT OF SPLITTER PLATE ON INLET DRAG

SECTION V

CONCLUSIONS

1. The presence of an aircraft forebody modifies the level of inlet and additive drag relative to that measured on an isolated inlet; however, it does not alter the variation of inlet drag with mass flow.
2. The variation of inlet drag with mass flow for all Two-Dimensional inlets (without louvers) tested in this program are essentially the same as that measured on the F-4 and Opposed-Ramp inlets reported in Reference 1.
3. The variation of inlet drag with mass flow for the Two-Dimensional inlets (without louvers) are essentially unaffected by the sideplate geometry at both subsonic and supersonic Mach number conditions.
4. The use of louvers in the sideplate reduces the effects of mass flow variations on inlet drag.
5. The addition of a cowl shape on the external contours of the compression surface of Two-Dimensional inlets lowers the drag at subsonic conditions. The drag "slope" is not changed.
6. The data from this test program revealed that the drag balance produces accurate and repeatable measurements of inlet drag characteristics for axisymmetric inlets; however, only drag increments and drag "slopes" are accurately determined for two-dimensional inlet configurations.
7. The accurate determination of cowl drag from integrated pressure data on axisymmetric inlets is reliable if sufficient instrumentation is incorporated near the cowl lip.

SECTION VI

REFERENCES

1. McVey, Francis D., Rejeske, John V., and Phillips, Edward J., "Experimental Evaluation of Inlet Drag Characteristics in the Transonic Mach Number Regime," Report AFAPL-TR-68-119, November 1968.
2. Mascitti, Vincent R., "Charts of Additive Drag Coefficient and Mass-Flow Ratio for Inlets Utilizing Right Circular Cones at Zero Angle of Attack," NASA TN D-3434, May 1966.
3. Rochow, Thomas C., "Calculation Procedure to Predict the Wave Drag for the Lip and External Cowl of Axisymmetric Inlets at Supersonic Flight Conditions," McDonnell Douglas Report EN-571, November 1967.
4. Rochow, Thomas C. and Sharp, Brooks M., "Axisymmetric Rotational Inviscid Supersonic Inlet Flow Field Calculations," McDonnell Douglas Report EN-550, August 1968.

BLANK PAGE

APPENDIX A

RUN SUMMARY

RUN SUMMARY

PHASE II - PART A

RUN	CONFIGURATION	M_∞	α (Degrees)	CORRELATION NUMBERS
1	F1Ps*	.70	0	14 - 20
2		.70	12	21 - 26
3		.90	0	27 - 34
4		.90	12	35 - 40
5		1.05	12	41 - 46
6	F1Po	.90	0	56 - 61
7		.70	0	62 - 69
8	F1Pf	1.05	0	85 - 91
9			6	96 - 103
10			6	104 - 109
11	F1Pf	1.05	12	110 - 116
12		.90	0	117 - 122
13			6	123 - 129
14			12	130 - 135
15		.80	0	136 - 142
16	F1Pf	.70	0	143 - 149
17			6	150 - 154
18			12	155 - 160
19		.90	0	161 - 166
20**	F3s	.70	0	178 - 183
21	F3s	.70	6	184 - 188
22		.90	0	189 - 194
23		.90	6	195 - 199
24		2.00	0	200 - 205
25		2.00	6	206 - 209
26	F3f	.70	0	218 - 223
27		.70	6	224 - 228
28		.90	0	229 - 234
29		.90	6	235 - 239
30		2.00	0	240 - 244
31	F3f	2.00	6	245 - 249
32	F1s	.70	0	257 - 262
33		.70	12	263 - 268
34		.90	0	270 - 275
35		.90	12	276 - 283
36	F1s	1.05	12	284 - 289
37	F1f	.70	0	415 - 421
38		.70	6	422 - 426

RUN SUMMARY
PHASE II - PART A (Continued)

RUN	CONFIGURATION	M_∞	α (Degrees)	CORRELATION NUMBERS
39	F1s	.70	0	525 - 531
40		.70	12	532 - 537
41	F1s	.90	0	538 - 549
42		1.05	12	582 - 588
43		.90	0	589 - 600
44		.90	12	601 - 606
45		.70	0	607 - 613
46	F1s	.70	12	614 - 619
47		.90	0	620 - 625
48	F1f	1.05	0	635 - 641
49		1.05	6	642 - 647
50		1.05	12	650 - 658
51	F1f	.90	0	659 - 665
52			6	667 - 672
53			12	673 - 677
54		.70	0	735 - 741
55		.70	6	742 - 747
56	F1f	.70	12	748 - 753
57	Flo	.90	0	762 - 768
58		.70	0	769 - 775
59	F3s	2.00	0	789 - 795
60		2.00	6	796 - 800
61	F3s	.90	0	801 - 806
62		.90	6	807 - 811
63		.70	0	812 - 817
64		.70	6	818 - 822
65		.90	0	823 - 827
66	F3f	2.00	0	838 - 841
67		2.00	6	842 - 846
68		.90	0	847 - 852
69		.90	6	853 - 857
70		.70	0	858 - 863
71	F3f	.70	6	864 - 868
72	A10P	.70	0	874 - 880
73		.90	0	881 - 887
74		1.05	0	888 - 895
75		2.00	0	896 - 904

RUN SUMMARY

PHASE II - PART A (Continued)

RUN	CONFIGURATION	M_∞	α (Degrees)	CORRELATION NUMBERS
76	A10	.70	0	917 - 923
77		.90	0	924 - 930
78		1.05	0	931 - 937
79		2.00	0	938 - 946

* The "P" designates Pressure Model.

**Runs 20 through 38 were no good because of balance problems,
and therefore were repeated.

RUN SUMMARY

PHASE II - PART B

RUN	CONFIGURATION	M_∞	α (Degrees)	CORRELATION NUMBERS
1	F3s	.70	0	11 - 15
2		.70	-	30 - 34
3		.90	-	35 - 39
4			+1° (yaw)	40 - 44
5			+2° (yaw)	45 - 49
6	F3s	2.00	0	50 - 54
7			+2° (yaw)	55 - 59
8	F3f		0	64 - 69
9		.90	0	70 - 75
10		.70	0	76 - 80
11	1	.90	0	91 - 102
12		.90	6	103 - 108
13		.70	0	109 - 115
14			6	116 - 122
15	3		0	131 - 138
16	3	.90	0	139 - 146
17	4	.70	-	150 - 156
18	4	.90	-	157 - 164
19	1	.70	-	174 - 181
20	1	.90	-	182 - 190
21	5	.70	0	194 - 201
22	5	.90	0	202 - 210
23	2	2.0	0	221 - 227
24			6	228 - 234
25			10	235 - 240
26	2	2.0	14	241 - 246
27		2.0	16	247
28		1.8	0	248 - 253
29		.90	0	254 - 261
30		.90	6	262 - 270
31	2	.70	0	271 - 278
32		.70	6	279 - 284
33		2.0	0	316 - 320
34		1.8	0	321 - 325
35		.90	0	326 - 332

RUN SUMMARY

PHASE II - PART B (Continued)

RUN	CONFIGURATION	M_∞	α (Degrees)	CORRELATION NUMBERS
36	2	.70	0	333 - 339
37	11	2.0	↑	343 - 348
38		1.8	↓	349 - 355
39		.90	↑	356 - 363
40		.70	↓	364 - 370
41	12	2.0	0	374 - 379
42		1.8	↑	380 - 386
43		.90	↓	387 - 394
44		.70	↑	395 - 402
45	6	2.0	↓	410 - 416
46	6	1.8	0	417 - 424
47		.90	↑	425 - 432
48		.70	↓	433 - 440
49	18	.70	↑	444 - 450
50	18	.90	↓	451 - 457
51	8	.90	0	462 - 470
52		.70	↑	471 - 477
53	16	2.0	↓	481 - 492
54	17	2.0	↑	499 - 506
55	18	2.0	↓	510 - 515
56	18	2.0	3	516 - 521
57			6	522 - 527
58			10	528 - 533
59			12	534 - 539

APPENDIX B
TEST RESULTS FOR THE
F-4 INLET MODELS

F-4 7.5% Model with Forebody
Ramp Configuration (10° - 0°)
 $\alpha = 0^\circ$

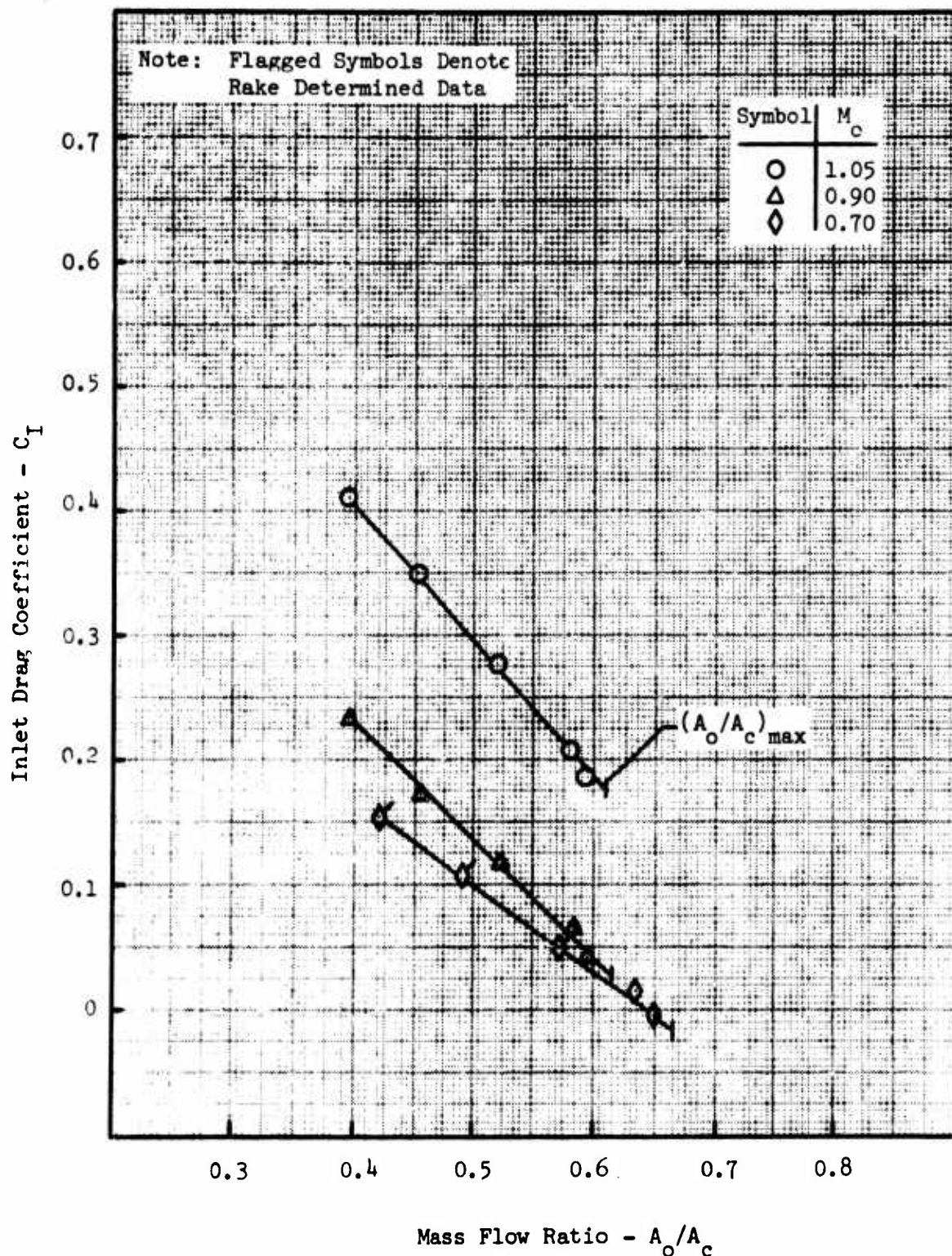


FIGURE B.1 - INLET DRAG COEFFICIENT

F-4 7.5% Model with Forebody
Ramp Configuration (10° - 0°)
 $\alpha = 6^\circ$

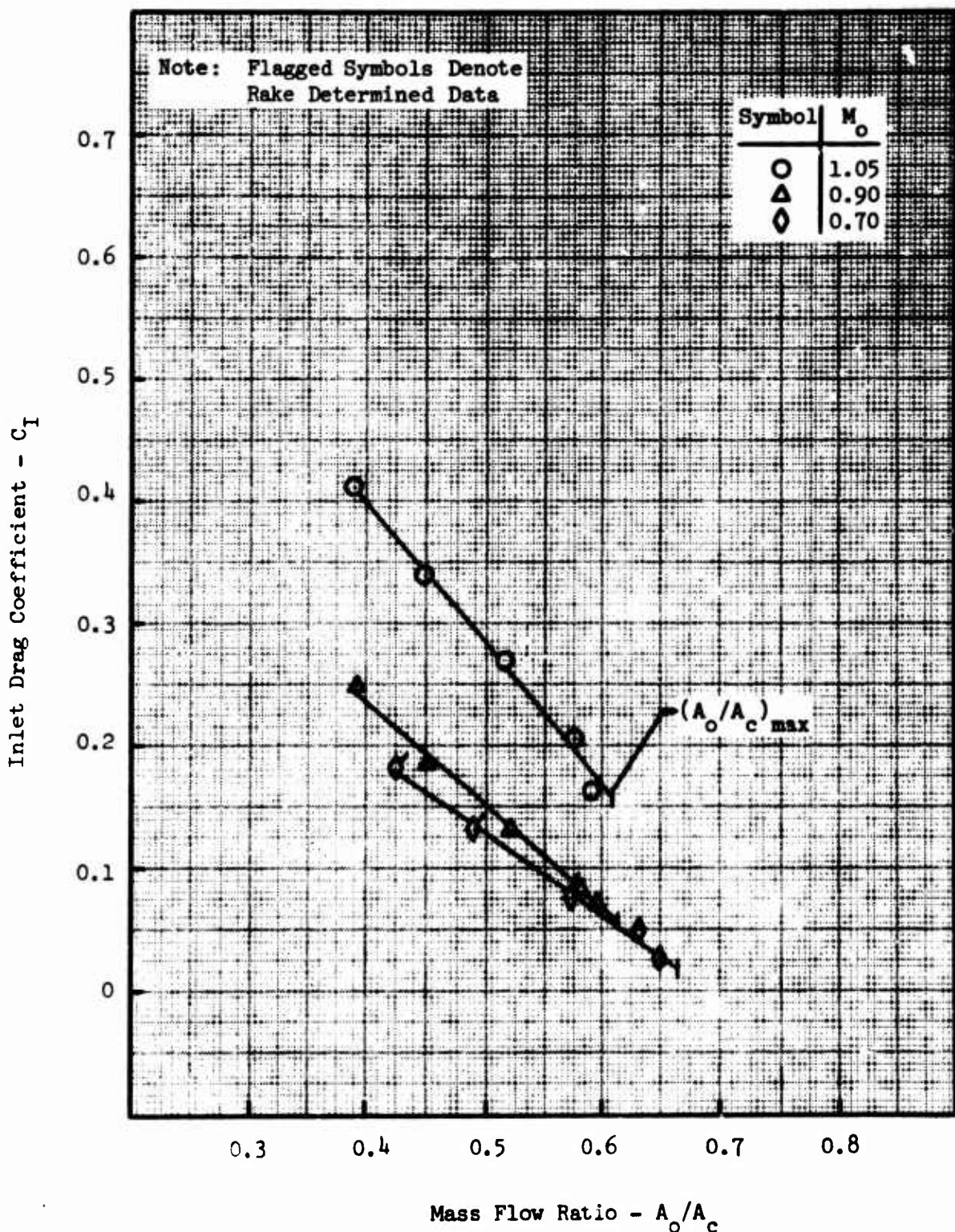


FIGURE B.2 - INLET DRAG COEFFICIENT

F-4 7.5% Model with Forebody
Ramp Configuration (10°-0°)
 $\alpha = 12^\circ$

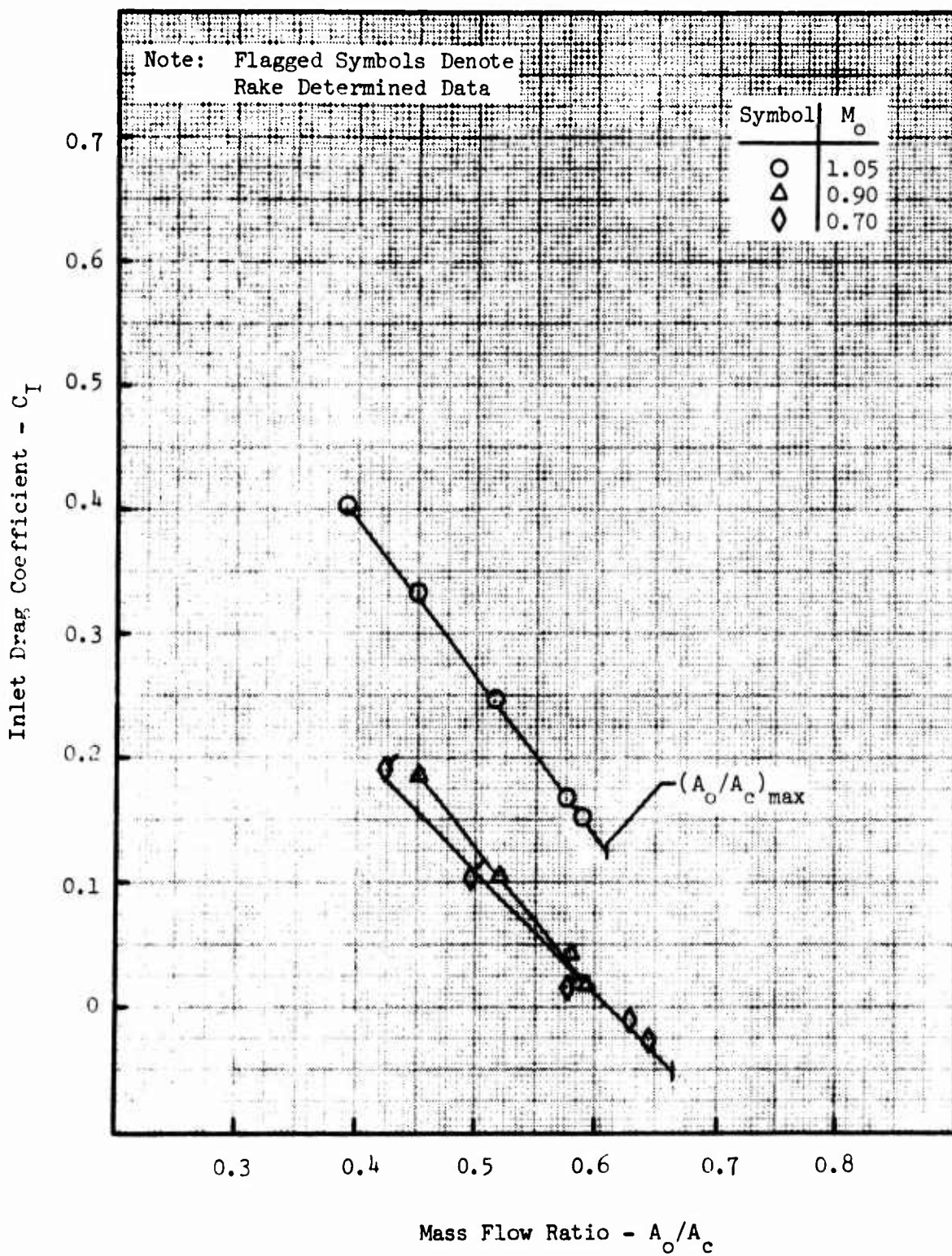


FIGURE B.3 - INLET DRAG COEFFICIENT

F-4 7.5% Model with Forebody
 Ramp Configuration (10° - 8°)
 $\alpha = 0^\circ$

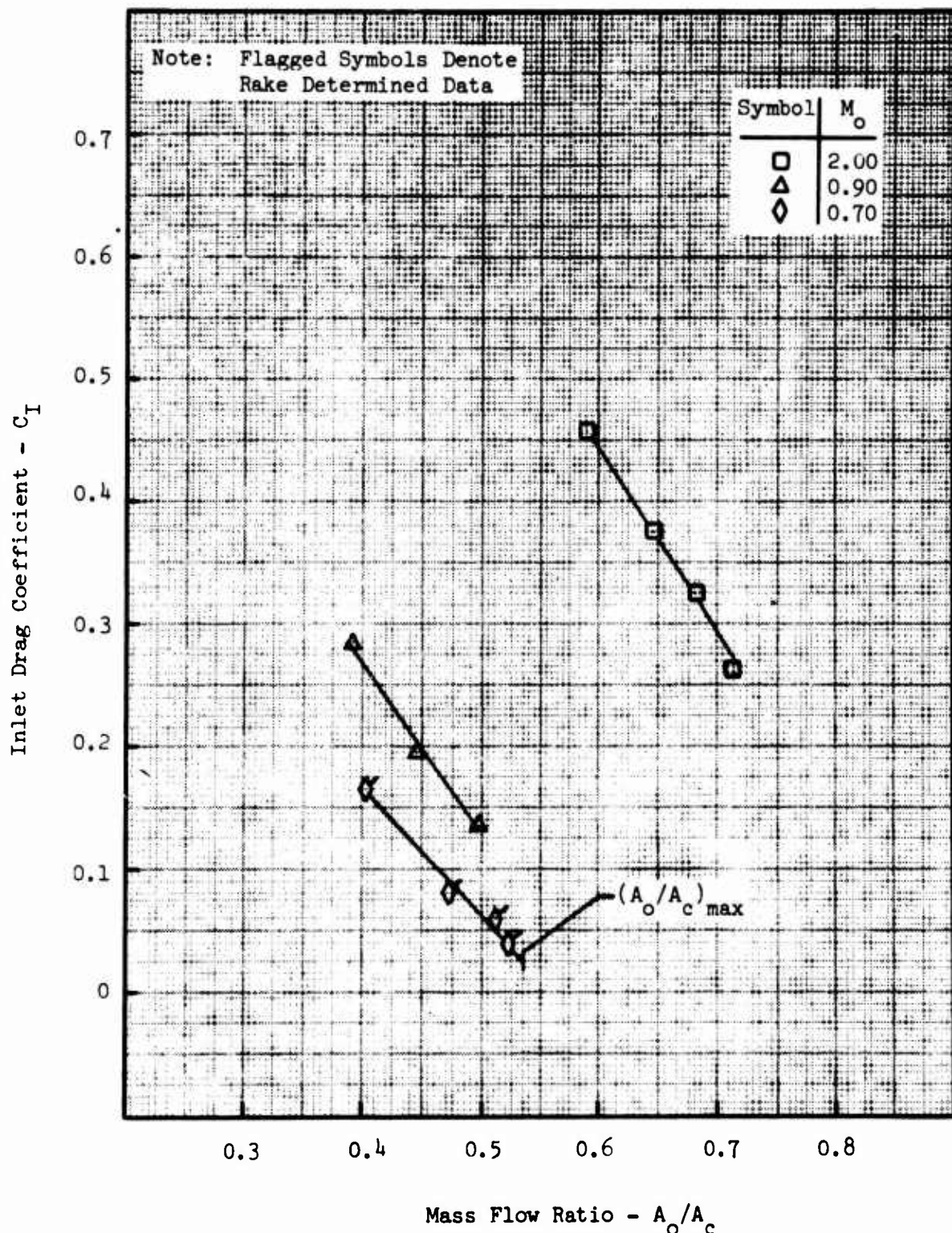


FIGURE B.4 - INLET DRAG COEFFICIENT

F-4 7.5% Model with Forebody
Ramp Configuration (10° - 8°)
 $\alpha = 6^\circ$

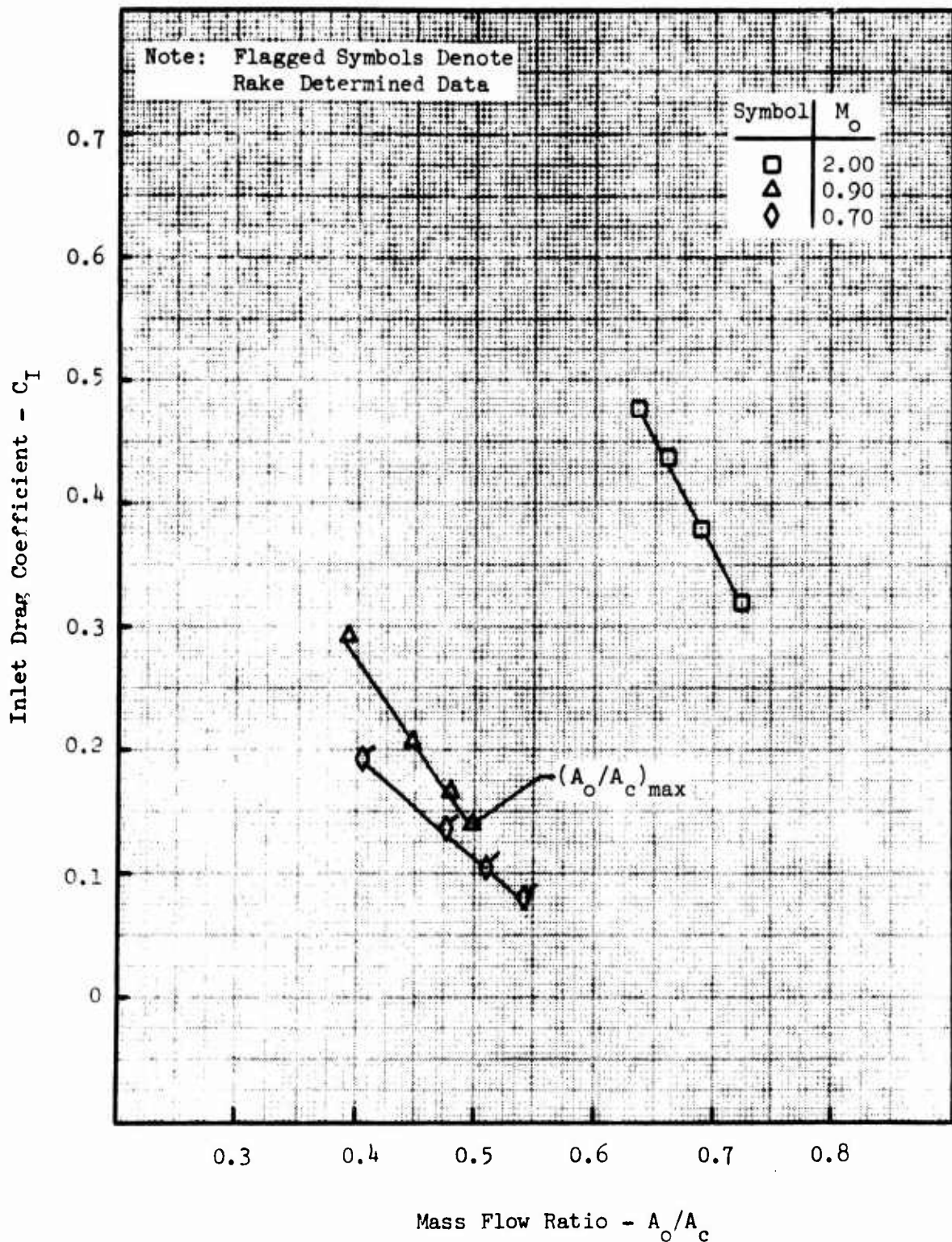


FIGURE B.5 - INLET DRAG COEFFICIENT

F-4 7.5% Model with No Forebody
 Ramp Configuration (10° - 0°)
 $\alpha = 0^\circ$

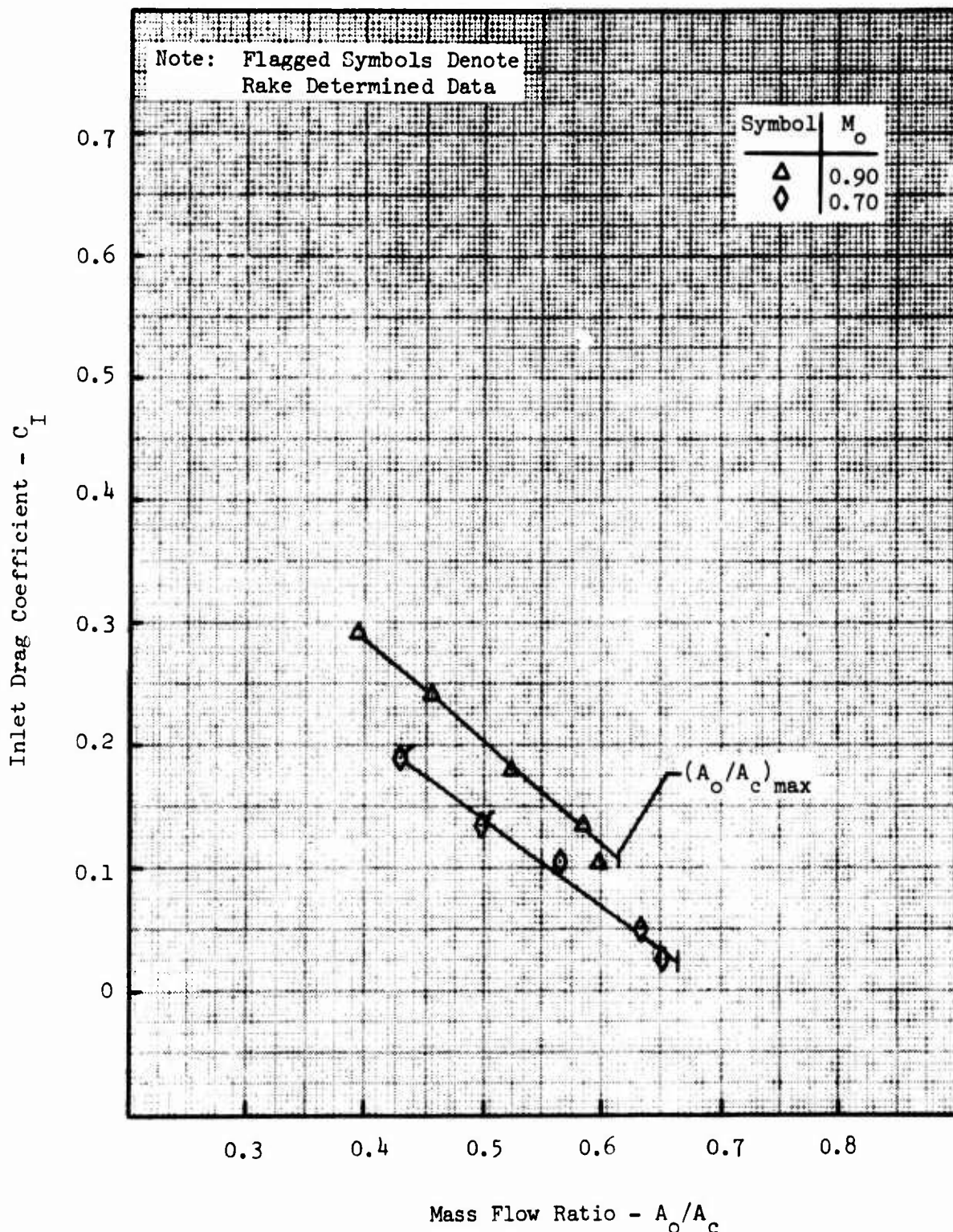


FIGURE B.6 - INLET DRAG COEFFICIENT

F-4 7.5% Model with Splitter Plate
 Ramp Configuration (10° - 0°)
 $\alpha = 12^\circ$

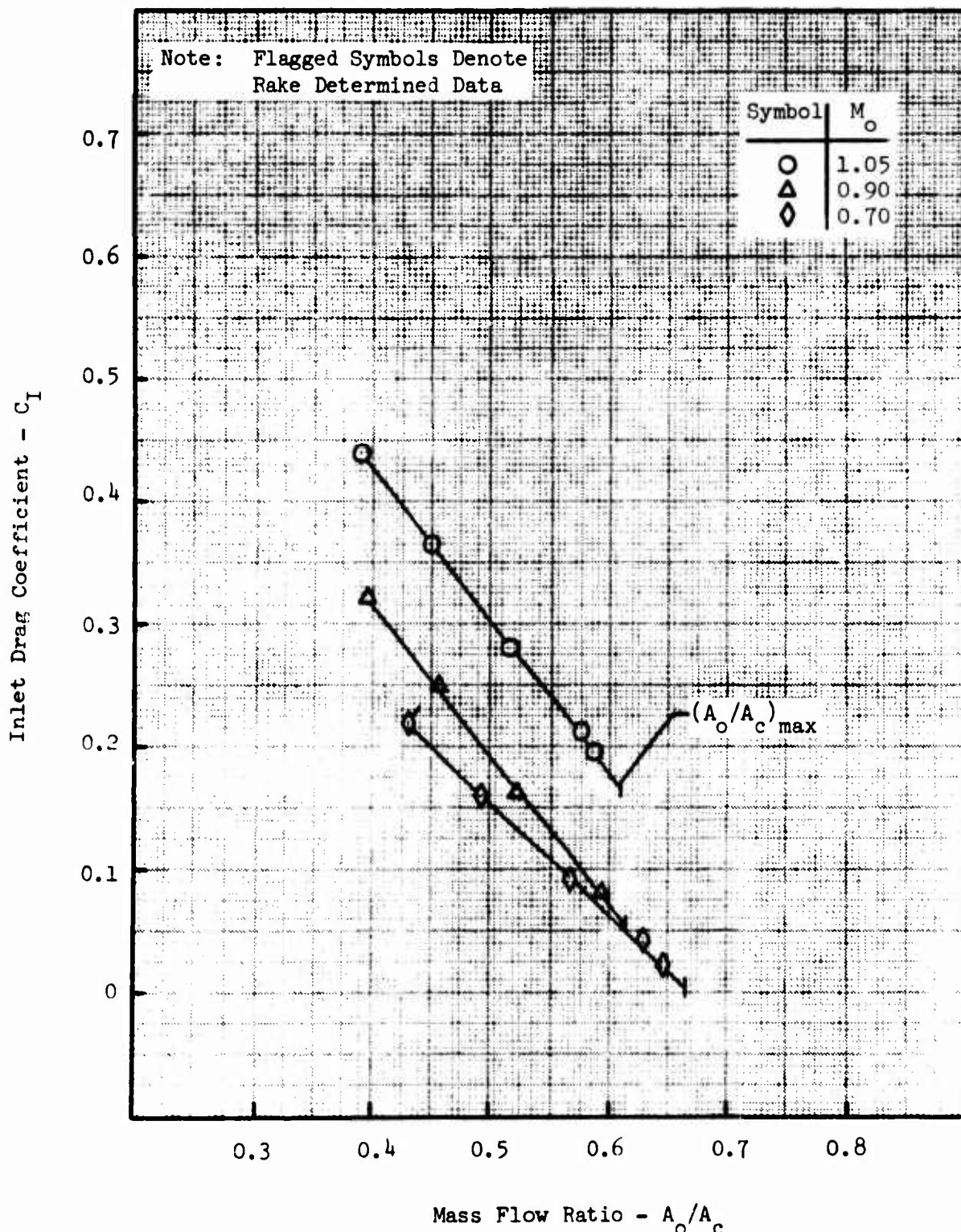


FIGURE B.7 - INLET DRAG COEFFICIENT

F-4 7.5% Model with Splitter Plate
 Ramp Configuration (10°-8°)
 $\alpha = 6^\circ$

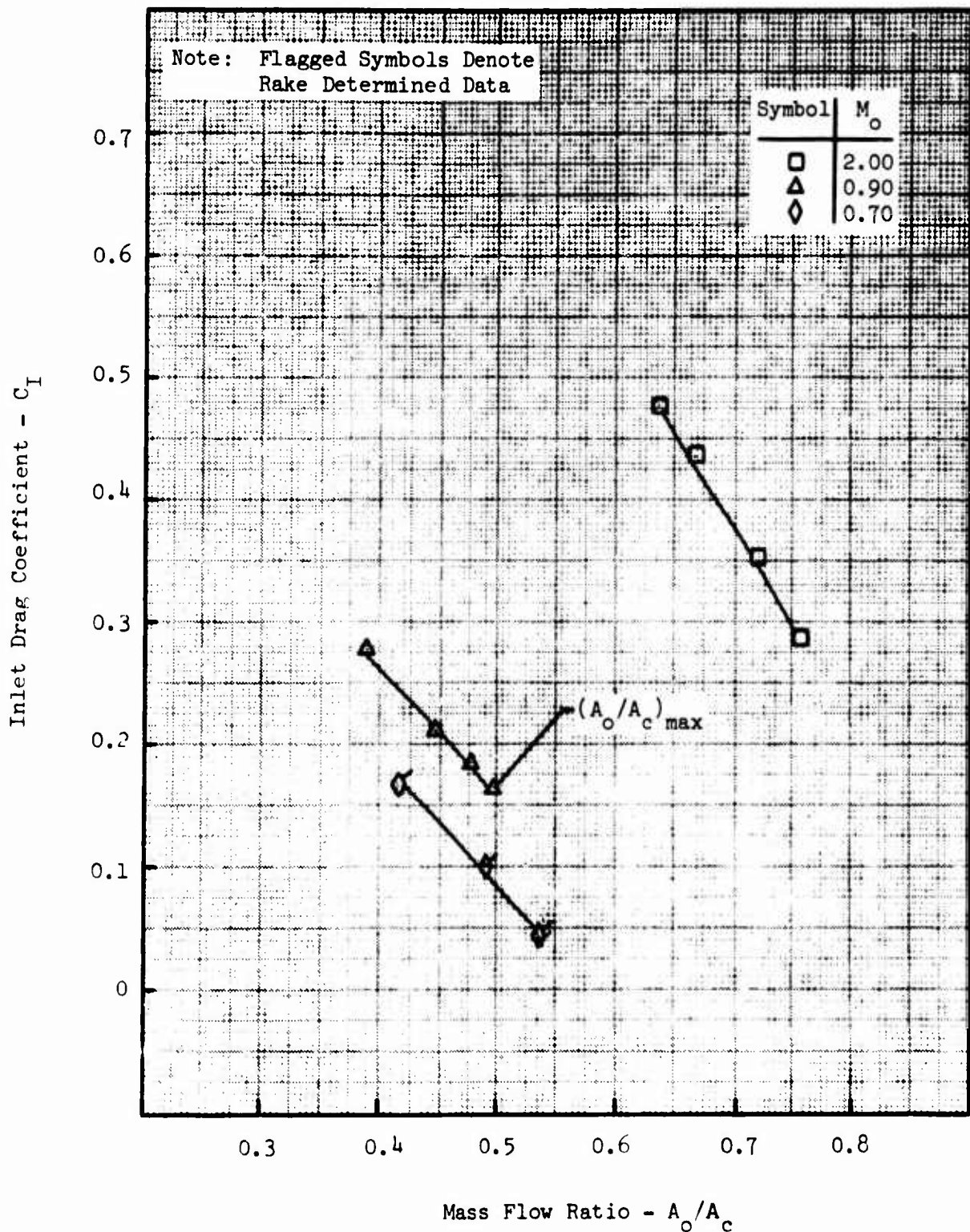


FIGURE B.8 - INLET DRAG COEFFICIENT

F-4 7.5% Model with Forebody
Ramp Configuration (10° - 0°)
 $\alpha = 0^\circ$

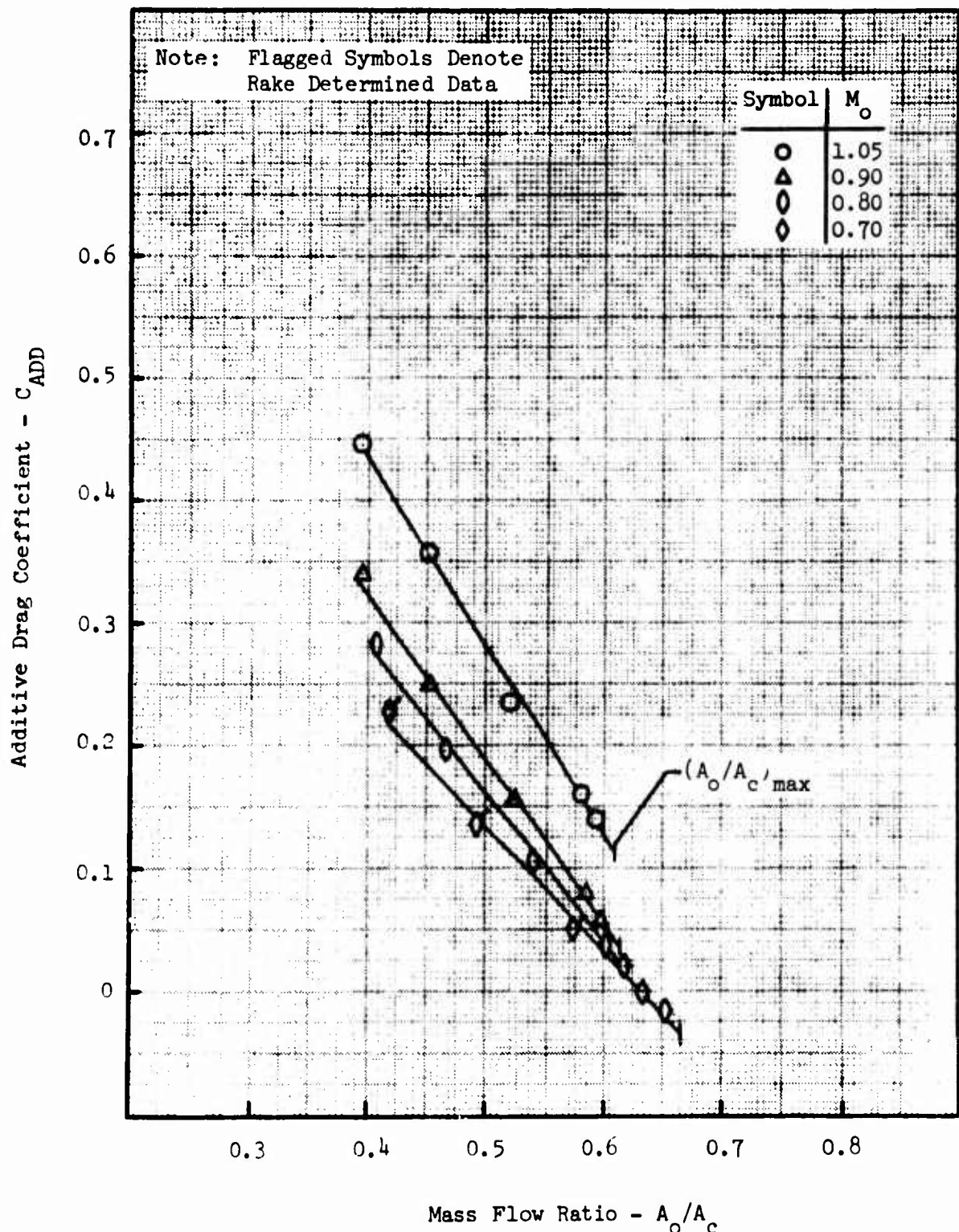


FIGURE B.9 - ADDITIVE DRAG COEFFICIENT

F-4 7.5% Model with Forebody
 Ramp Configuration (10°-0°)
 $\alpha = 6^\circ$

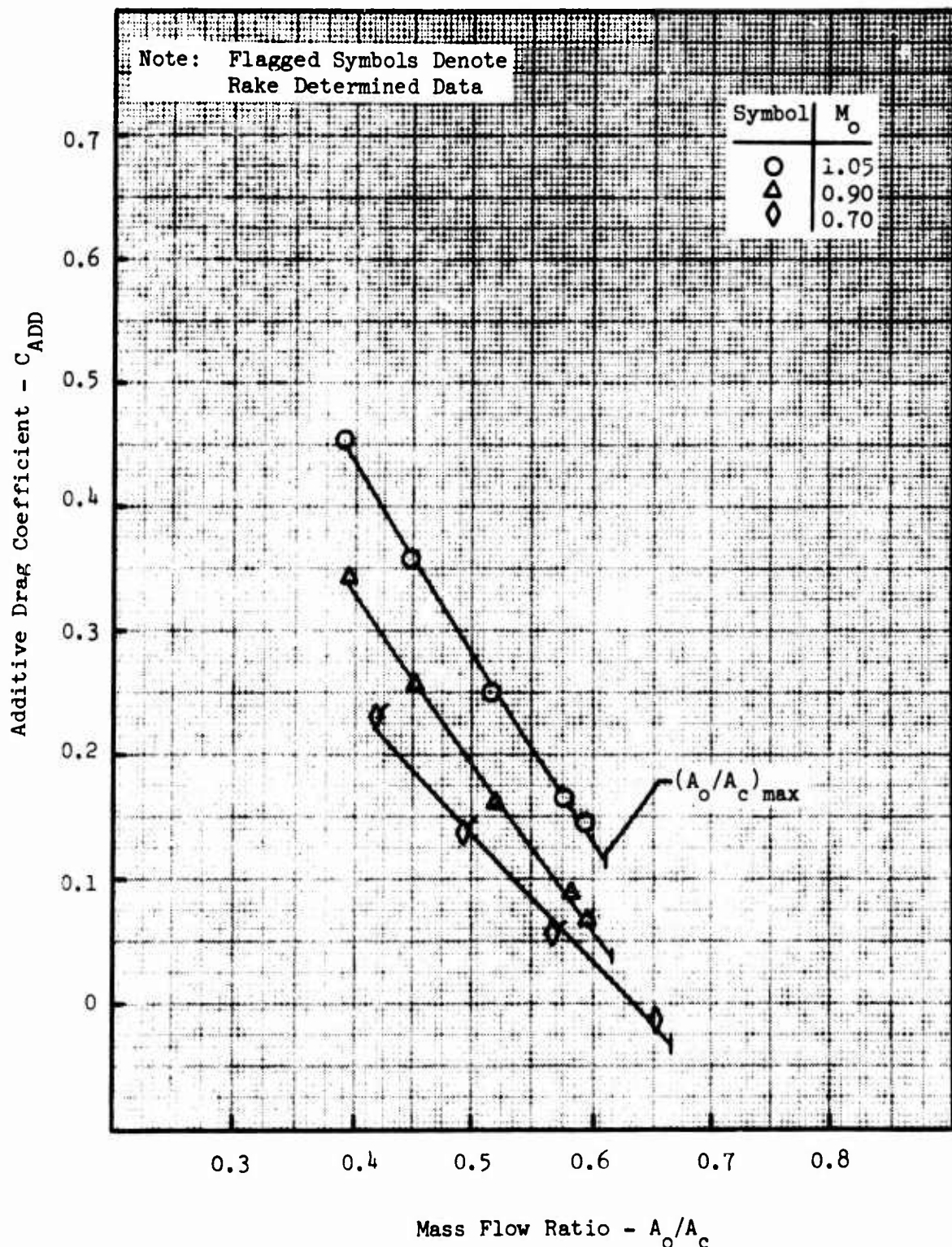


FIGURE B.10 - ADDITIVE DRAG COEFFICIENT

F-4 7.5% Model with Forebody
Ramp Configuration (10° - 0°)
 $\alpha = 12^\circ$

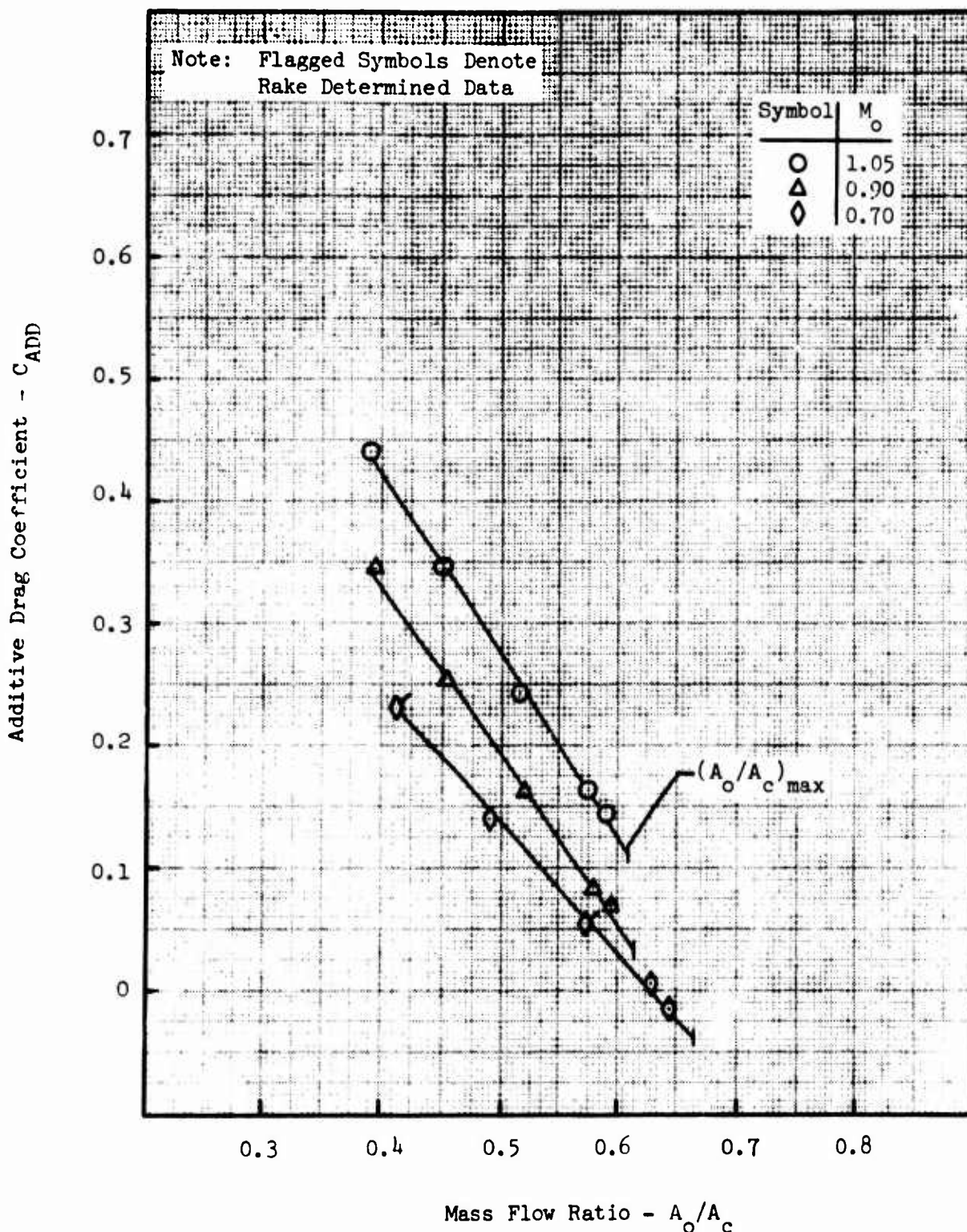


FIGURE B.11 - ADDITIVE DRAG COEFFICIENT

F-4 7.5% Model with No Forebody
 Ramp Configuration (10°-0°)
 $\alpha = 0^\circ$

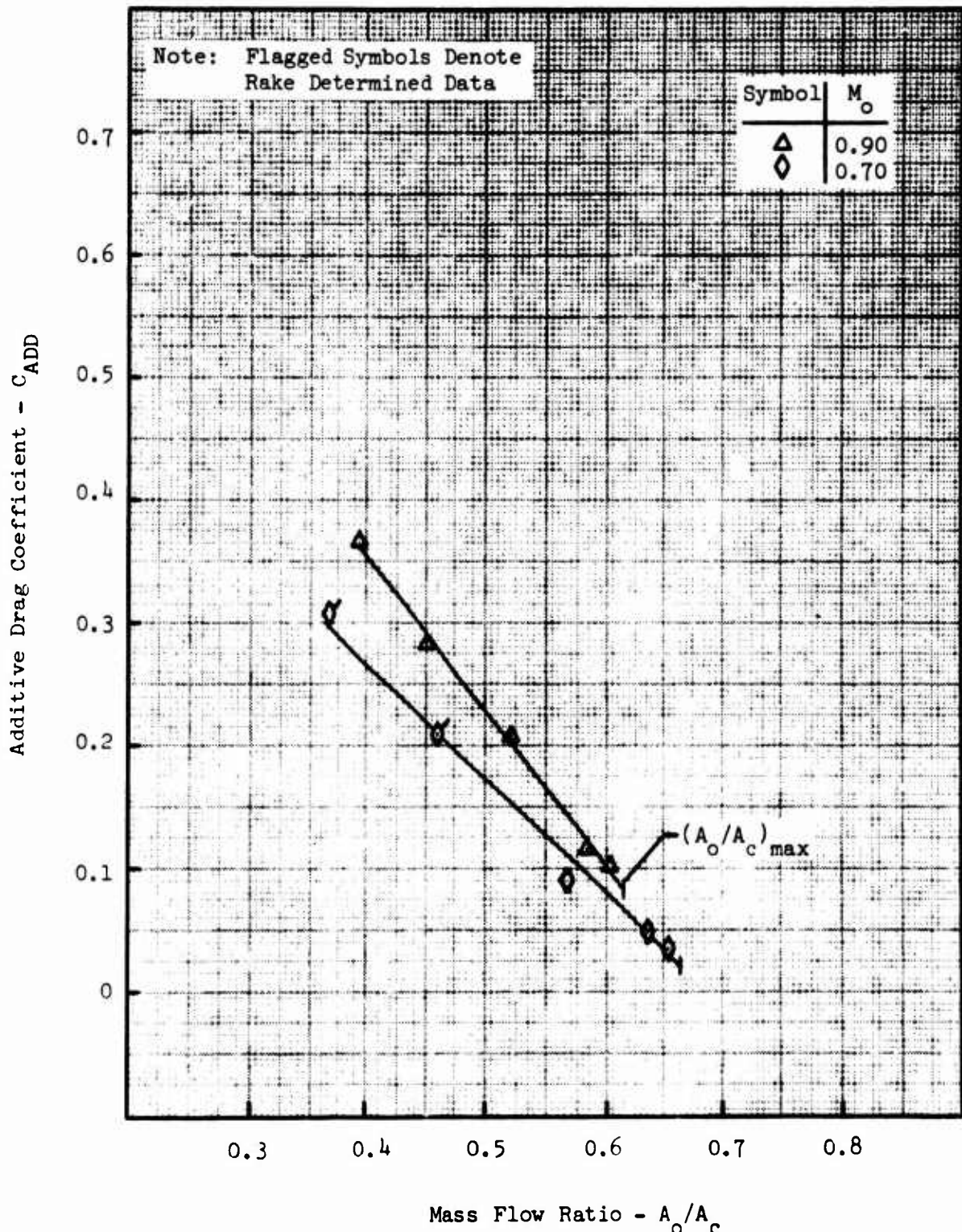


FIGURE B.12 - ADDITIVE DRAG COEFFICIENT

F-4 7.5% Model with Splitter Plate
 Ramp Configuration (10° - 0°)
 $\alpha = 12^\circ$

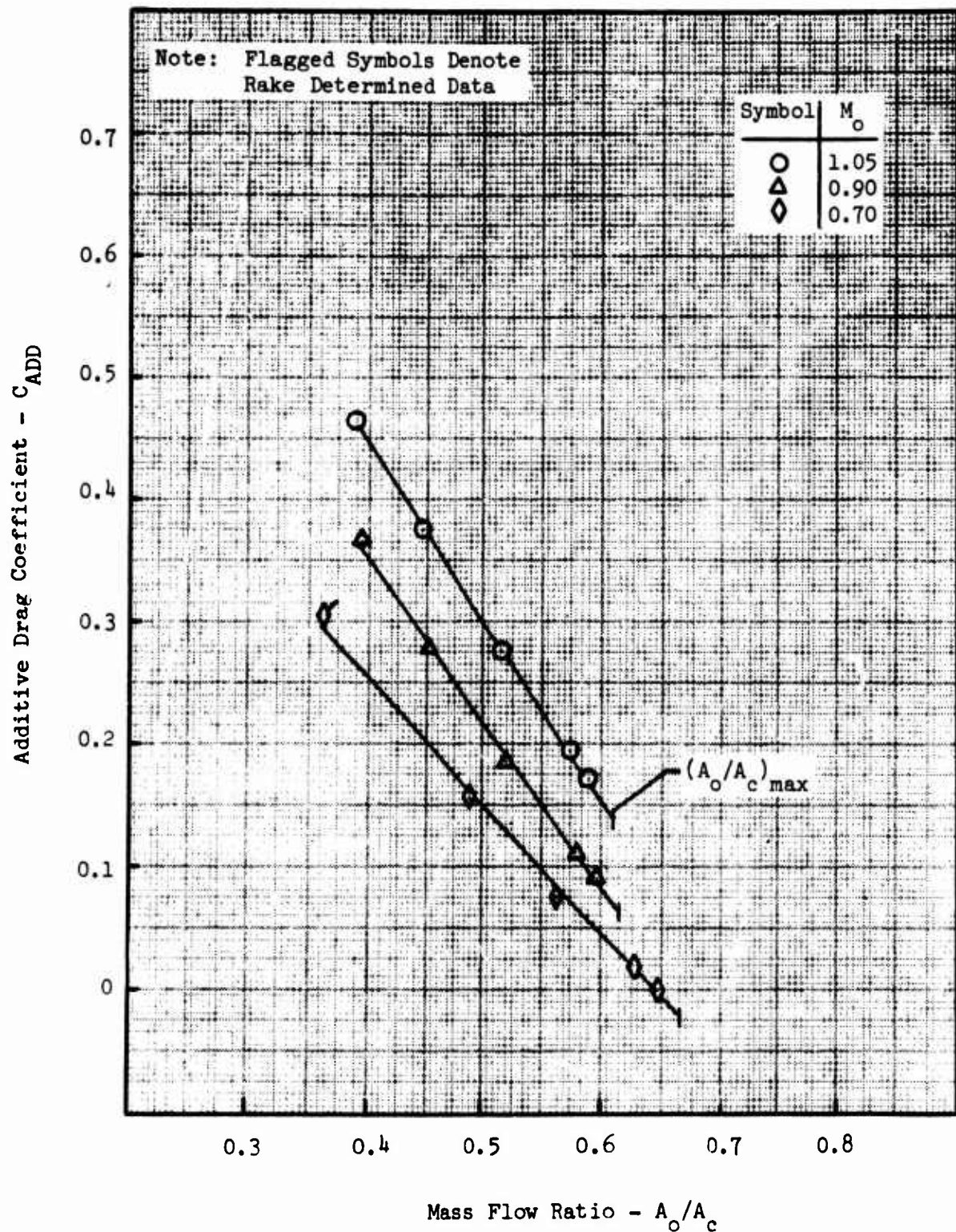


FIGURE B.13 - ADDITIVE DRAG COEFFICIENT

F-4 7.5% Model with Forebody
Ramp Configuration (10°-0°)
 $\alpha = 0^\circ$

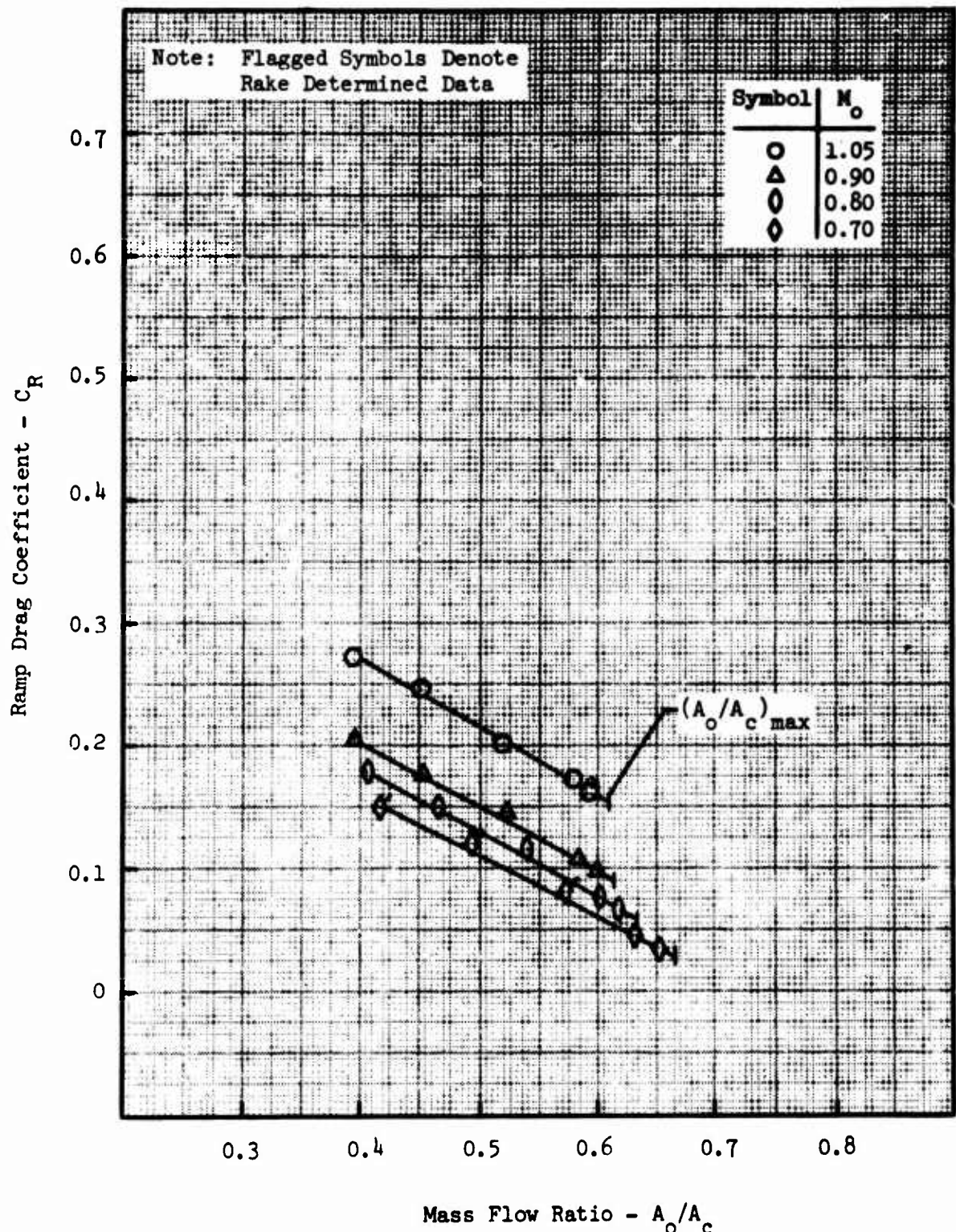


FIGURE B.14 - RAMP DRAG COEFFICIENT

F-4 7.5% Model with Forebody
 Ramp Configuration (10° - 0°)
 $\alpha = 6^\circ$

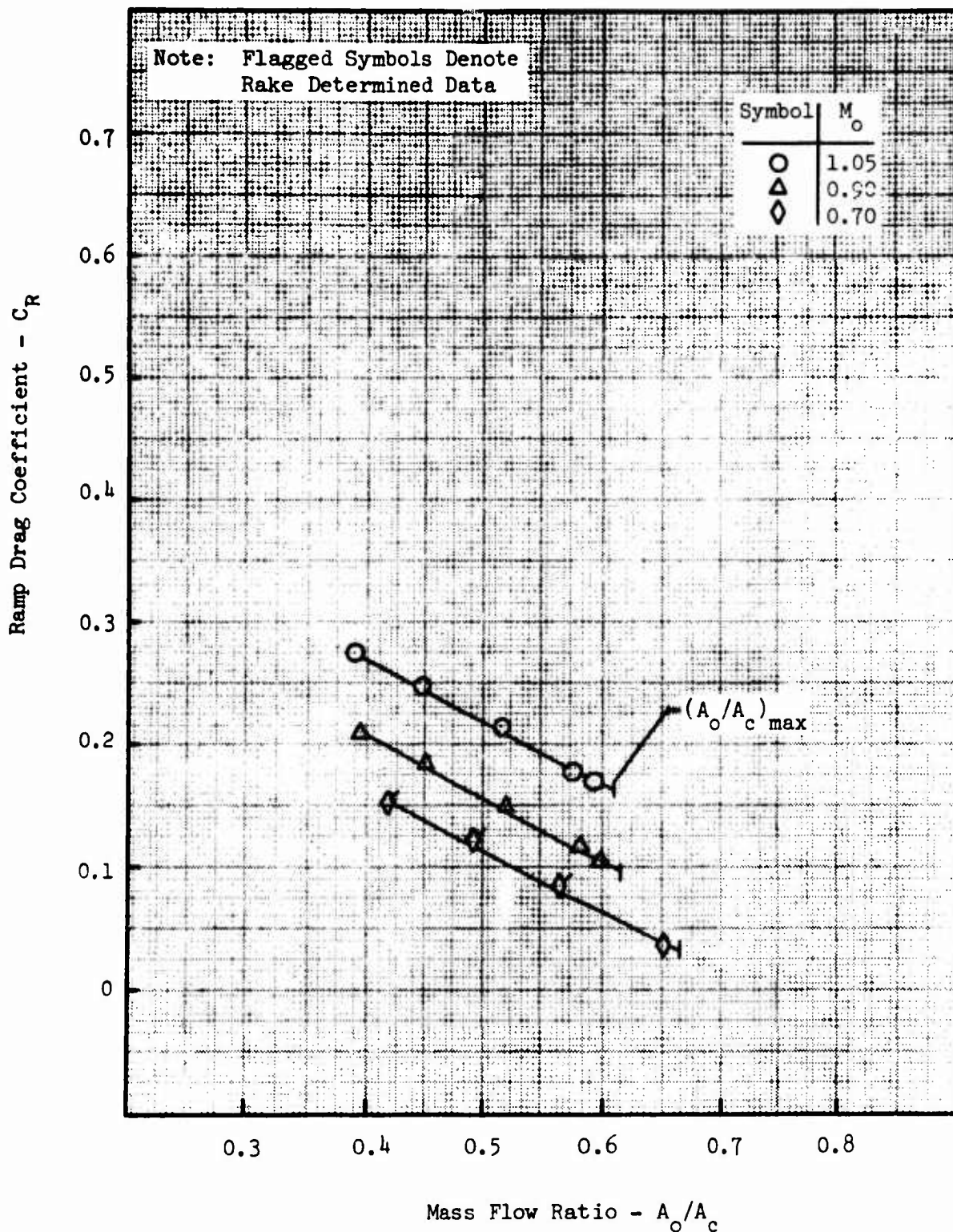


FIGURE B.15 - RAMP DRAG COEFFICIENT

F-4 7.5% Model with Forebody
Ramp Configuration (10° - 0°)
 $\alpha = 12^\circ$

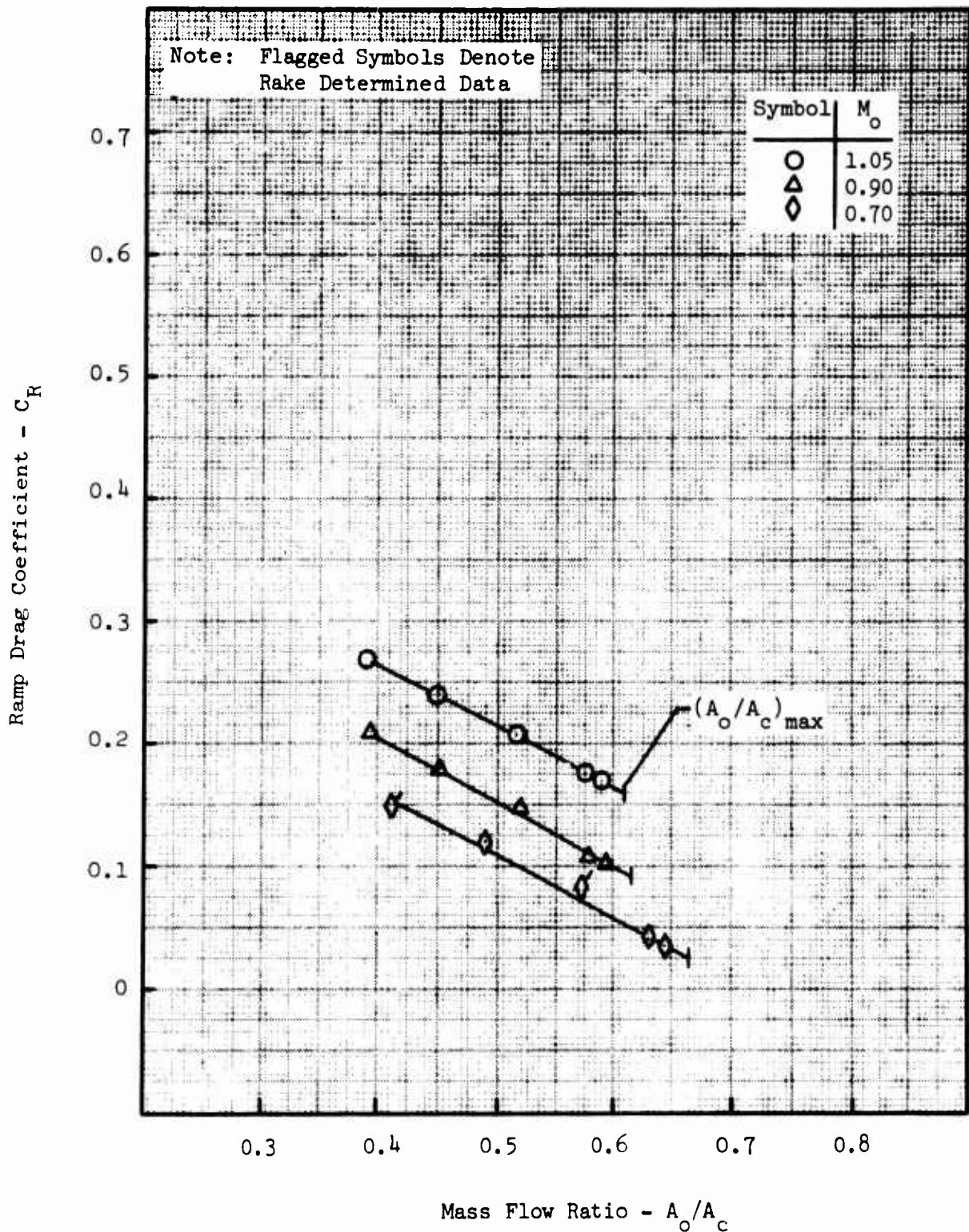


FIGURE B.16 - RAMP DRAG COEFFICIENT

F-4 7.5% Model with No Forebody
 Ramp Configuration (10° - 0°)
 $\alpha = 0^\circ$

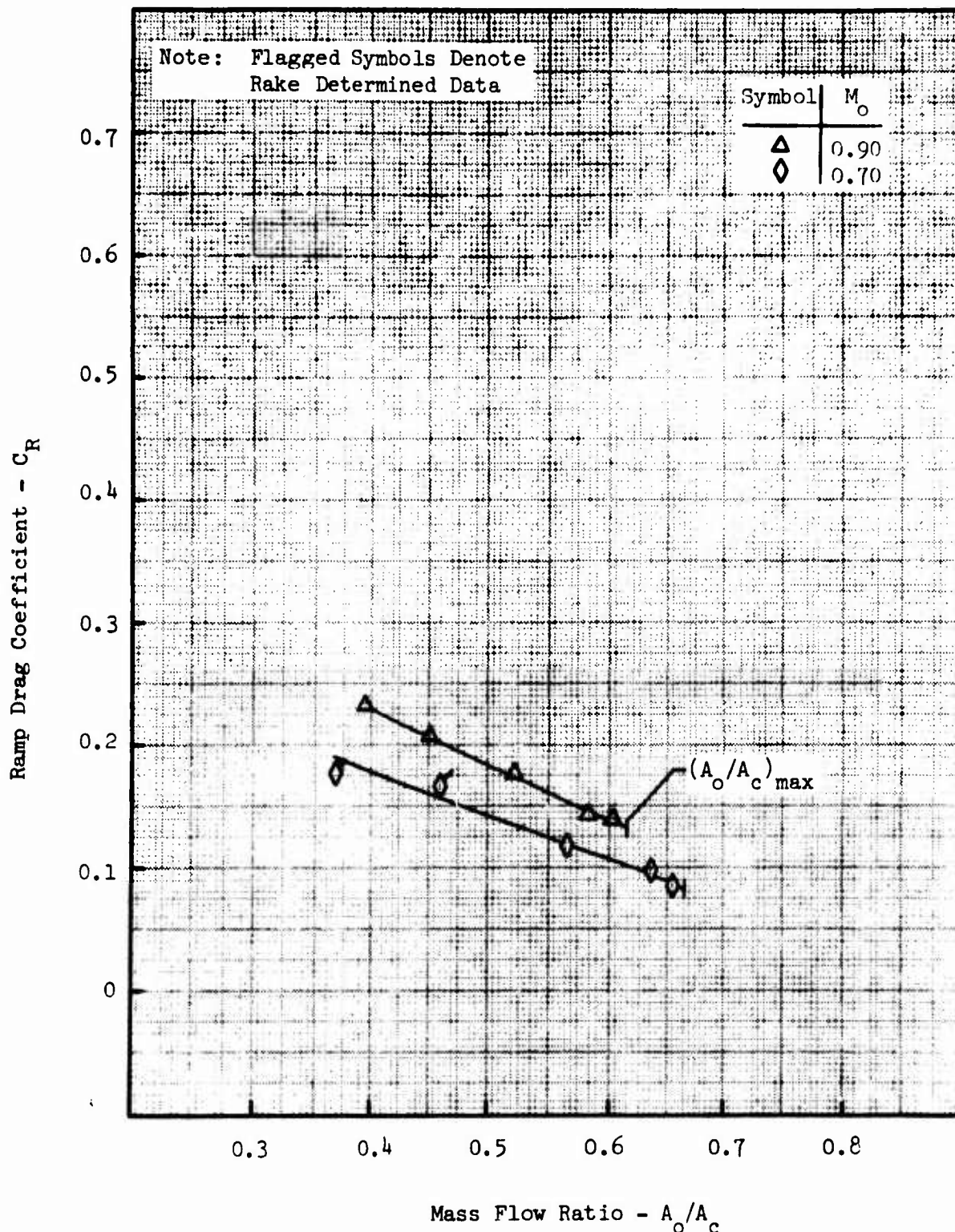


FIGURE B.17 - RAMP DRAG COEFFICIENT

F-4 7.5% Model with Splitter Plate
 Ramp Configuration (10°-0°)
 $\alpha = 12^\circ$

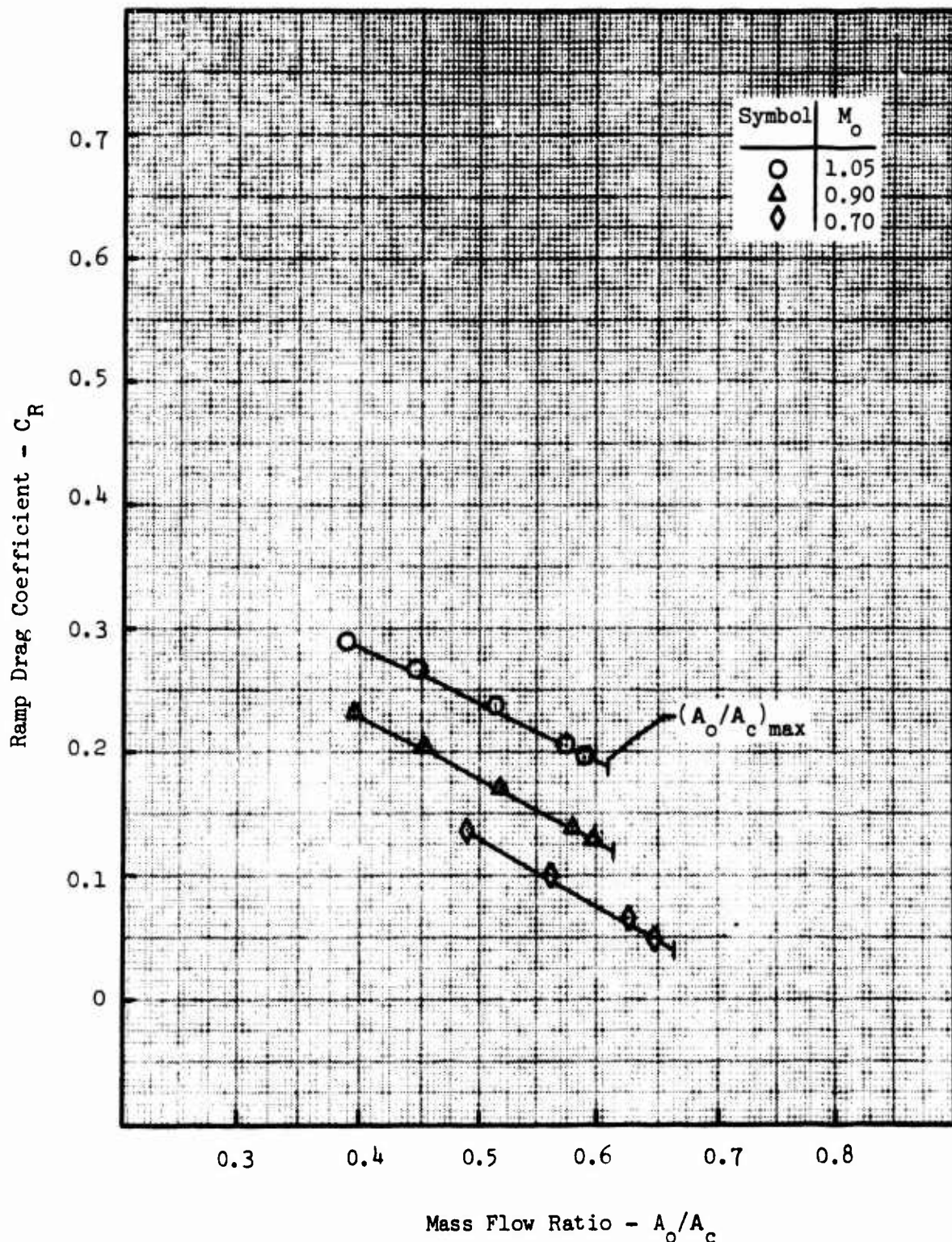


FIGURE B.18 - RAMP DRAG COEFFICIENT

APPENDIX C
AXISYMMETRIC INLET
PRESSURE DISTRIBUTIONS

Axisymmetric Single Cone Inlet Model
Configuration A10
 $\alpha = 0^\circ$

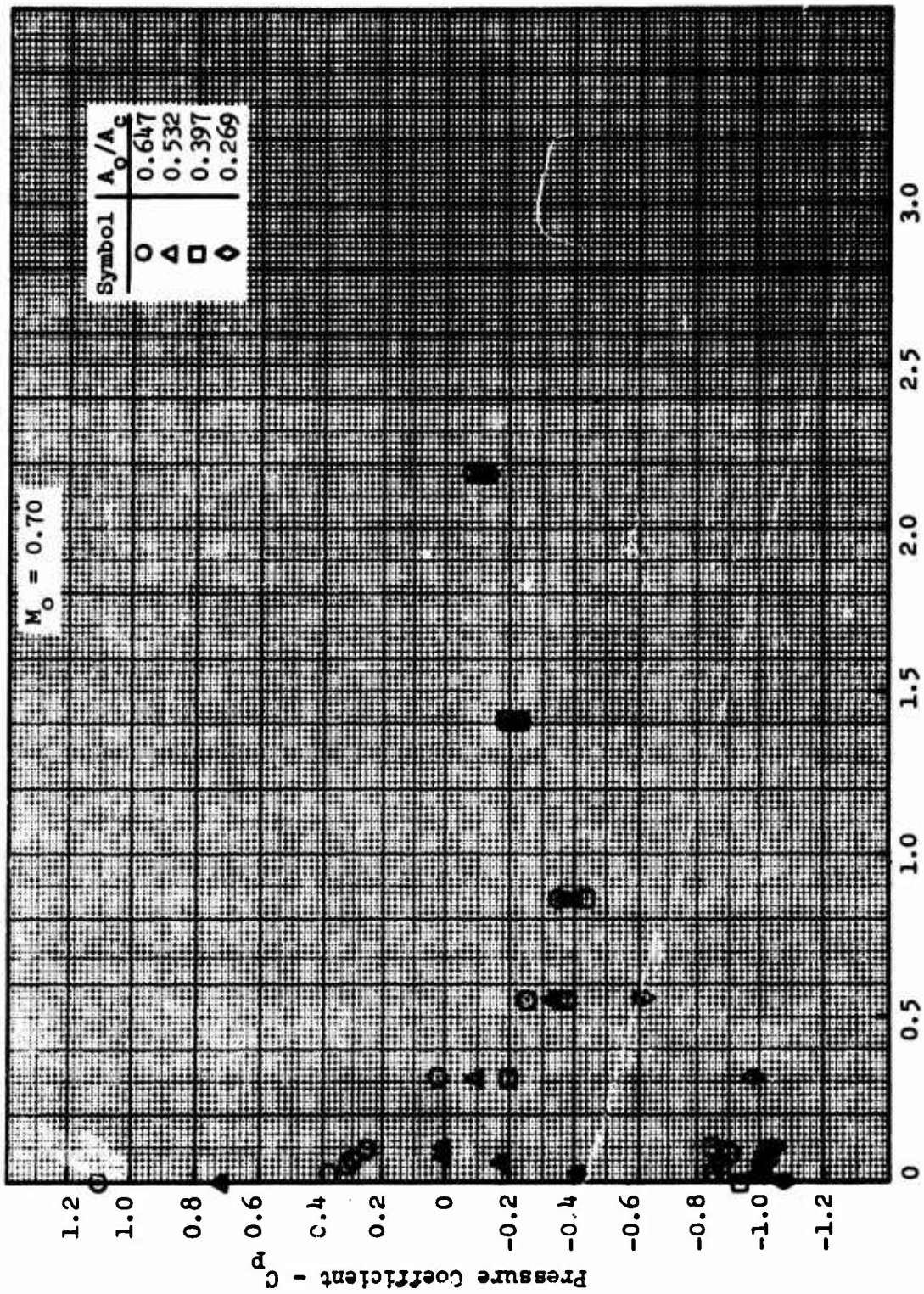


FIGURE C.1 - COWL PRESSURE COEFFICIENT

Axisymmetric Single Cone Inlet Model
Configuration A10
 $\alpha = 0^\circ$

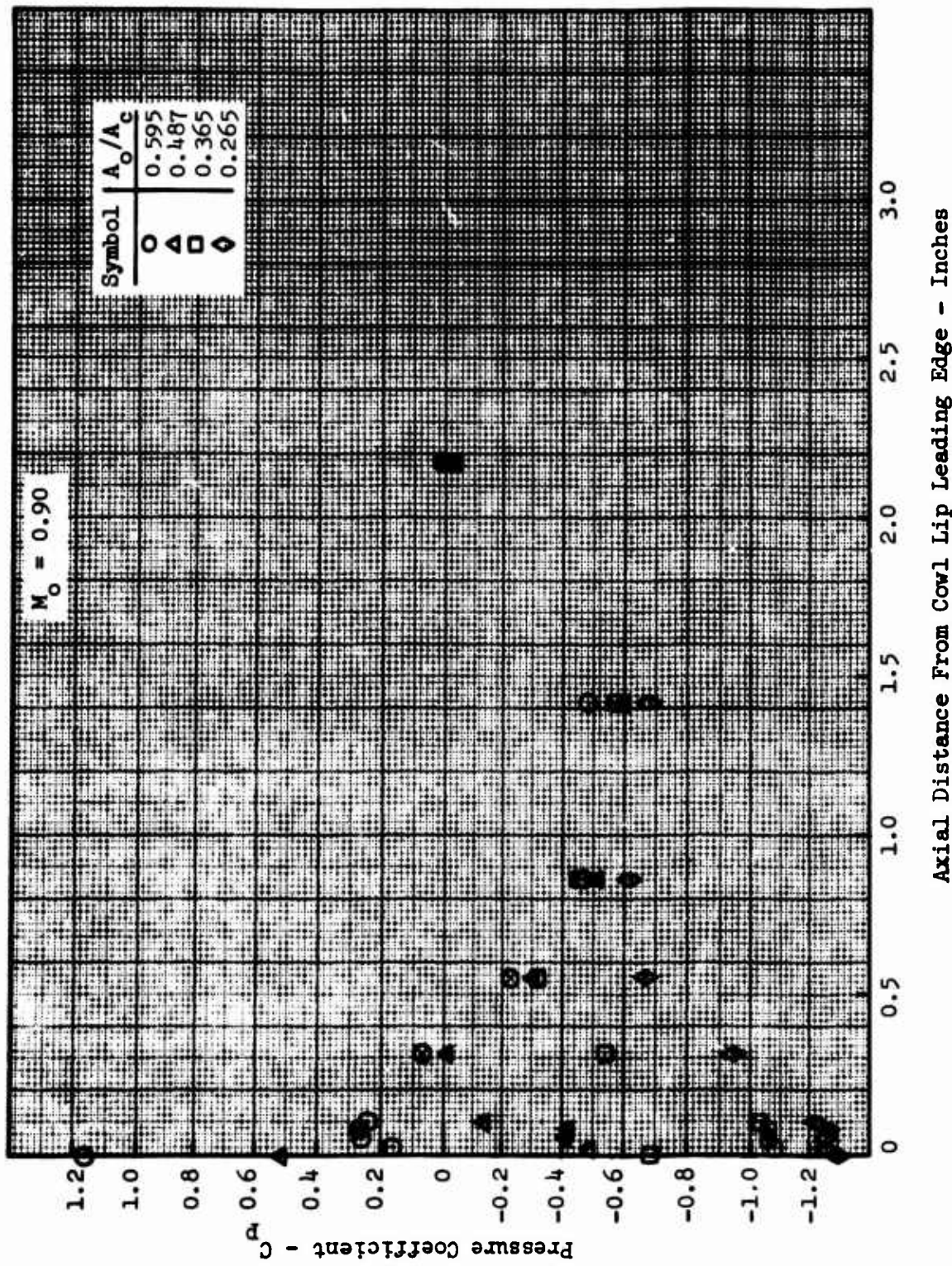


FIGURE C.2 - COWL PRESSURE COEFFICIENT

Axisymmetric Single Cone Inlet Model
Configuration A10
 $\alpha = 0^\circ$

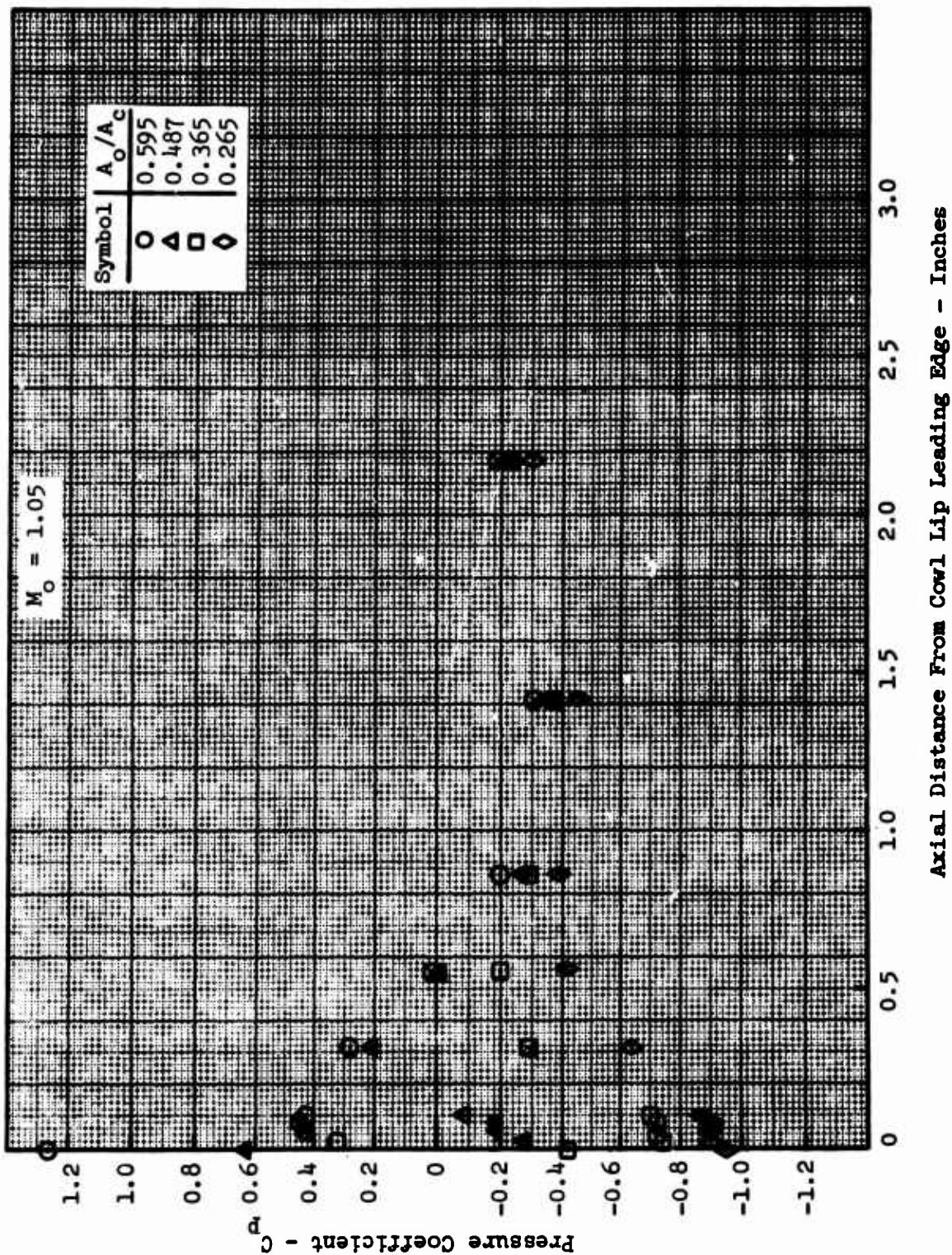


FIGURE C.3 - COWL PRESSURE COEFFICIENT

Axisymmetric Single Cone Inlet Model
 Configuration A10
 $\alpha = 0^\circ$

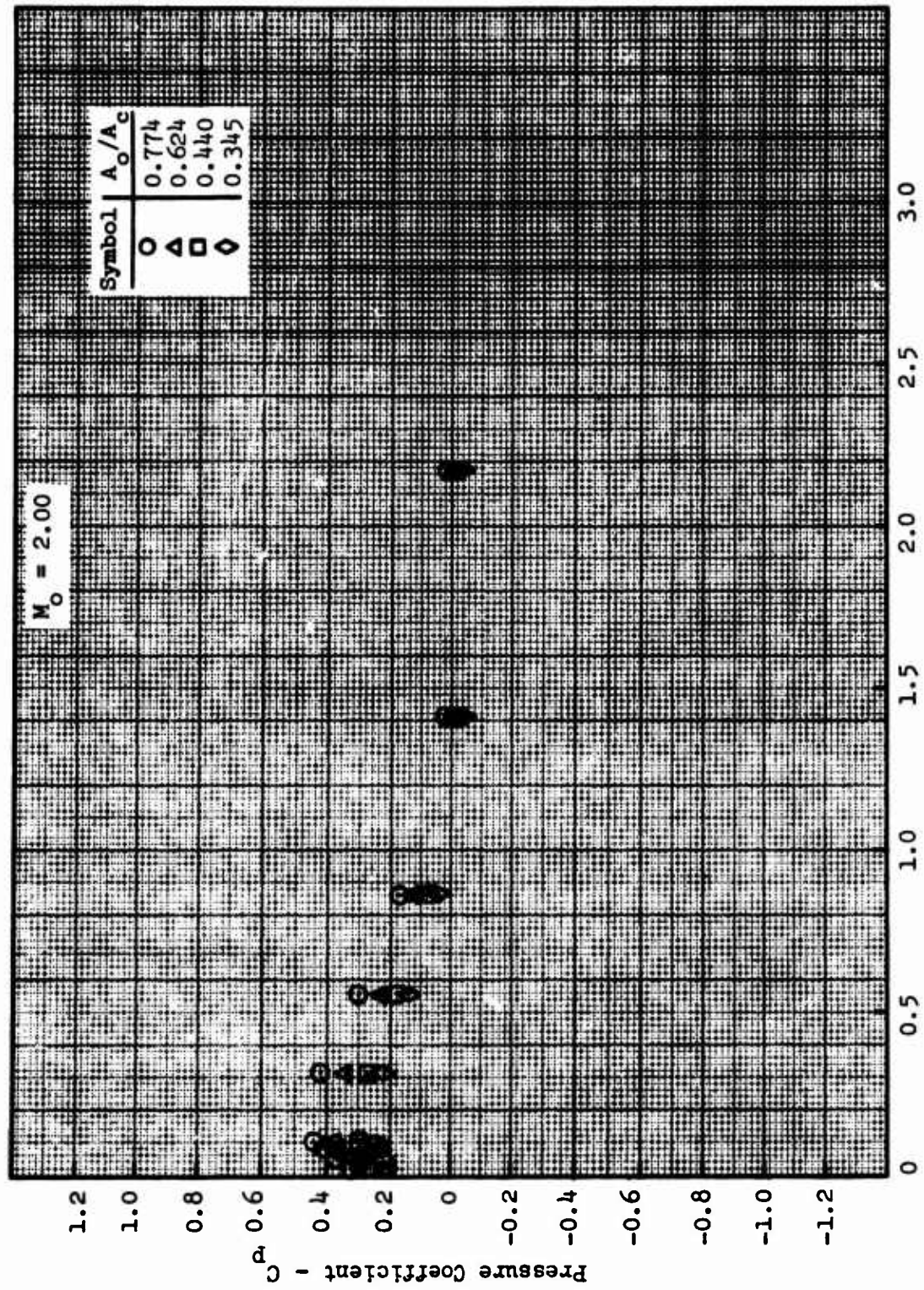


FIGURE C.4 - COWL PRESSURE COEFFICIENT

**Axisymmetric Single Cone Inlet Model
Configuration A10**

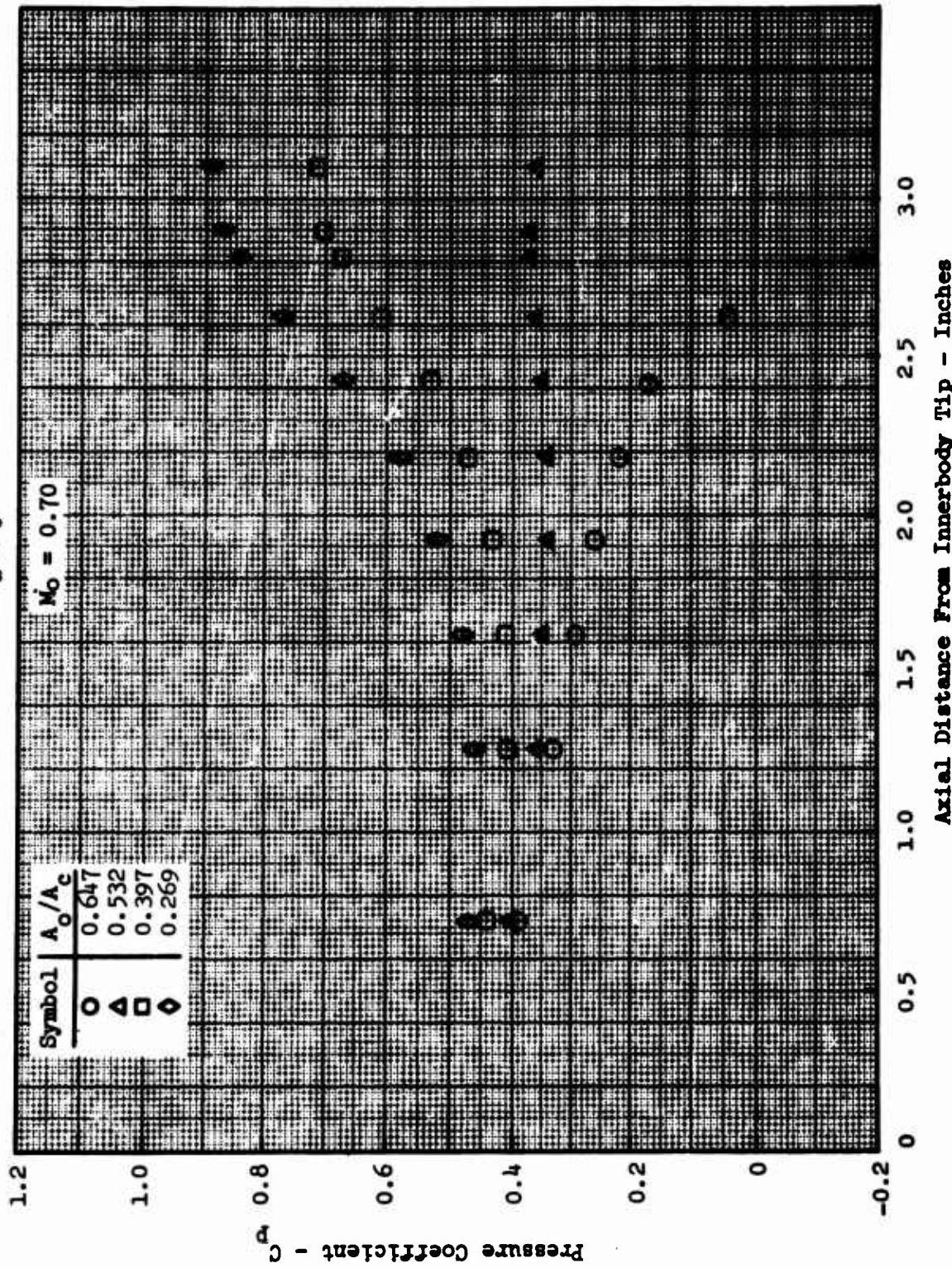


FIGURE C.5 - INNERBODY PRESSURE COEFFICIENT

Axisymmetric Single Cone Inlet Model
Configuration A10
 $\alpha = 0^\circ$

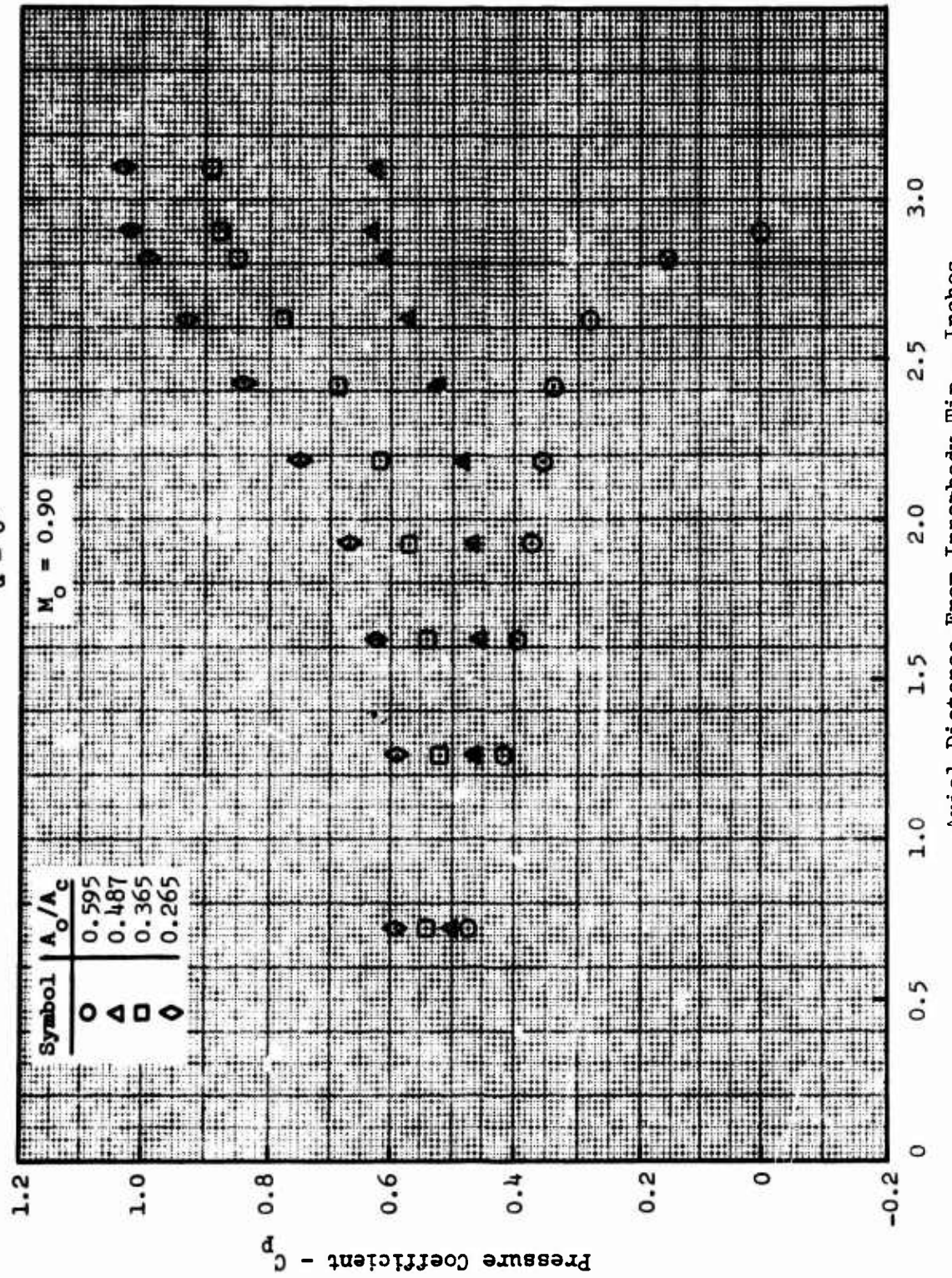


FIGURE C.6 - INNERBODY PRESSURE COEFFICIENT

Axisymmetric Single Cone Inlet Model
Configuration A10
 $\alpha = 0^\circ$

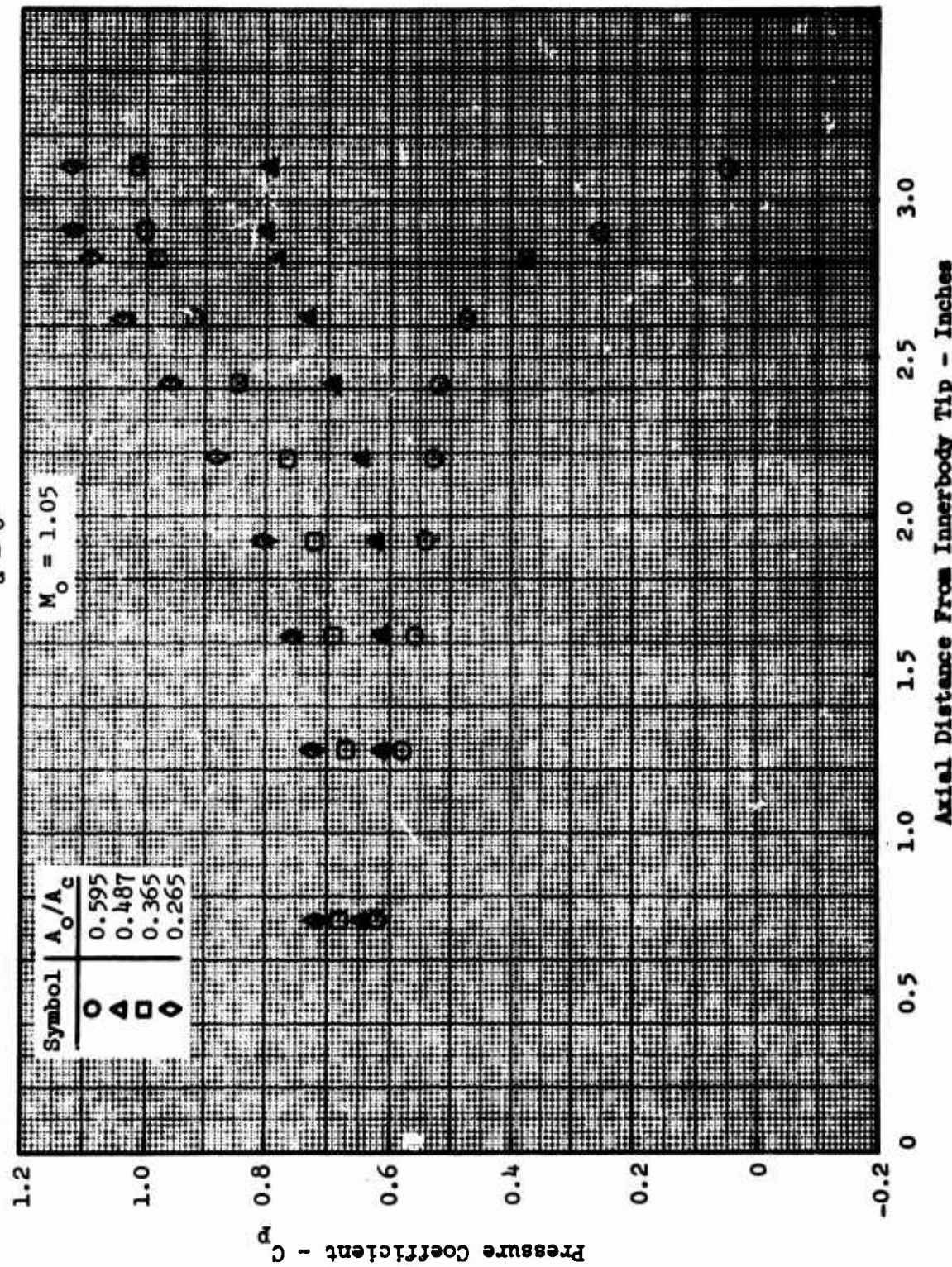


FIGURE C.7 - INNERBODY PRESSURE COEFFICIENT

Axisymmetric Single Cone Inlet Model
Configuration A10
 $\alpha = 0^\circ$

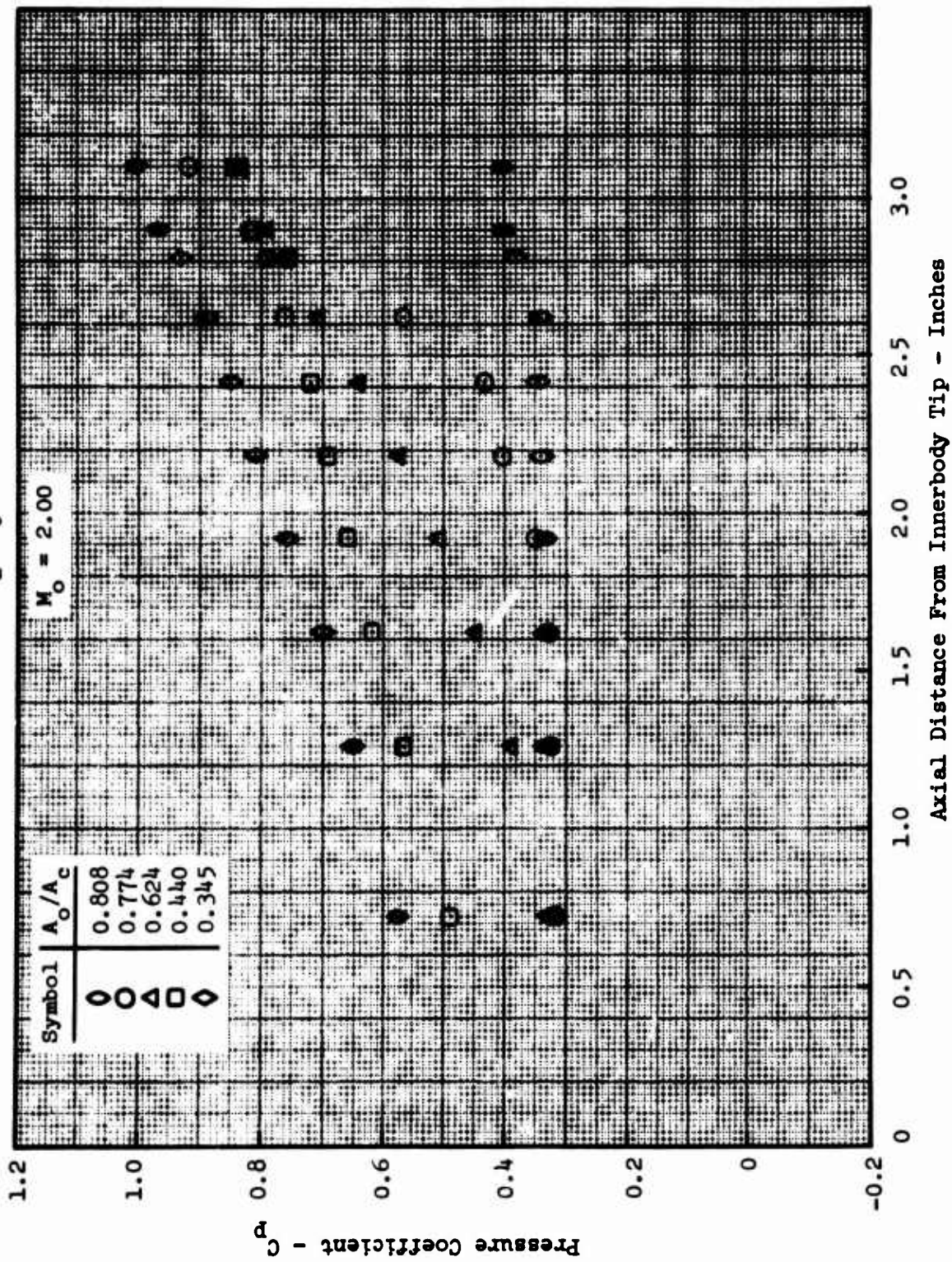


FIGURE C.8 - INNERBODY PRESSURE COEFFICIENT

APPENDIX D
TEST RESULTS FOR THE
TWO-DIMENSIONAL INLET MODELS

Two-Dimensional Inlet Model
Configuration 1
 $\alpha = 0^\circ$

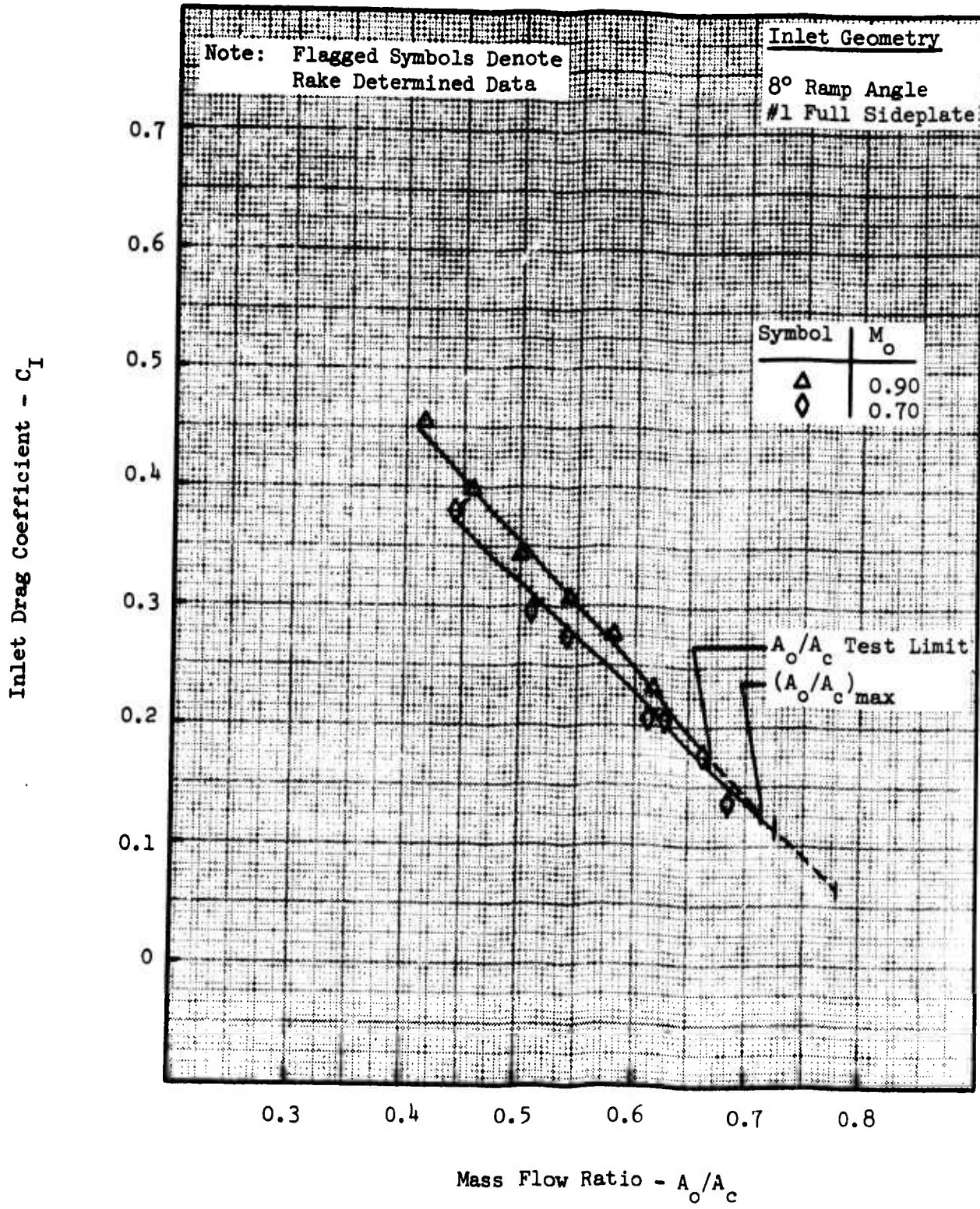


FIGURE D.1 - INLET DRAG COEFFICIENT

Two-Dimensional Inlet Model
Configuration 2
 $\alpha = 0^\circ$

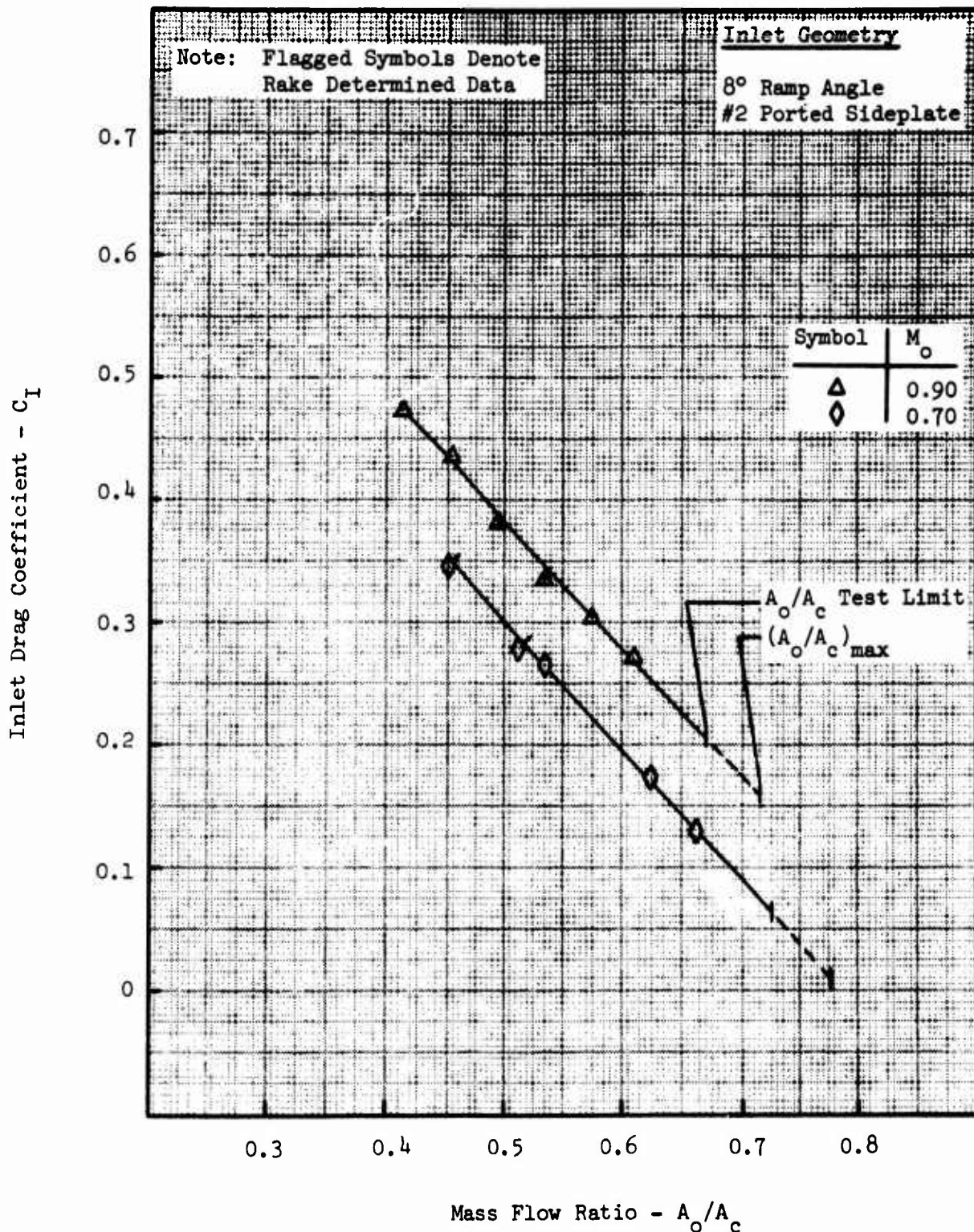


FIGURE D.2 - INLET DRAG COEFFICIENT

Two-Dimensional Inlet Model
Configuration 3
 $\alpha = 0^\circ$

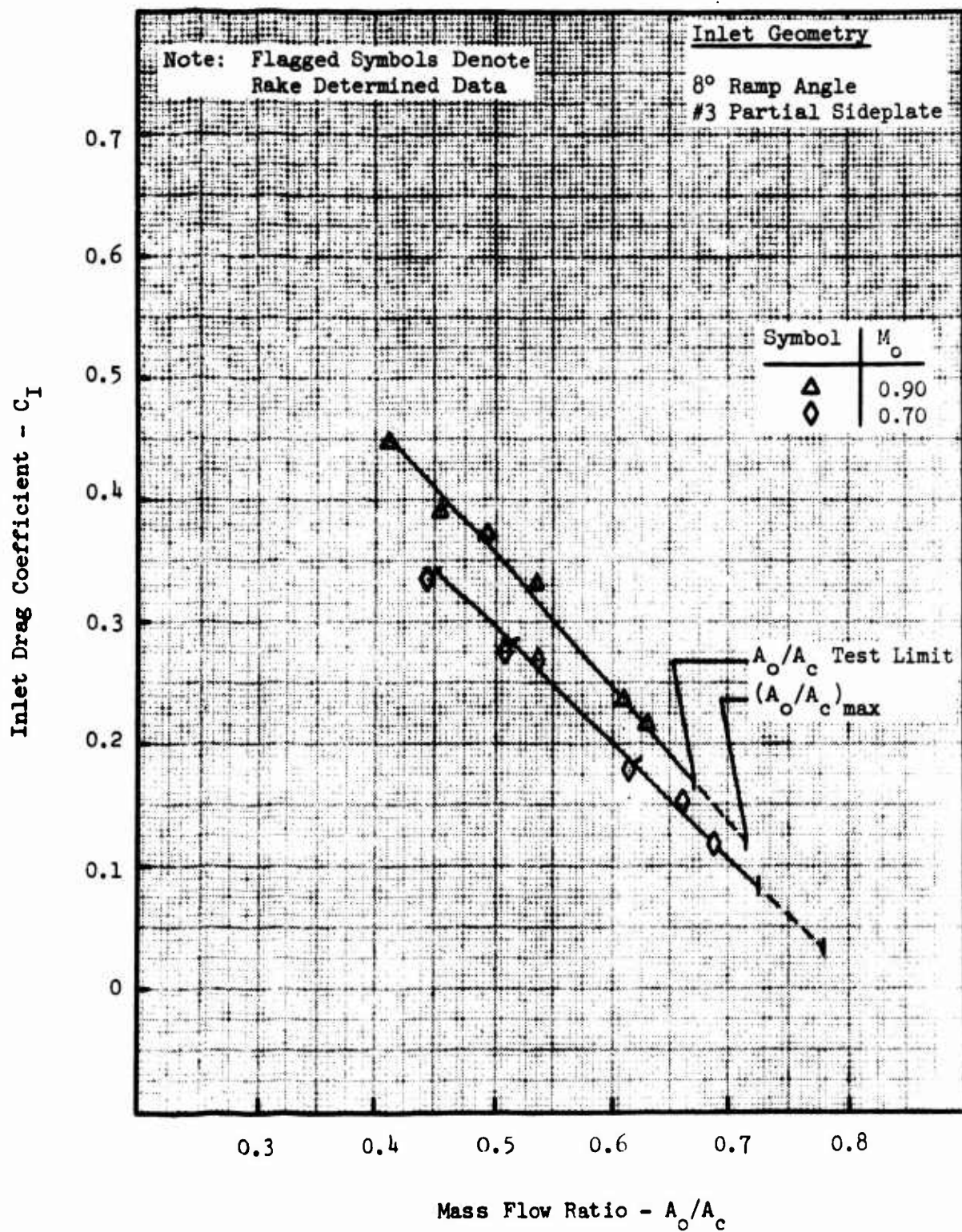


FIGURE D.3 - INLET DRAG COEFFICIENT

Two-Dimensional Inlet Model
Configuration 4
 $\alpha = 0^\circ$

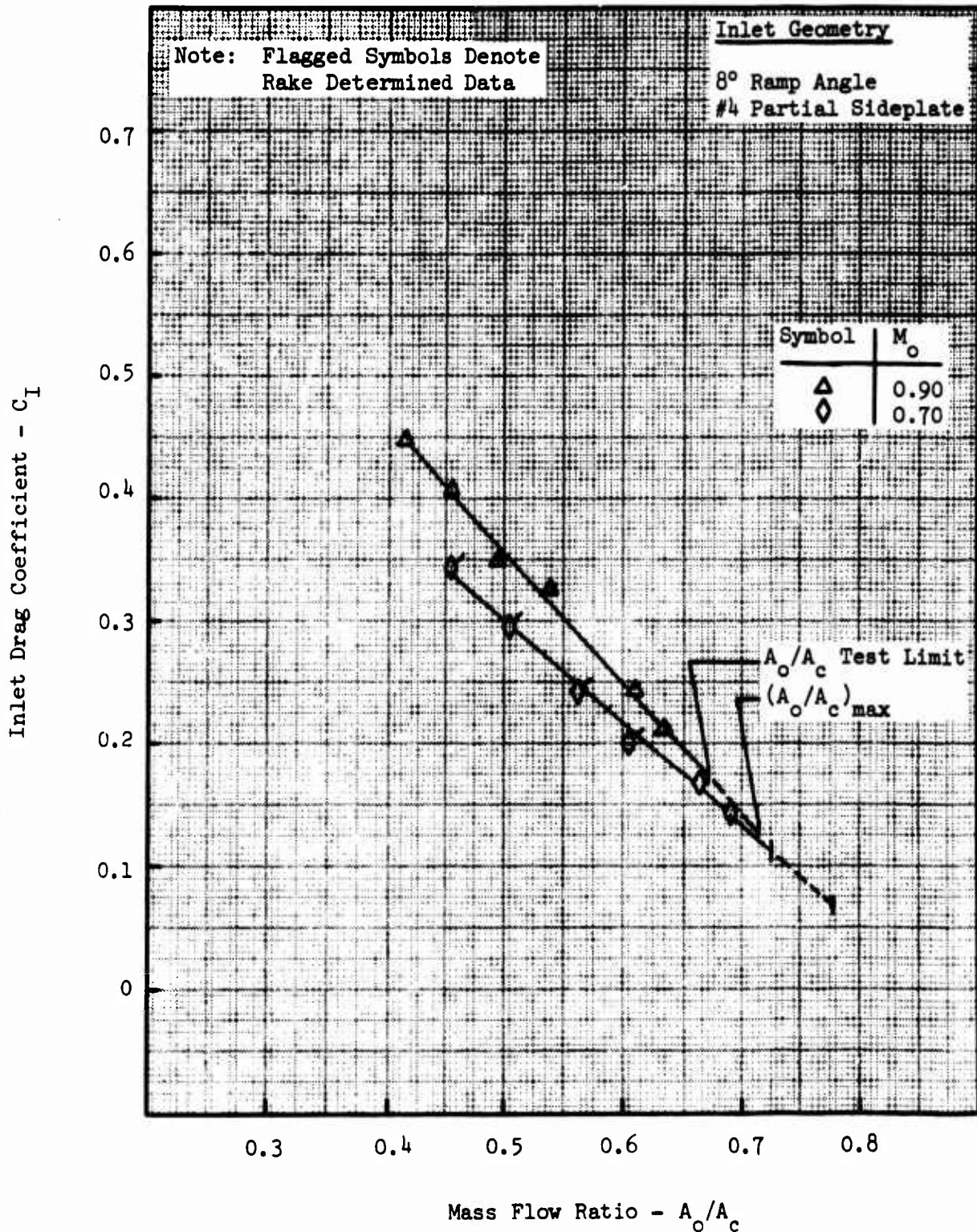


FIGURE D.4 - INLET DRAG COEFFICIENT

Two-Dimensional Inlet Model
 Configuration 5
 $\alpha = 0^\circ$

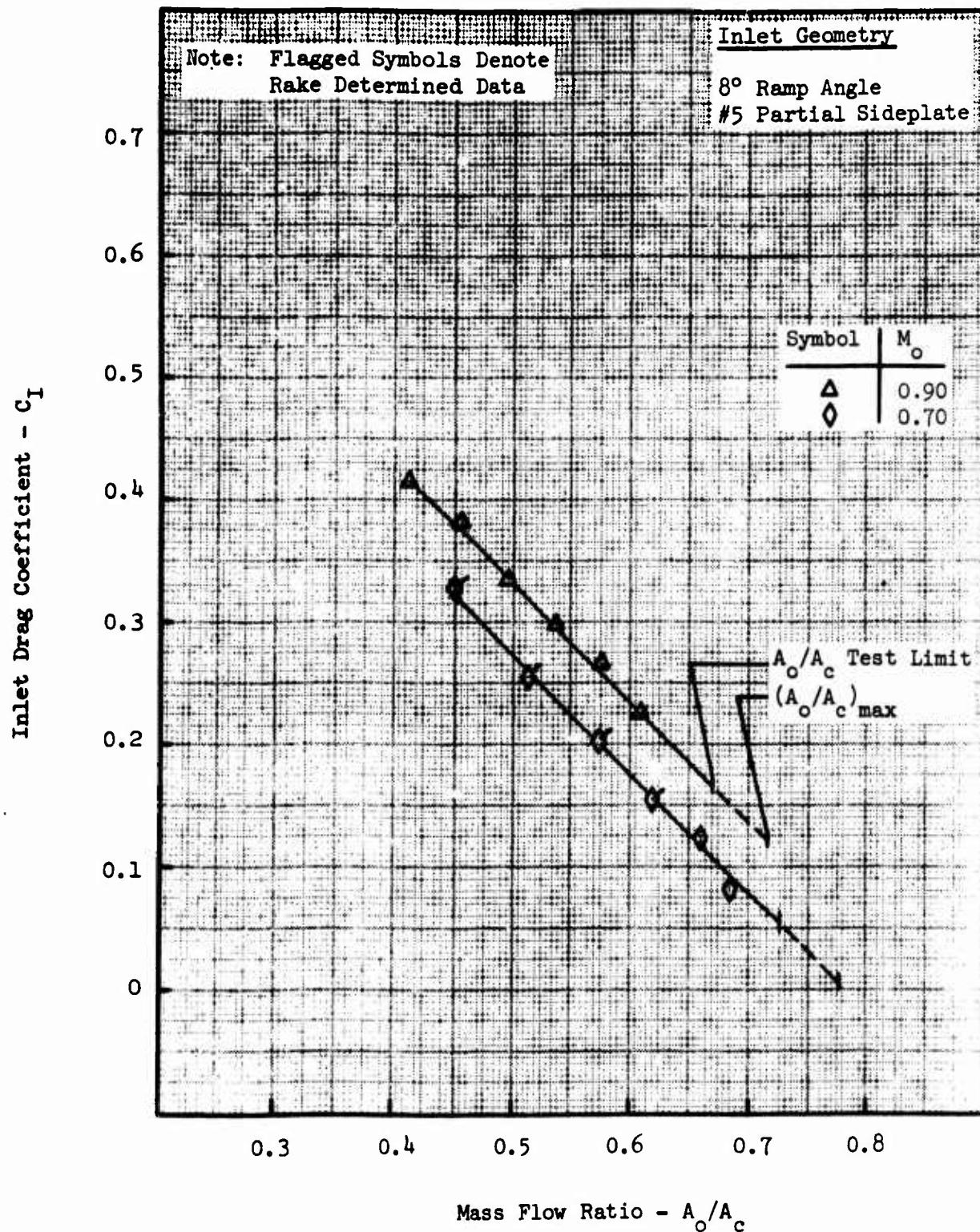


FIGURE D.5 - INLET DRAG COEFFICIENT

Two-Dimensional Inlet Model
Configuration 6
 $\alpha = 0^\circ$

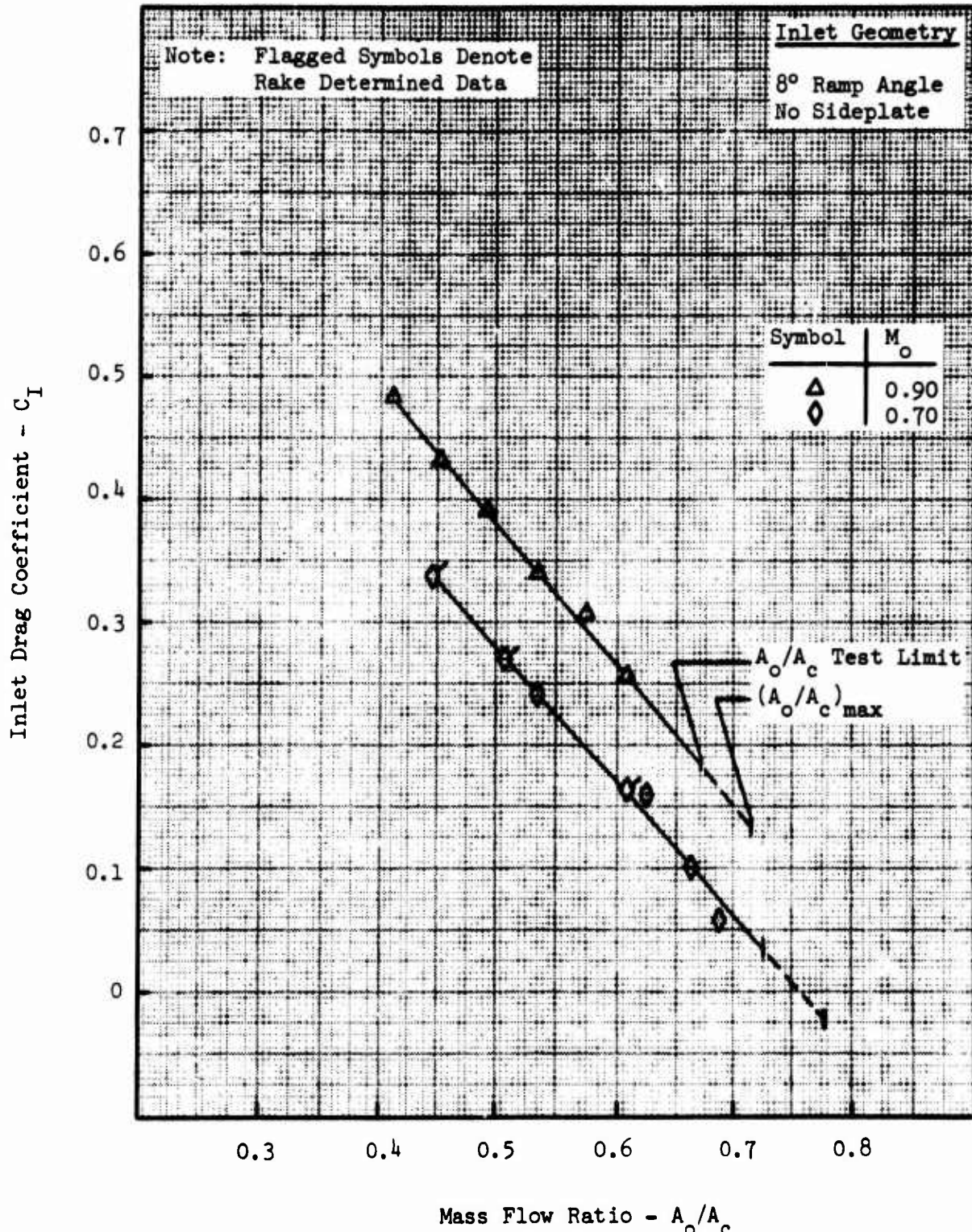


FIGURE D.6 - INLET DRAG COEFFICIENT

Two-Dimensional Inlet Model
Configuration 8
 $\alpha = 0^\circ$

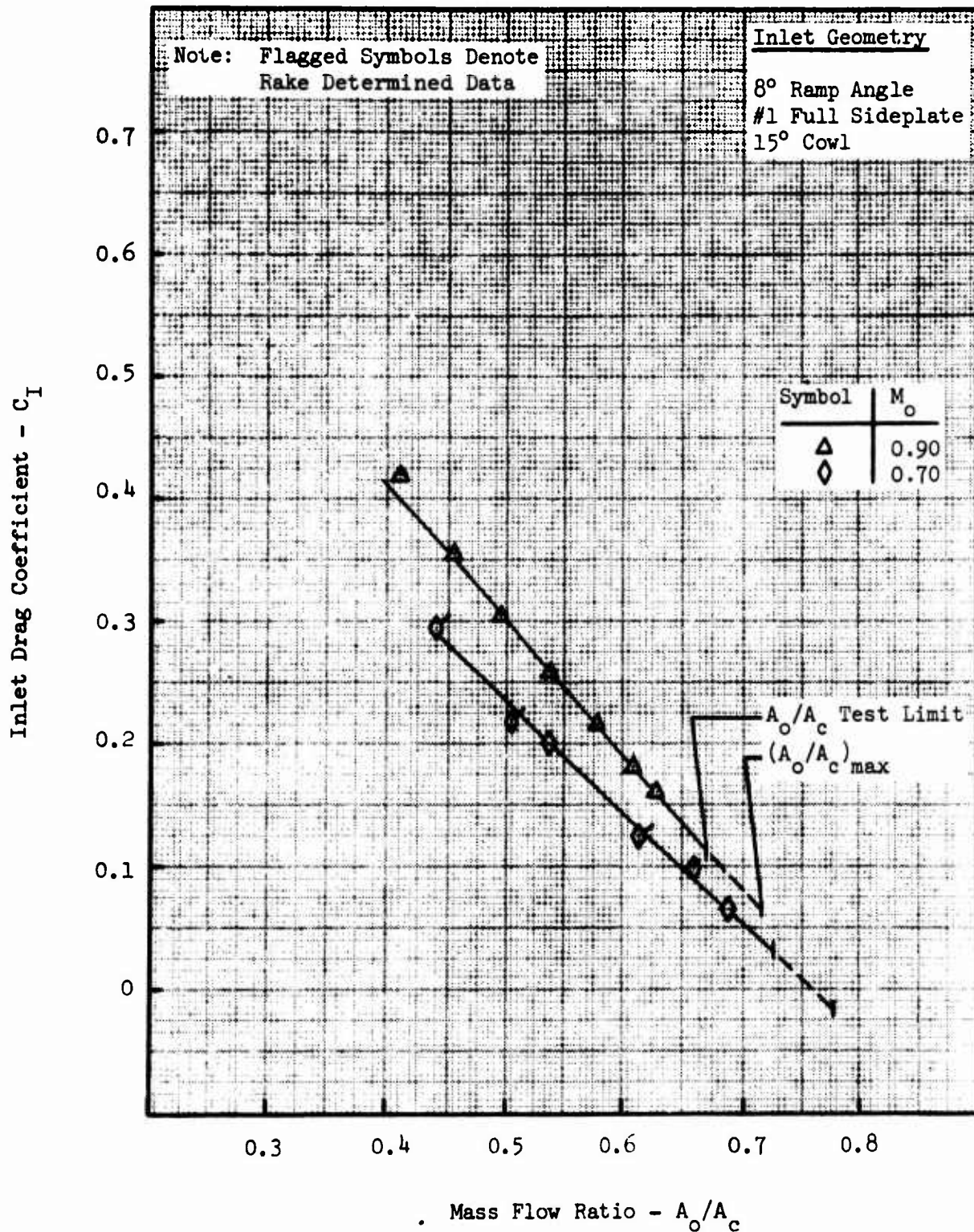


FIGURE D.7 - INLET DRAG COEFFICIENT

Two-Dimensional Inlet Model
 Configuration 11
 $\alpha = 0^\circ$

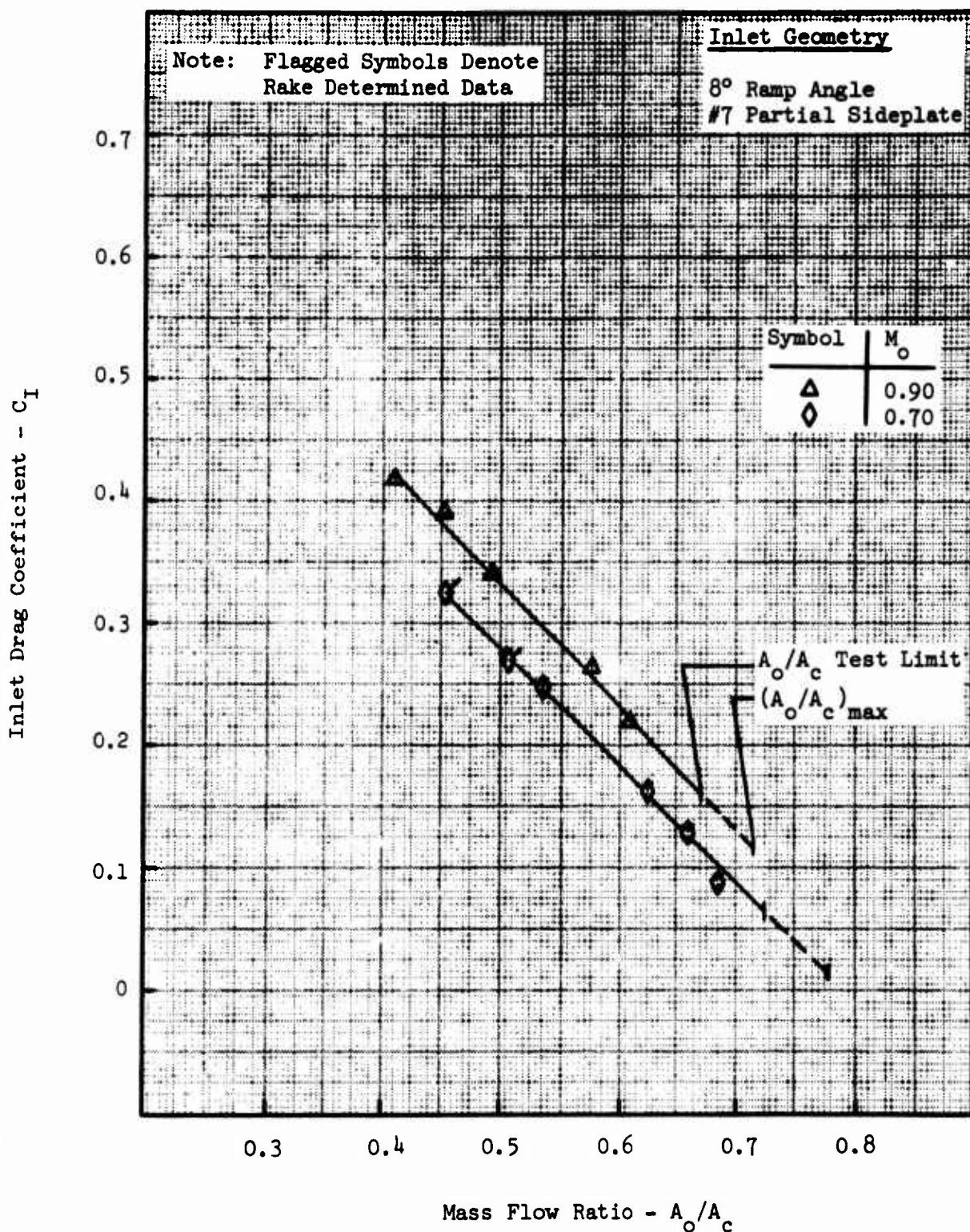


FIGURE D.8 - INLET DRAG COEFFICIENT

Two-Dimensional Inlet Model
Configuration 12
 $\alpha = 0^\circ$

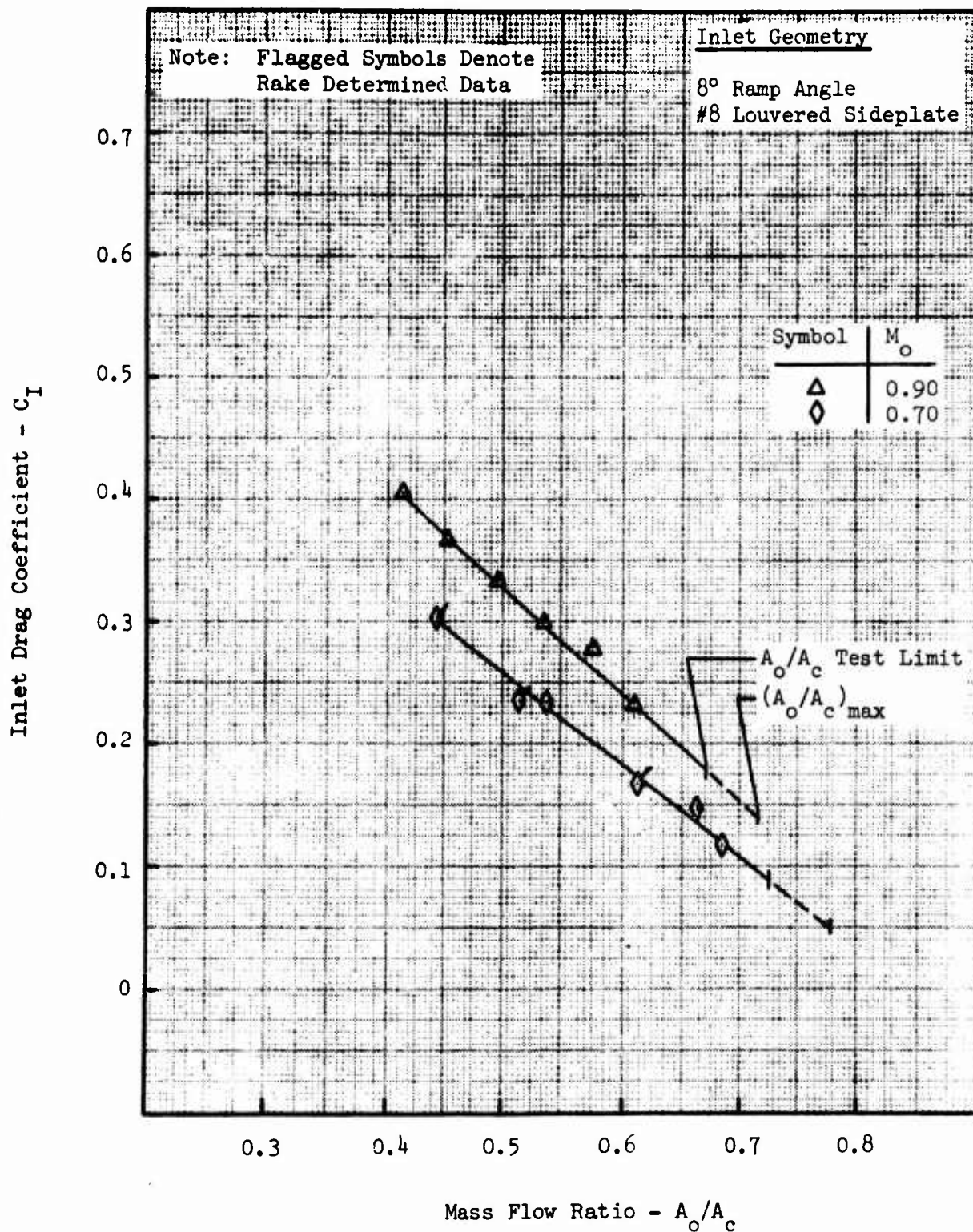


FIGURE D.9 - INLET DRAG COEFFICIENT

Two-Dimensional Inlet Model
Configuration 1s
 $\alpha = 0^\circ$

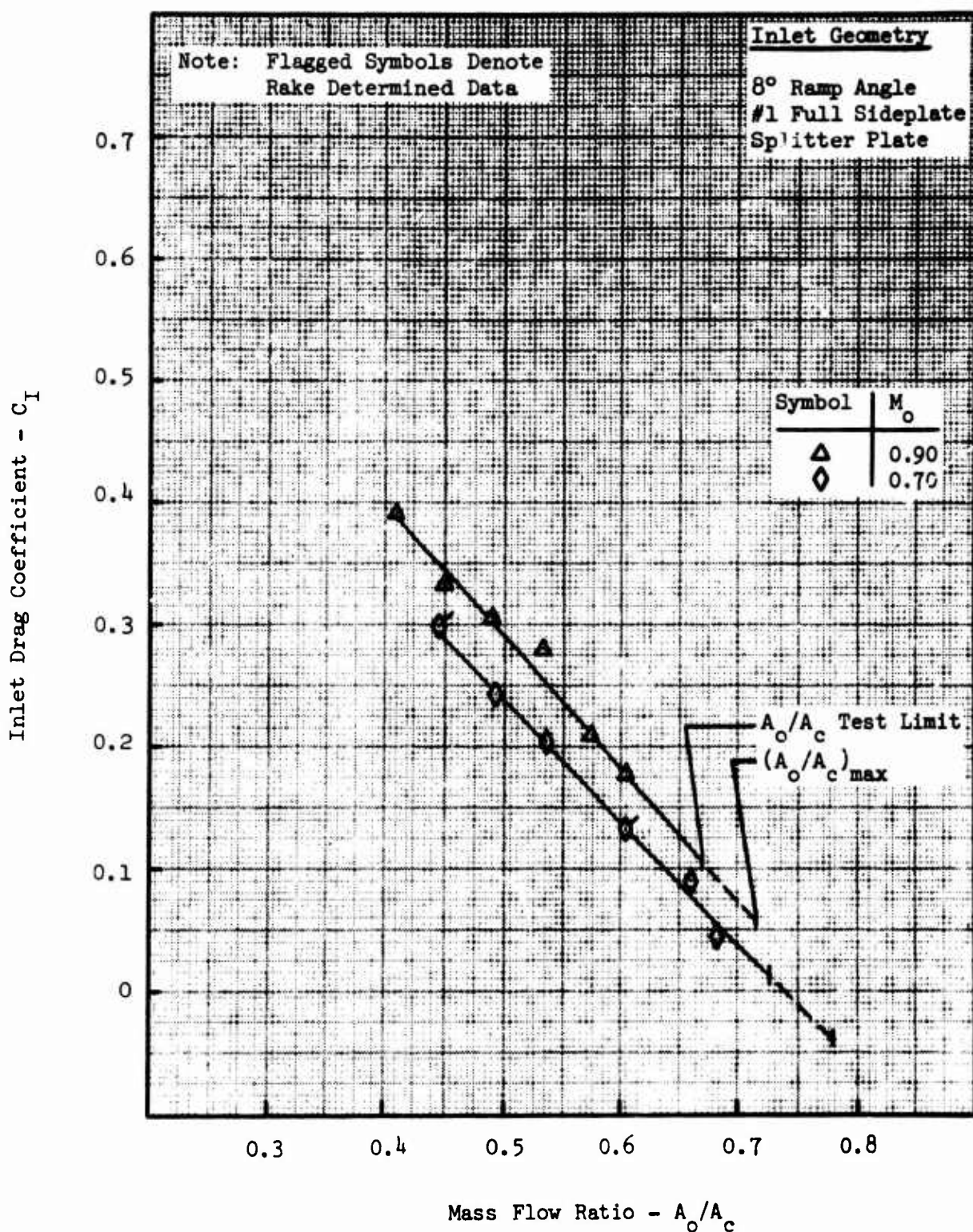


FIGURE D.10 - INLET DRAG COEFFICIENT

Two-Dimensional Inlet Model
Configuration 1
 $\alpha = 6^\circ$

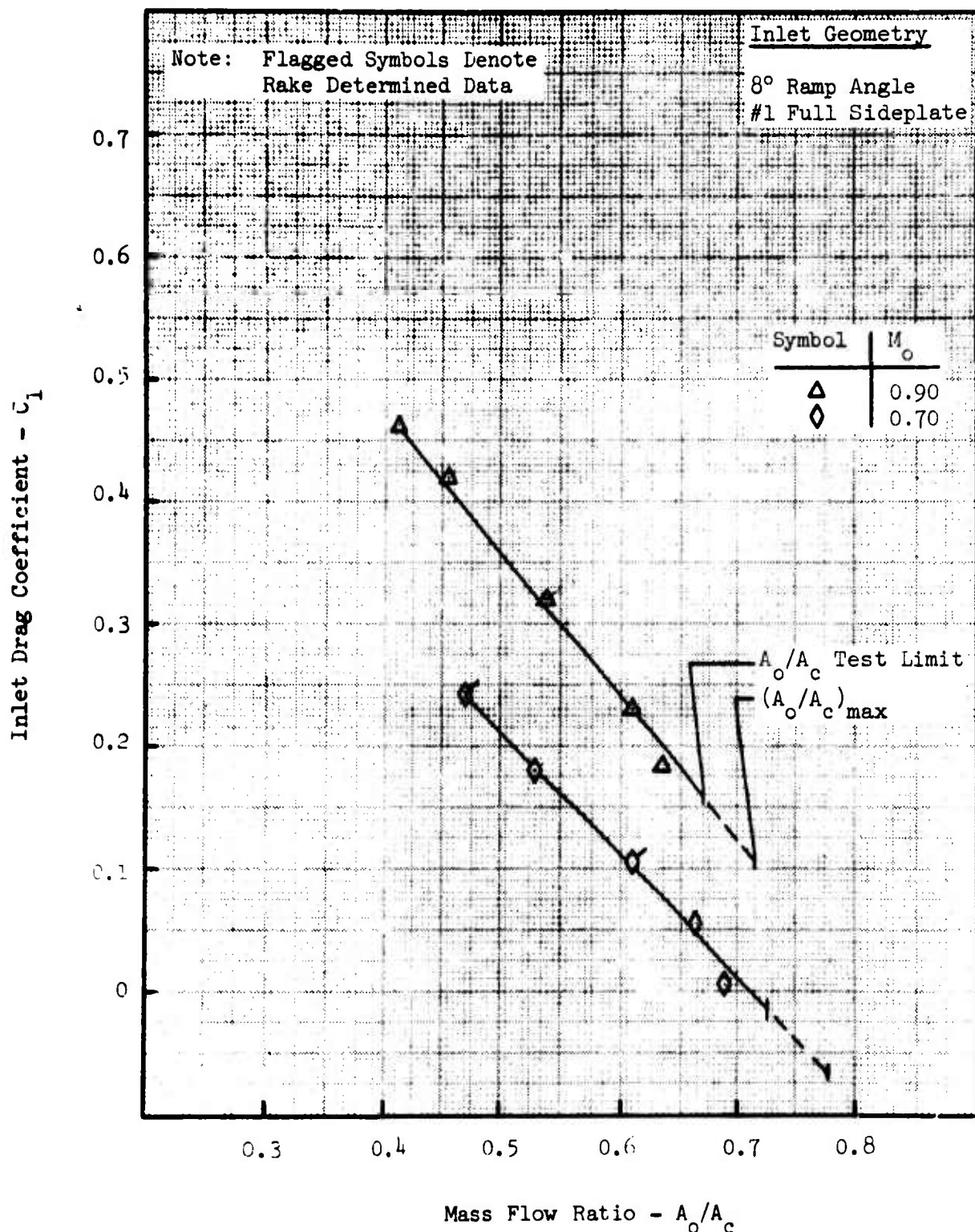


FIGURE D.11 - INLET DRAG COEFFICIENT

Two-Dimensional Inlet Model
Configuration 2
 $\alpha = 6^\circ$

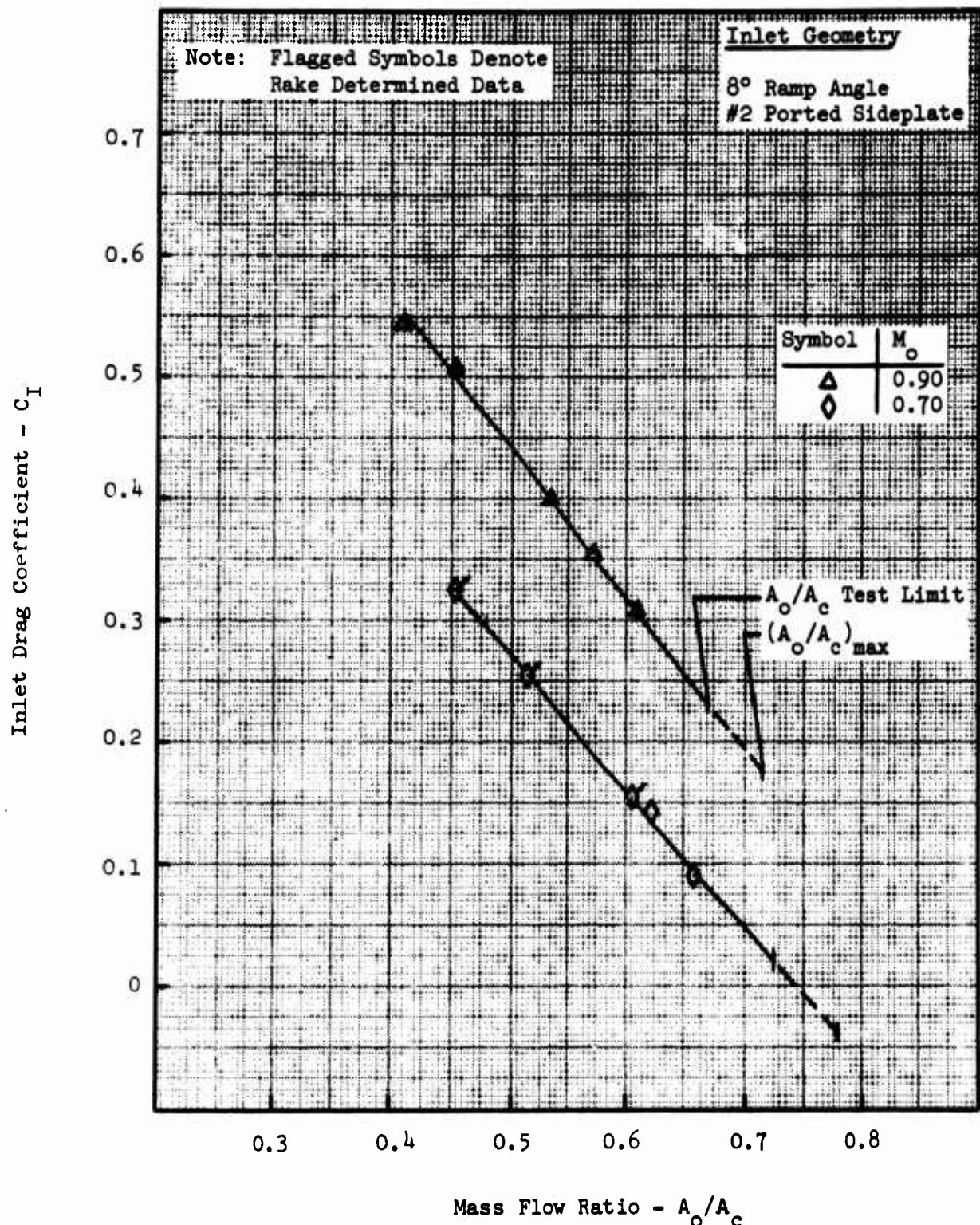


FIGURE D-12 - INLET DRAG COEFFICIENT

Unclassified

Security Classification

DOCUMENT CONTROL DATA - R&D

(Security classification of title, body of abstract and indexing annotation must be entered when the overall report is classified)

1. ORIGINATING ACTIVITY (Corporate author) McDonnell Douglas Corporation St. Louis, Missouri		2a. REPORT SECURITY CLASSIFICATION Unclassified
		2b. GROUP N/A
3. REPORT TITLE Experimental Evaluation of Inlet Drag Characteristics in the Transonic Mach Number Regime		
4. DESCRIPTIVE NOTES (Type of report and inclusive dates) Final Report, Supplement I		
5. AUTHOR(S) (Last name, first name, initial) McVey, Francis D., Rejeske, John V., Phillips, Edward J.		
6. REPORT DATE November 1969	7a. TOTAL NO. OF PAGES 105	7b. NO. OF REFS 4
8a. CONTRACT OR GRANT NO. F33615-68-C-1520	8b. ORIGINATOR'S REPORT NUMBER(S) None	
8c. PROJECT NO. 3066	8d. OTHER REPORT NO(S) (Any other numbers that may be assigned this report) AFAPL-TR-68-119, Supplement I	
9. AVAILABILITY/LIMITATION NOTICES This document is subject to special export controls and each transmittal to foreign governments or foreign nationals may be made only with the approval of Air Force Aero Propulsion Laboratory, Wright-Patterson AFB, Ohio 45433	10. SPONSORING MILITARY ACTIVITY Air Force Aero Propulsion Laboratory Attn: (APTA) Wright-Patterson AFB, Ohio 45433	
11. SUPPLEMENTARY NOTES None	12. ABSTRACT → This report presents the results of a test program to determine the drag of supersonic inlets operating at transonic Mach number conditions. It is a supplement to Air Force Report AFAPL-TR-68-119 describing the results of additional tests conducted under Air Force Contract F33615-68-C-1520. Data are presented showing the additive drag and total inlet drag of the F-4 aircraft inlet measured in the presence of the aircraft forebody and in an undisturbed stream. Inlet drag test data are also presented for a series of thirteen configurations where the sideplate geometry is the primary variable. All thirteen configurations are variations on a single two-dimensional inlet. Tests to reproduce some of the data reported in AFAPL-TR-68-119 were conducted to evaluate the accuracy of the experimental procedure.	

Unclassified
Security Classification

14. KEY WORDS	LINK A		LINK B		LINK C	
	ROLE	WT	ROLE	WT	ROLE	WT
Inlet Drag Additive Drag Cowl Drag Subsonic, Transonic, and Supersonic Inlet Drag Axisymmetric Inlet Drag Two-Dimensional Inlet Drag F-4 Inlet Drag Forebody Effects on Inlet Drag						

INSTRUCTIONS

1. ORIGINATING ACTIVITY: Enter the name and address of the contractor, subcontractor, grantees, Department of Defense activity or other organization (corporate author) issuing the report.

2a. REPORT SECURITY CLASSIFICATION: Enter the overall security classification of the report. Indicate whether "Restricted Data" is included. Marking is to be in accordance with appropriate security regulations.

2b. GROUP: Automatic downgrading is specified in DoD Directive 5200.10 and Armed Forces Industrial Manual. Enter the group number. Also, when applicable, show that optional markings have been used for Group 3 and Group 4 as authorized.

3. REPORT TITLE: Enter the complete report title in all capital letters. Titles in all cases should be unclassified. If a meaningful title cannot be selected without classification, show title classification in all capitals in parenthesis immediately following the title.

4. DESCRIPTIVE NOTES: If appropriate, enter the type of report, e.g., interim, progress, summary, annual, or final. Give the inclusive dates when a specific reporting period is covered.

5. AUTHOR(S): Enter the name(s) of author(s) as shown on or in the report. Enter last name, first name, middle initial. If military, show rank and branch of service. The name of the principal author is an absolute minimum requirement.

6. REPORT DATE: Enter the date of the report as day, month, year, or month, year. If more than one date appears on the report, use date of publication.

7a. TOTAL NUMBER OF PAGES: The total page count should follow normal pagination procedures, i.e., enter the number of pages containing information.

7b. NUMBER OF REFERENCES: Enter the total number of references cited in the report.

8a. CONTRACT OR GRANT NUMBER: If appropriate, enter the applicable number of the contract or grant under which the report was written.

8b, 8c, & 8d. PROJECT NUMBER: Enter the appropriate military department identification, such as project number, subproject number, system numbers, task number, etc.

9a. ORIGINATOR'S REPORT NUMBER(S): Enter the official report number by which the document will be identified and controlled by the originating activity. This number must be unique to this report.

9b. OTHER REPORT NUMBER(S): If the report has been assigned any other report numbers (either by the originator or by the sponsor), also enter this number(s).

10. AVAILABILITY/LIMITATION NOTICES: Enter any limitations on further dissemination of the report, other than those

imposed by security classification, using standard statements such as:

- (1) "Qualified requesters may obtain copies of this report from DDC."
- (2) "Foreign announcement and dissemination of this report by DDC is not authorized."
- (3) "U. S. Government agencies may obtain copies of this report directly from DDC. Other qualified DDC users shall request through _____."
- (4) "U. S. military agencies may obtain copies of this report directly from DDC. Other qualified users shall request through _____."
- (5) "All distribution of this report is controlled. Qualified DDC users shall request through _____."

If the report has been furnished to the Office of Technical Services, Department of Commerce, for sale to the public, indicate this fact and enter the price, if known.

11. SUPPLEMENTARY NOTES: Use for additional explanatory notes.

12. SPONSORING MILITARY ACTIVITY: Enter the name of the departmental project office or laboratory sponsoring (paying for) the research and development. Include address.

13. ABSTRACT: Enter an abstract giving a brief and factual summary of the document indicative of the report, even though it may also appear elsewhere in the body of the technical report. If additional space is required, a continuation sheet shall be attached.

It is highly desirable that the abstract of classified reports be unclassified. Each paragraph of the abstract shall end with an indication of the military security classification of the information in the paragraph, represented as (TS), (S), (C), or (U).

There is no limitation on the length of the abstract. However, the suggested length is from 150 to 225 words.

14. KEY WORDS: Key words are technically meaningful terms or short phrases that characterize a report and may be used as index entries for cataloging the report. Key words must be selected so that no security classification is required. Identifiers, such as equipment model designation, trade name, military project code name, geographic location, may be used as key words but will be followed by an indication of technical context. The assignment of links, roles, and weights is optional.

Unclassified
Security Classification